

The analytical theory of self-consistent current structures in a relativistic collisionless plasma

¹Vl.V.Kocharovsky, ^{1,2}V.V.Kocharovsky, ³V.Ju.Martyanov, ¹S.V.Tarasov

¹Institute of Applied Physics RAS, Nizhny Novgorod, Russia

²Department of Physics and Astronomy, Texas A&M University, College Station, TX, USA

³Intel Corporation, 5000 W Chandler Blvd, Chandler, AZ 85226, USA

We outline the most-studied classes of exact solutions to Vlasov-Maxwell equations for stationary neutral current structures, which allow the particle distribution functions to be chosen at will (Physics - Uspekhi **59** (2016) 1165).

A number of new analytical solutions are given.

The Harris current sheet solution, 1962

$$f_{e,i} = \frac{N(x, z)}{(2\pi m_{e,i} T_{e,i})^{3/2}} \exp\left(\frac{-p_x^2 - (p_y - m_{e,i} V_{e,i})^2 - p_z^2}{2m_{e,i} T_{e,i}}\right)$$

PDF of exponential type:

$$p_y \rightarrow p_y + q_{e,i} A / c$$

Vector potential $\mathbf{A} = A(x)$

$$B_z = 2kA_0 \tanh(kx)$$

$$V_e, V_i = \text{const}$$

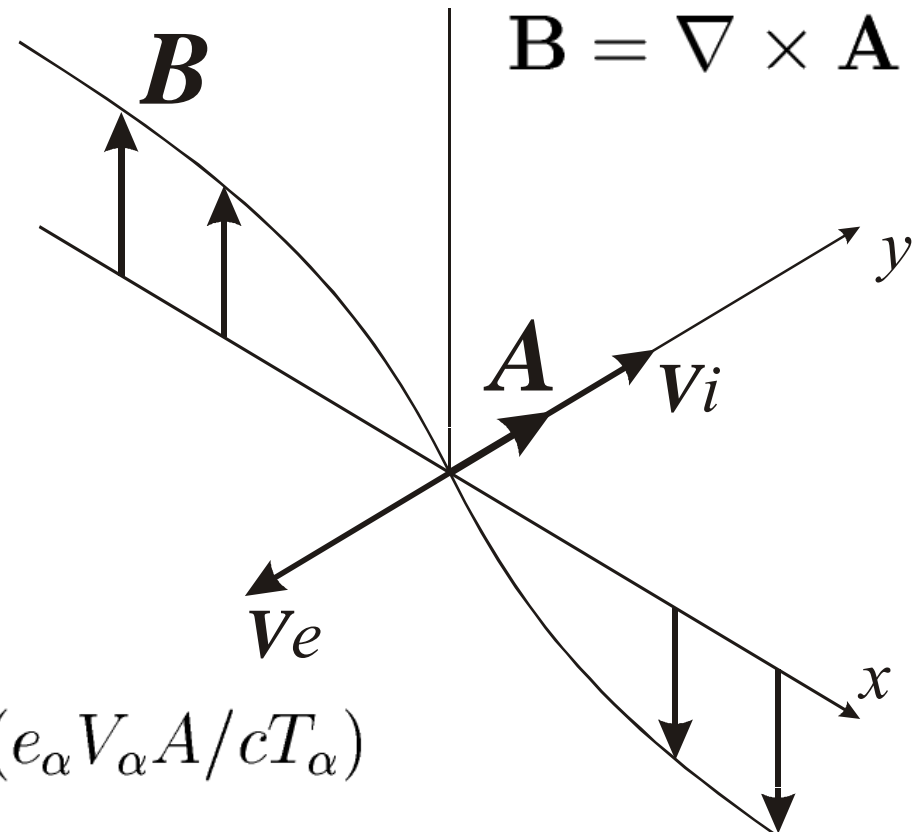
$$V_e / T_e = V_i / T_i$$

$$\Delta A = -\frac{4\pi}{c} \sum_{\alpha} e_{\alpha} N_{0\alpha} V_{\alpha} \exp(e_{\alpha} V_{\alpha} A / c T_{\alpha})$$

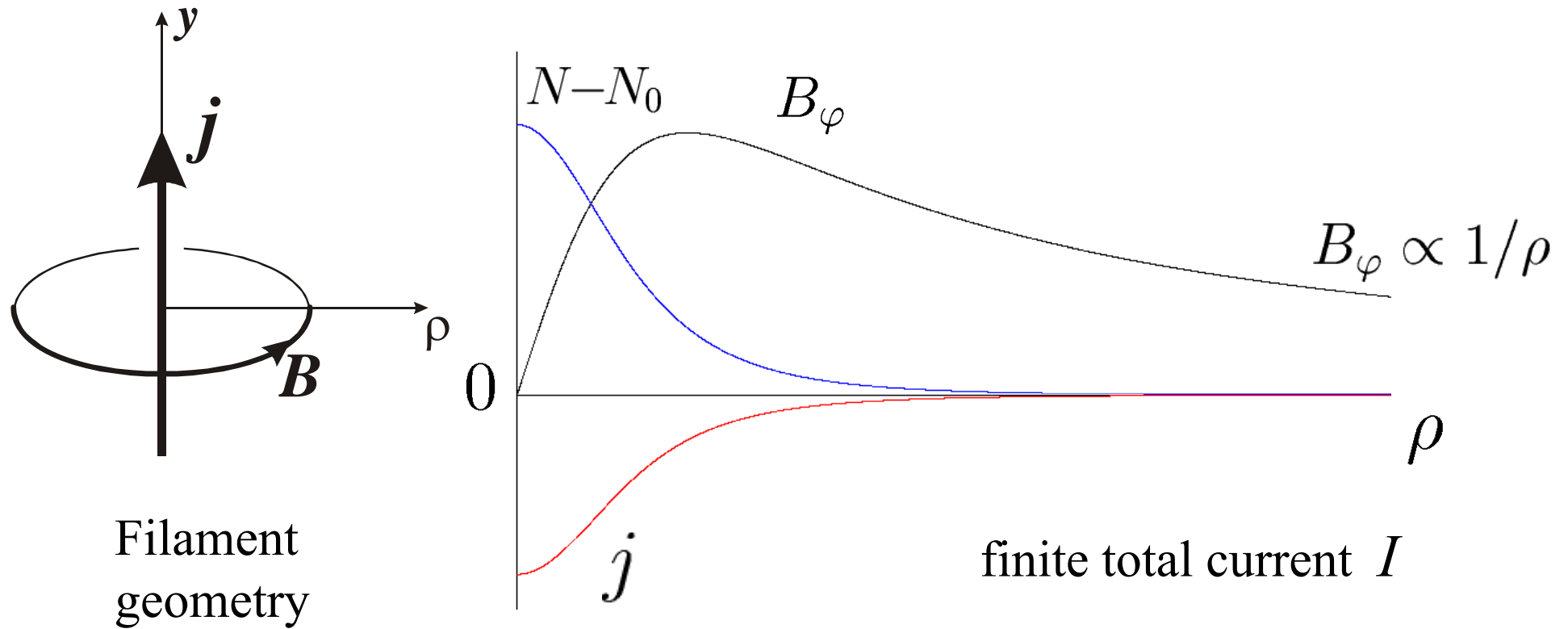
$$\Delta \varphi = 4\pi \rho, \quad \rho \sim \exp(-e\varphi / T) \quad (\text{ion' frame of reference})$$

$$\text{Balance of forces: } e_{\alpha} E_{\alpha} = T_{\alpha} \nabla N_{\alpha}$$

$\varphi \approx 0$ and $\rho \approx 0$ in De Hoffmann-Teller' frame of reference



Bennett pinch, 1934 (PDF of exponential type)



$$A = -2A_0 \ln \left[1 + \frac{\alpha(x^2 + y^2)}{8A_0} \right], \quad B = \frac{4A_0\alpha\rho}{8A_0 + \alpha\rho^2}, \quad N_j = N_{j\max} \left[1 + \frac{\alpha(x^2 + y^2)}{8A_0} \right]^{-2}$$

Basic nonlinear equations describing stationary self-consistent current configurations in collisionless multicomponent plasma

$$\mathbf{p} \frac{\partial f_\alpha}{\partial \mathbf{r}} + \frac{e_\alpha}{c} [\mathbf{p} \times [\nabla \times \mathbf{A}]] \frac{\partial f_\alpha}{\partial \mathbf{p}} = 0$$

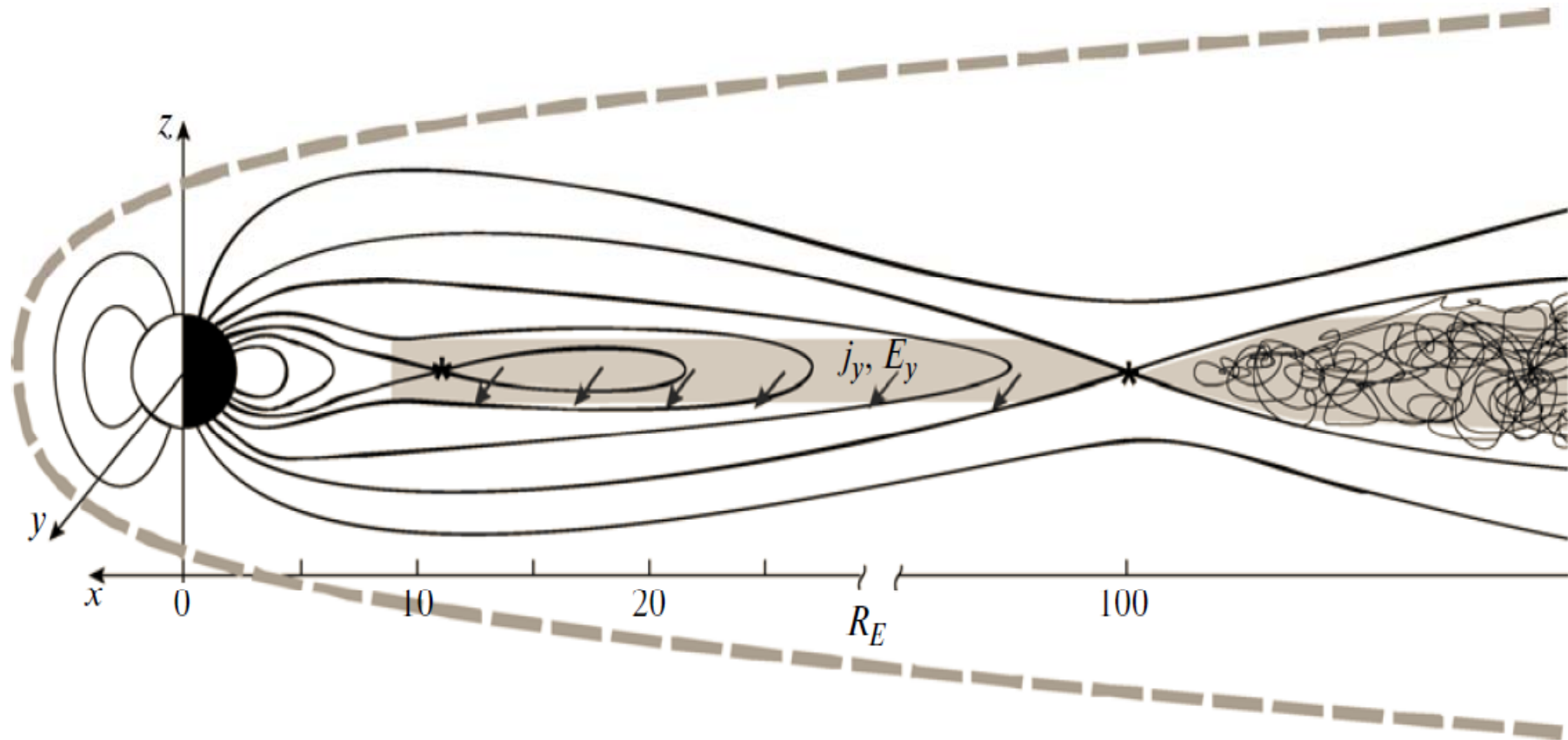
$$[\nabla \times [\nabla \times \mathbf{A}]] = \frac{4\pi}{c} \sum_\alpha e_\alpha \int f_\alpha \frac{\mathbf{p}}{m_\alpha \gamma_a} d^3 \mathbf{p}$$

The solutions are found via **the method of integrals of particle motion** and extend far beyond the known generalizations of the non-relativistic Harris and Bennett models.

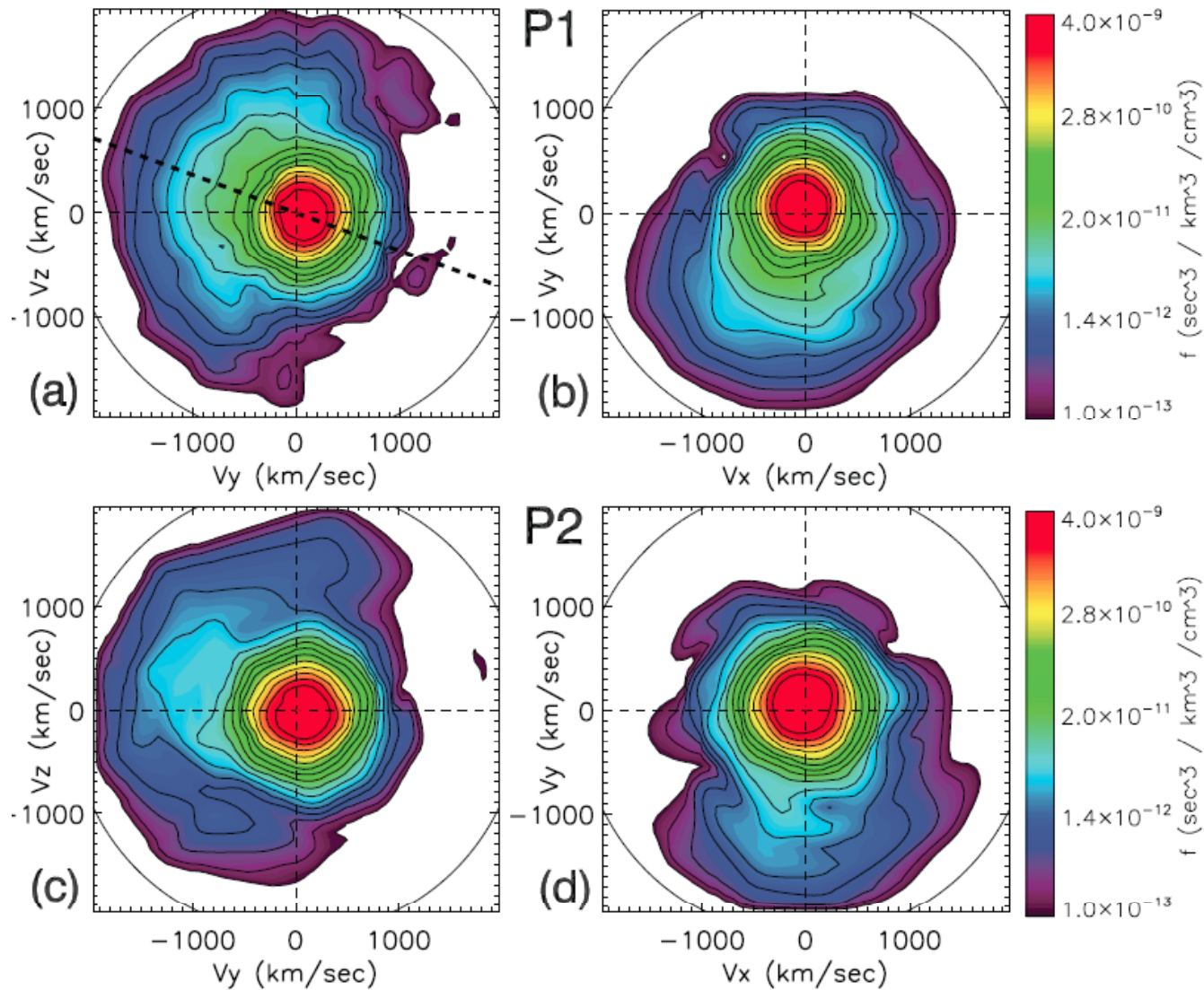
We come to the nonlinear Grad-Shafranov type equation which allows us to analytically investigate and compare general properties of self-consistent structures: the ratio of magnetic field energy to that of particles, the anisotropy of particle momentum distribution, the spatial scales and profiles of particle density, current and magnetic field, etc.

V.Ju. Martyanov, Vl.V. Kocharovsky, V.V. Kocharovsky, JETP **107**, 1049 (2008);
Radiophys. Quant. Electr. **52**, n. 2 (2009); Astronomy Lett. **36**, 396 (2010);
Phys. Rev. Lett. **104**, 215002 (2010); Physics of Plasmas **22**, 083303 (2015);
Physics - Uspekhi **59** (2016) 1165.

Current sheet in Earth's magnetosphere



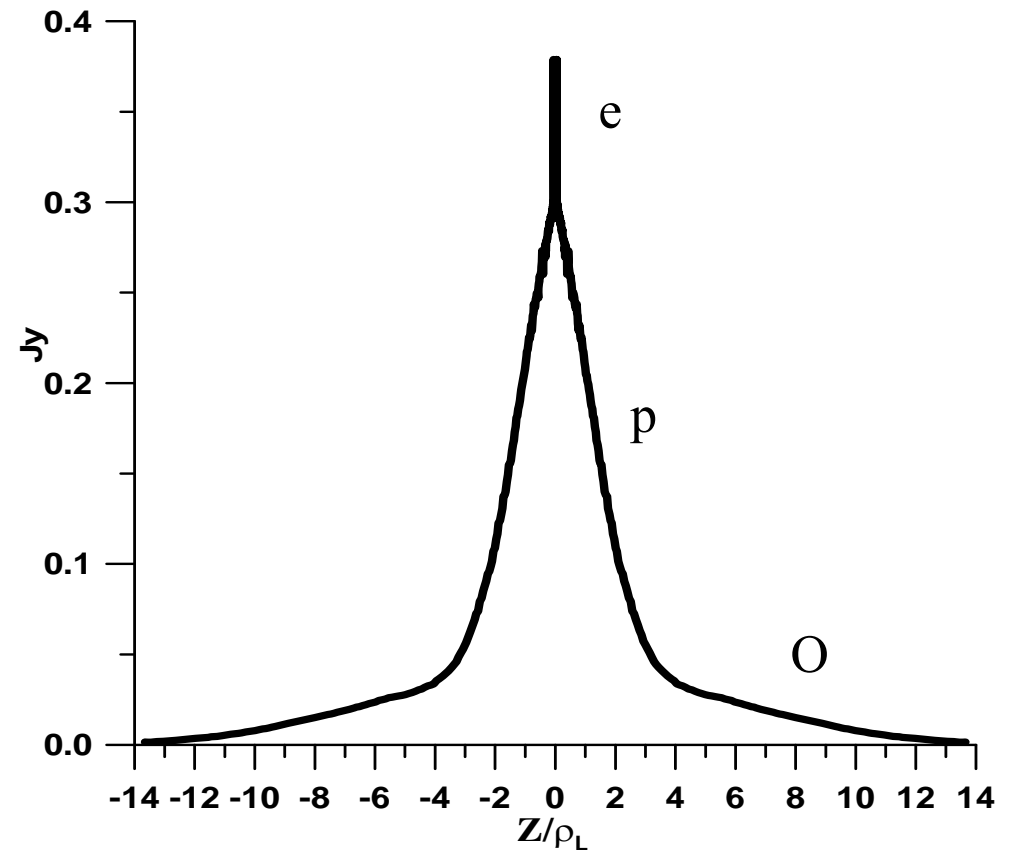
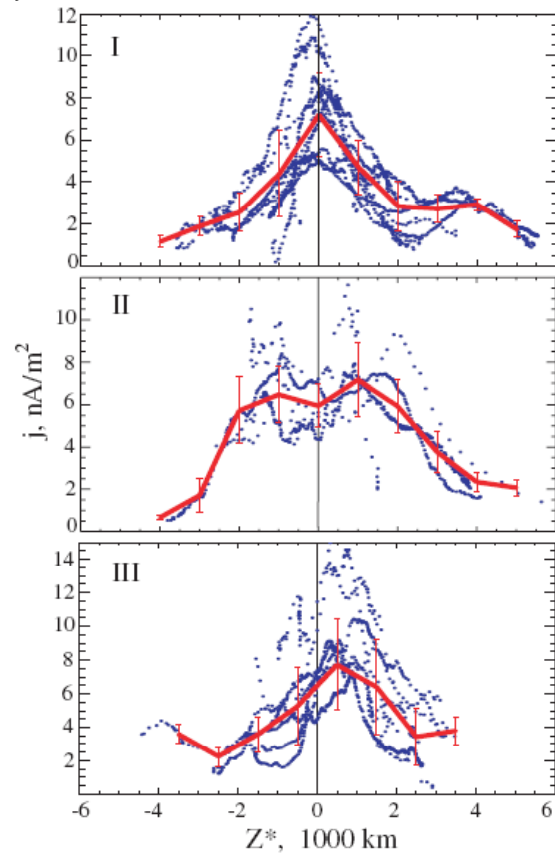
Cluster data show a complicated structure of the current sheet



THEMIS P1 and P2 observations of the ion distribution functions in the despun spacecraft coordinates (+x is Earthward, +y is downward, and +z is southward) during the substorm event of 26 February 2008.

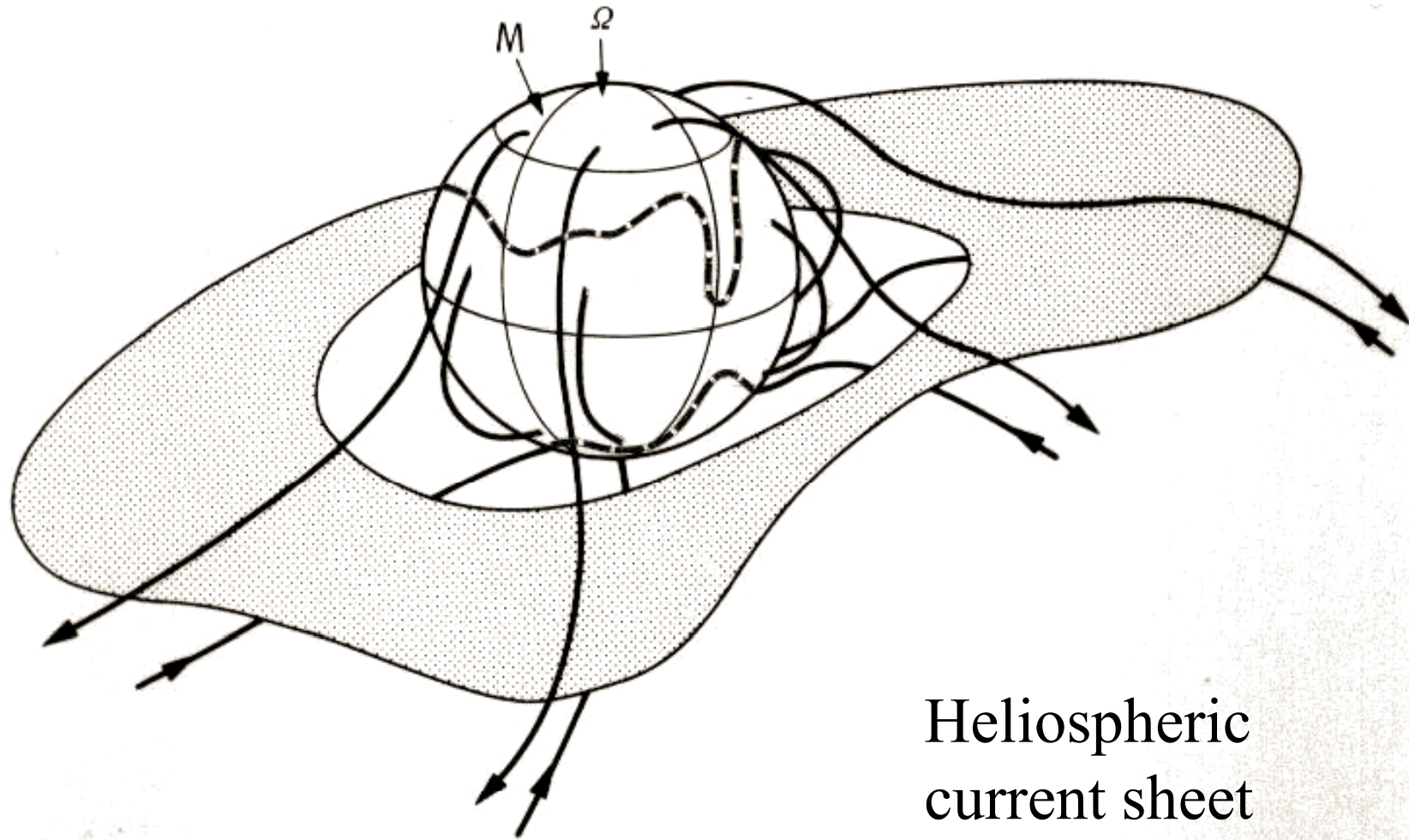
Multi-scale and asymmetric current sheets in the Earth magnetosphere

Runov et al., Annales Geophysicae, 24, 247, 2006; Artemyev et al., Annales Geophysicae, 26, 2749, 2008; Zelenyi et al., Plasma Physics Reports, 37, 118, 2011.



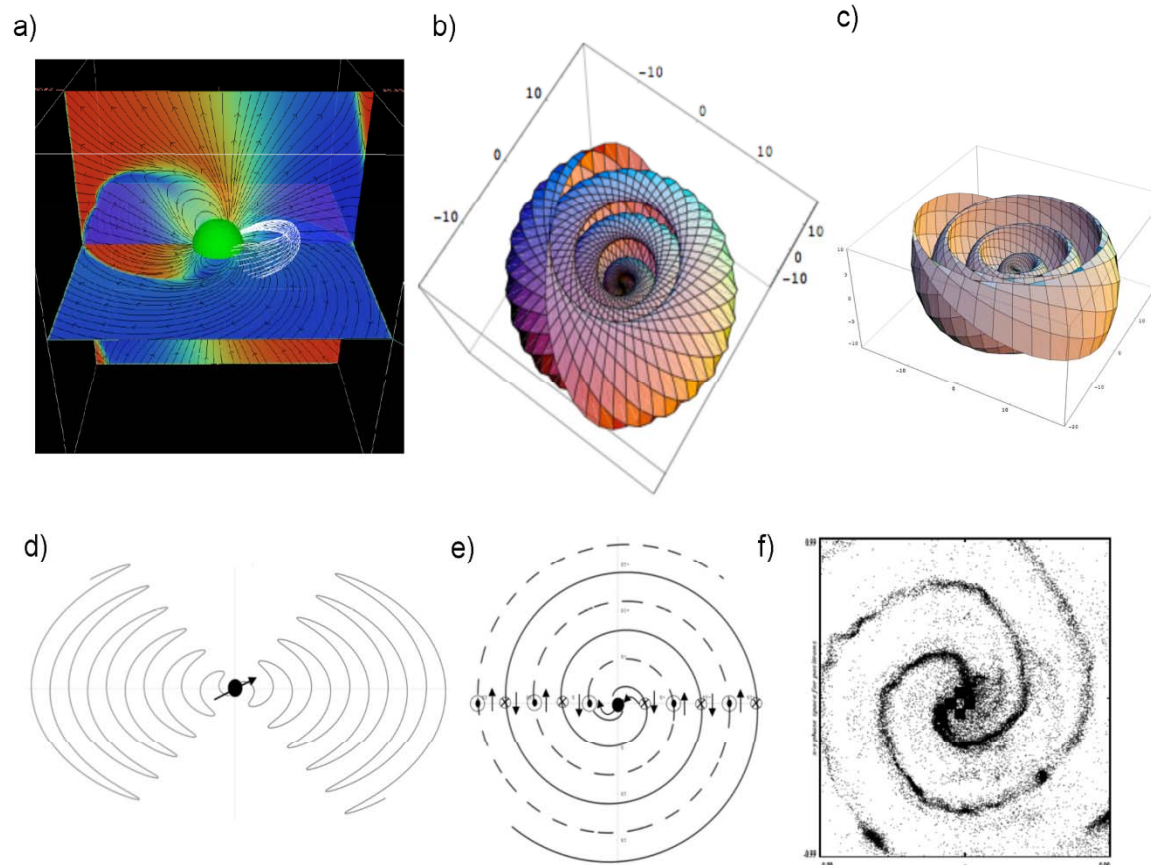
Current sheets and filaments in the solar corona:

Non-equilibrium particle distributions and variety of spatial profiles



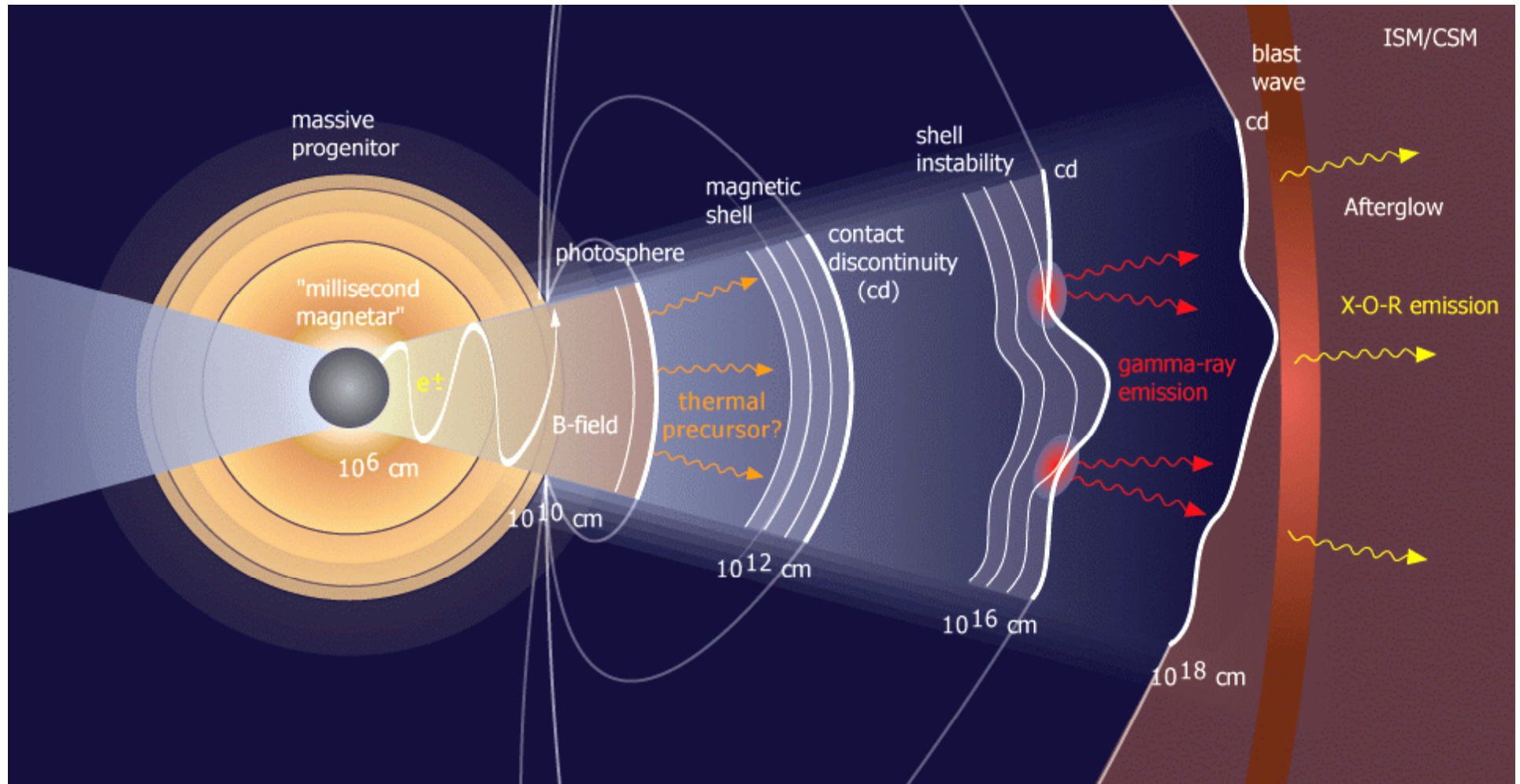
Heliospheric
current sheet

Current sheets in a pulsar wind nebula



a) Magnetic Geometry of a Force-Free Rotator for $r < 2RL$ and $i = 60$, from Spitkovsky (2006). The rapid transition to inclined split monopole field geometry for $r > RL$ is apparent. b) Geometry of the current sheet from the split monopole model for $i = 60$, $r > RL$. For clarity, only one of the two spirally wound current sheets is shown. As $i=90$, the sheets almost completely enclose the star; for $r>RL$, the spirals are tightly wrapped and the current sheet surfaces closely approximate nested spheres. c) One sheet for $i=30$, shown for clarity. d) Meridional cross section of the current sheet for $i = 60$. e) Equatorial cross section snapshot of the current sheet, showing the two arm spiral form. The arrows show the local directions of the magnetic field; the dots and crosses show the direction of the current flow. f)

Relativistic shock model of Gamma-Ray Bursts (an extremely non-equilibrium collisionless plasma with a long-living turbulent magnetic field)



How large is a set of self-consistent current sheets?

Quasistationary magnetic fields maintained by intrinsic currents in a collisionless plasma determine to a large extent its kinetic, dynamic, and radiative properties. The energy distribution of particles may be far from a Maxwellian one in different physical conditions prevailing in both, cosmic and laboratory (including laser) plasmas. Despite the lack of quantitative data, results of in situ observations, laboratory experiments, and numerical simulations have one thing in common: they all suggest the existence of various long-lived current structures considerably different in terms of particle distribution functions, spatial configuration of the current density, and magnetic fields produced by the current.

Numerous publications report attempts to kinetically describe magnetostatic self-consistent structures. Most of them refer to analytical studies, because numerical simulation does not provide an approach to the solution to this complicated nonlinear problem. Unfortunately, many authors confine themselves to considering a very limited set of anisotropic particle distributions (usually a shifted Maxwellian distribution), which leaves only a narrow choice of spatial current density distributions.

The few studies that allow an arbitrary particle distribution over energies and/or arbitrary spatial current profiles fail to provide a clear understanding of possible types of current structures; see, e.g.,

Tur A et al. *J. Plasma Phys.* **66** (2001) 97; Mottez F, *Phys. Plasmas* **10** (2003) 2501, **11** (2004) 336; Balikhin M, Gedalin M, *J. Plasma Phys.* **74** (2008) 749; Ghosh A et al., *Chaos* **24** (2014) 013117.

A consistent analytical theory of neutral current structures in a collisionless plasma with arbitrary energy distribution of particles has only recently attracted the serious attention of researchers, with the most interesting results obtained by our method based on the invariants of particle motion.

The present talk is restricted mainly by the planar structures. We consider variety of current and magnetic field profiles, both localized and nonlocalized, taking into account the complicated motion of trapped and transit particles and the inhomogeneity of the anisotropy of their distribution function.

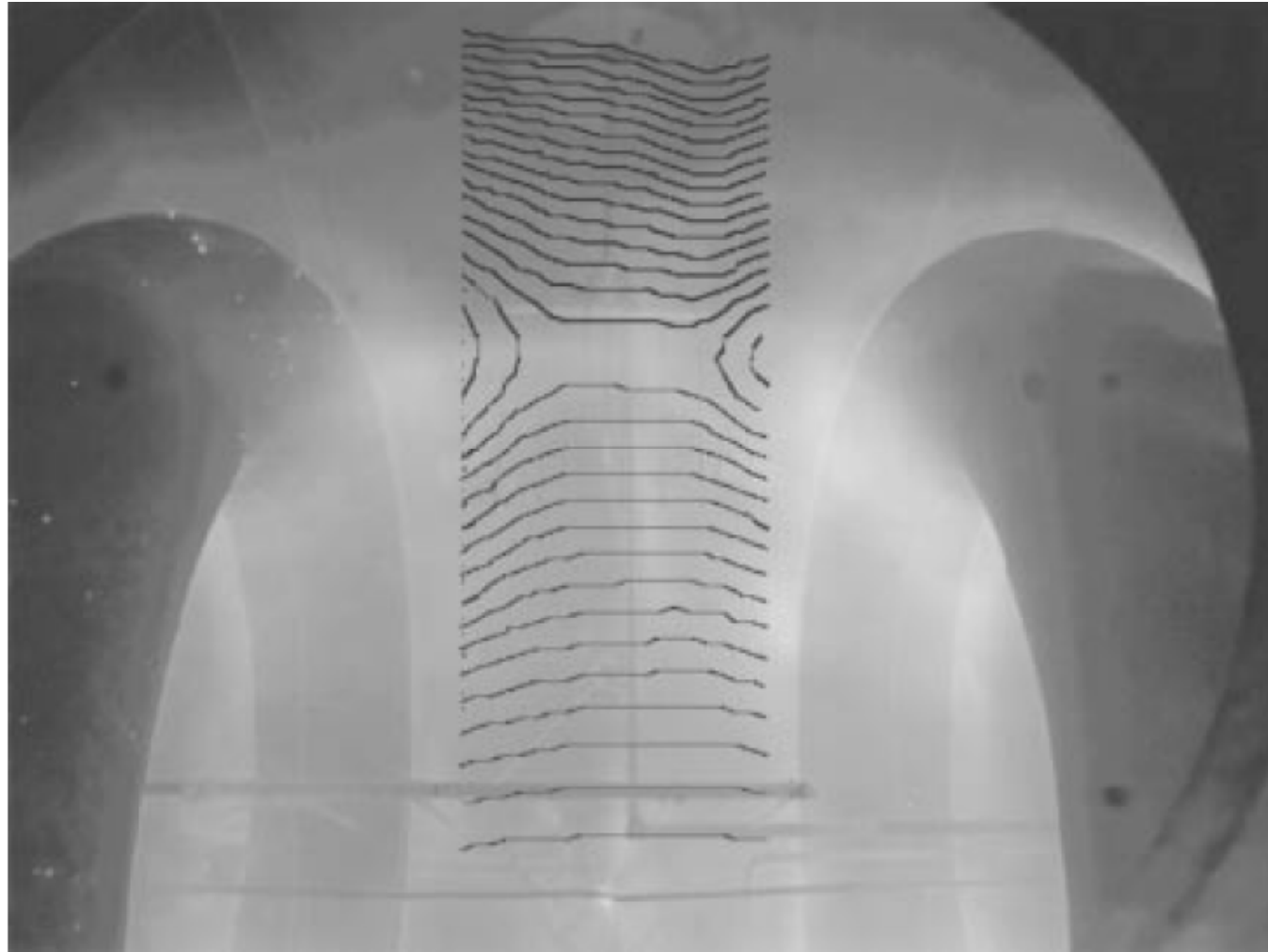
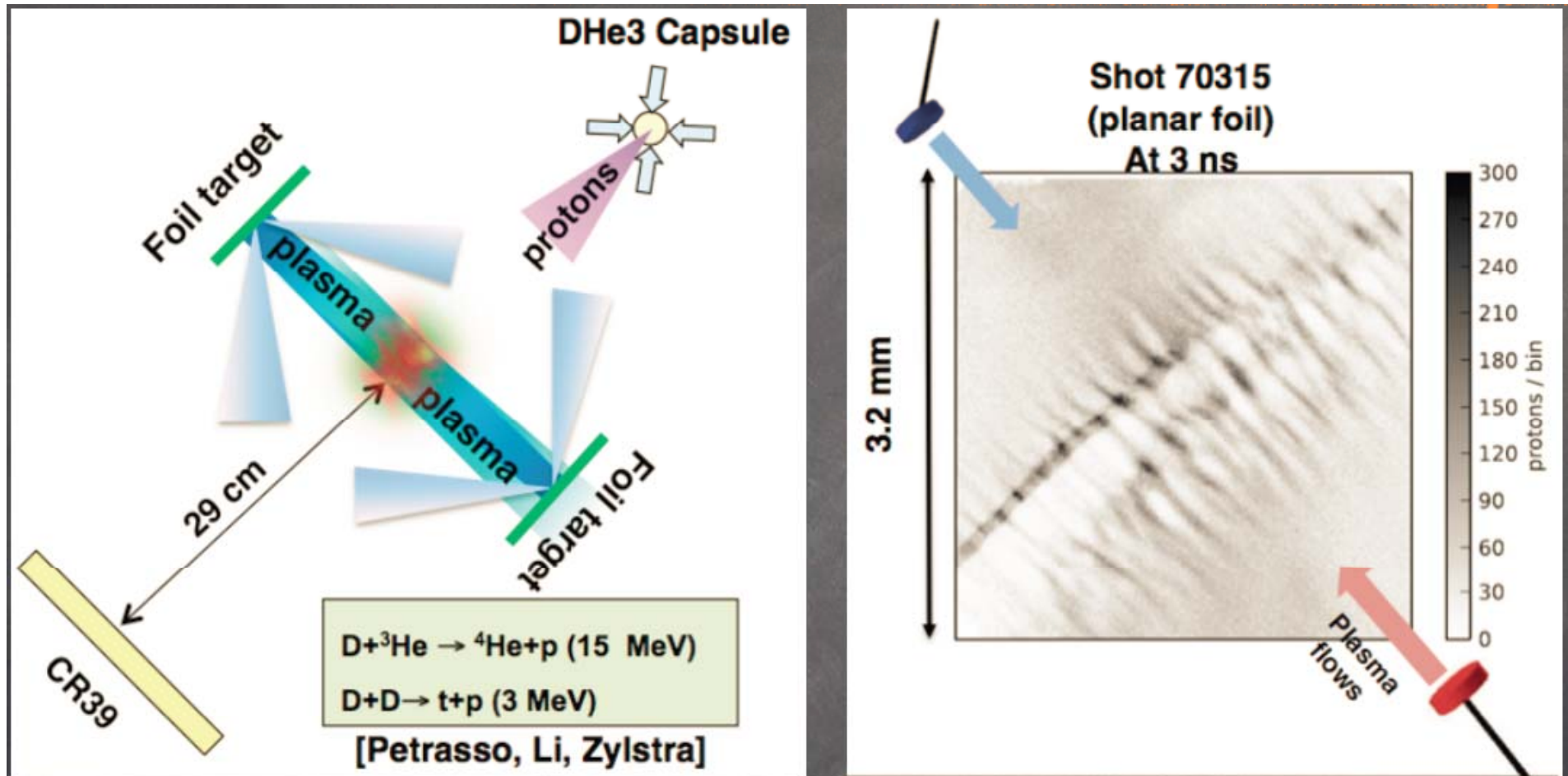


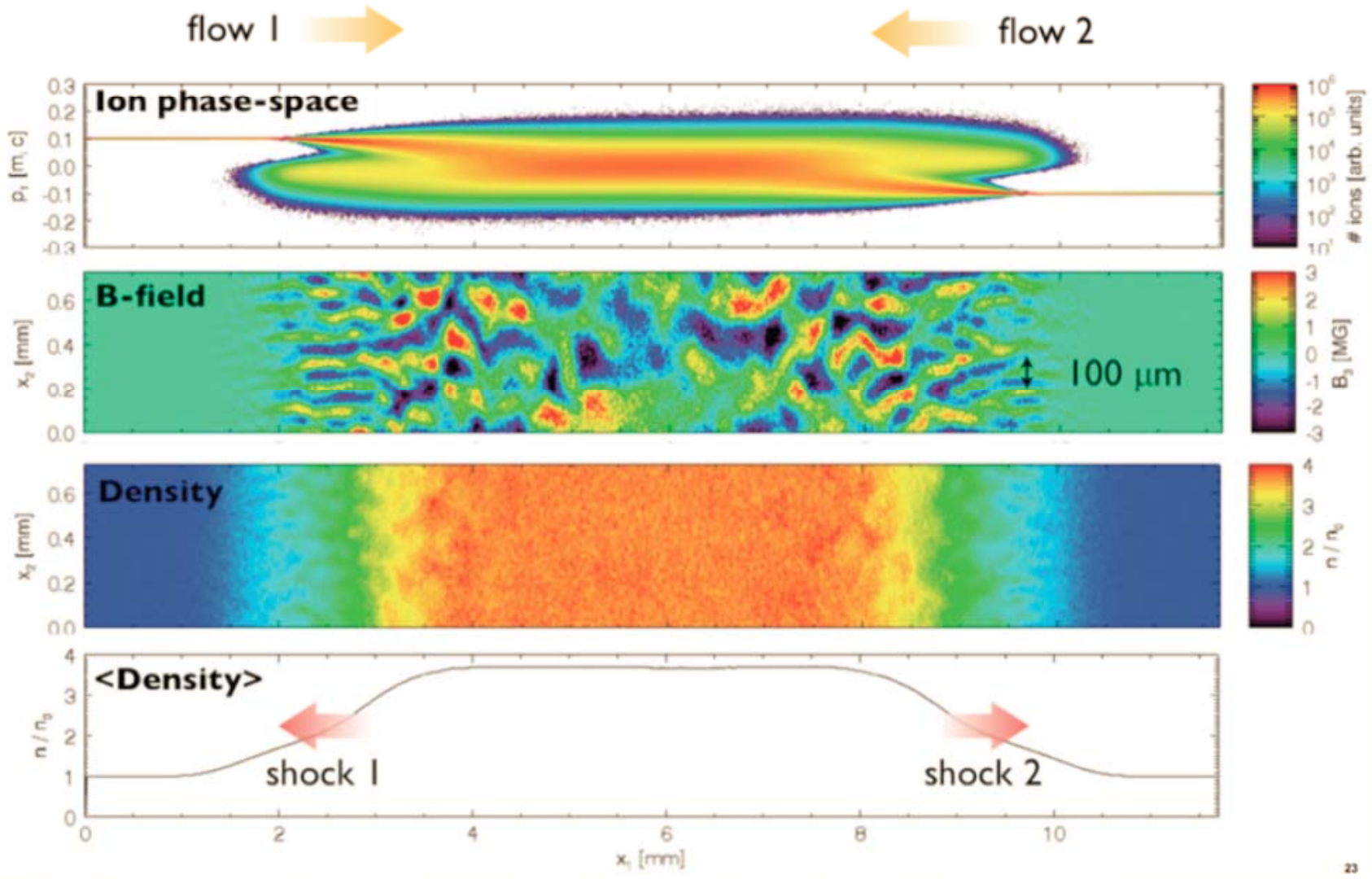
Figure 26. Typical plasma distribution (as a background) and magnetic field lines (cross section) in the vicinity of the current sheet formed in the force lines reconnection region (MRX facility, Princeton, www.pppl.gov)

Yoo J et al. *Phys. Rev. Lett.* **113** 095002 (2014), Ji H et al. *Phys. Rev. Lett.* **92** 115001 (2004)

Collision of laser collisionless plasma jets



- First clearly seen filamentation from DHe3 capsule implosion protons. Later confirmed that same filamentation is seen with EP protons on Omega

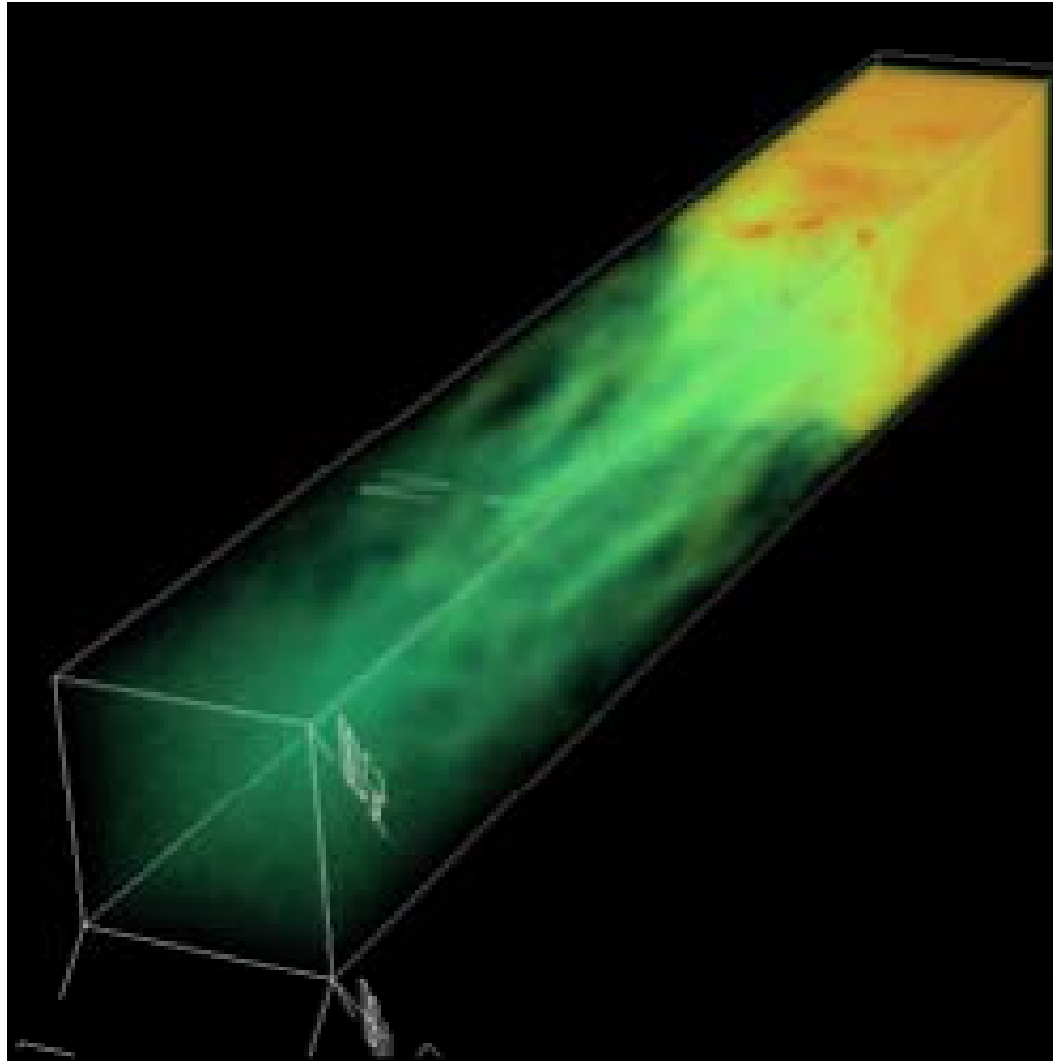


PIC simulation with OSIRIS code (Fiuza)

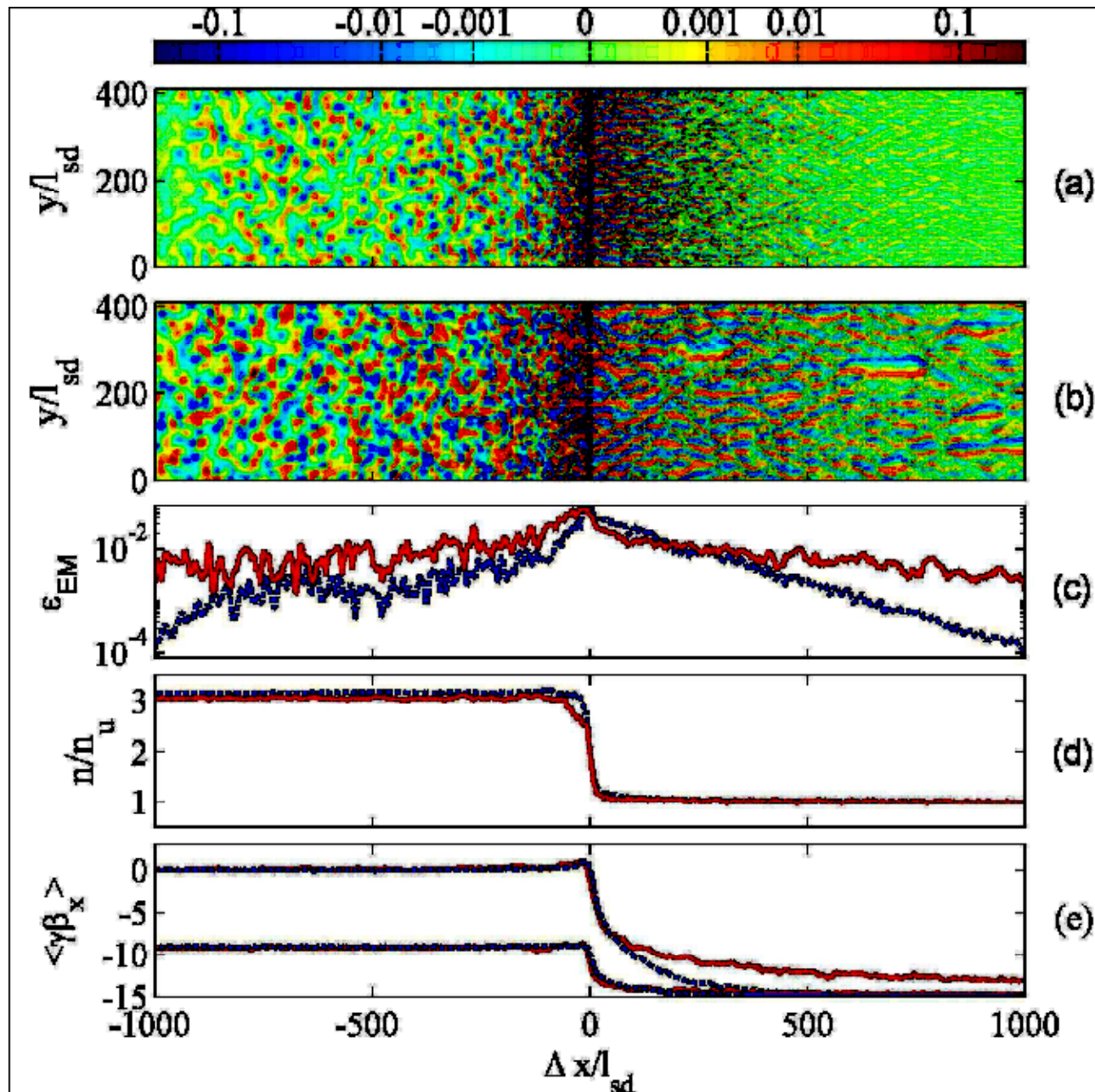
Higher density allows to have > 300 ion skin depths between targets.

Current structures in relativistic collisionless shocks

(Numerical simulation, A.Spitkovsky, 2006)

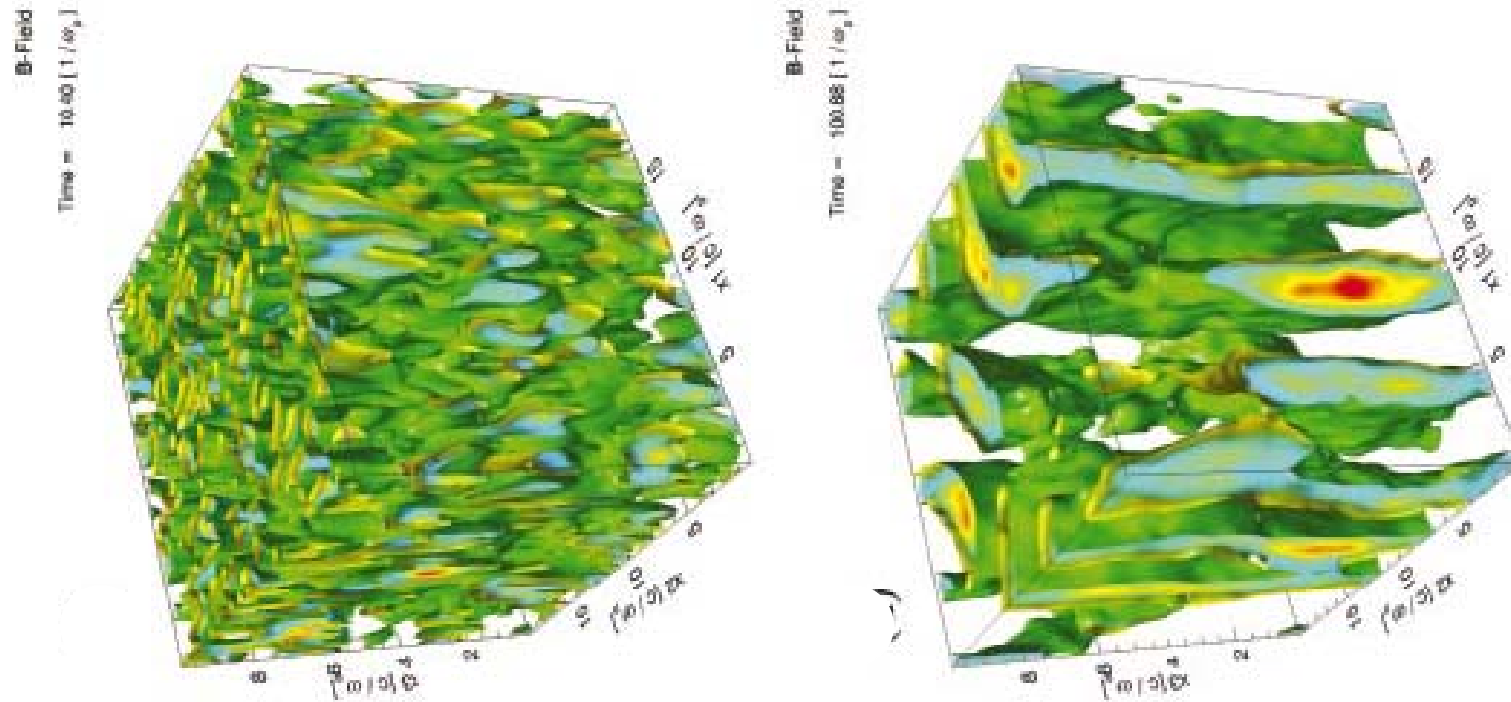


Collisionless shock wave in e^-e^+ plasma



Keshet, Katz,
Spitkovsky,
Waxman
(2008)

3D Weibel instability in $e^- - e^+$ plasma



Magnetic field energy density for values of 15% of the maximum energy density. Results are shown slightly before saturation and in the quasi-static stage ($\epsilon_B \sim 1\%$).

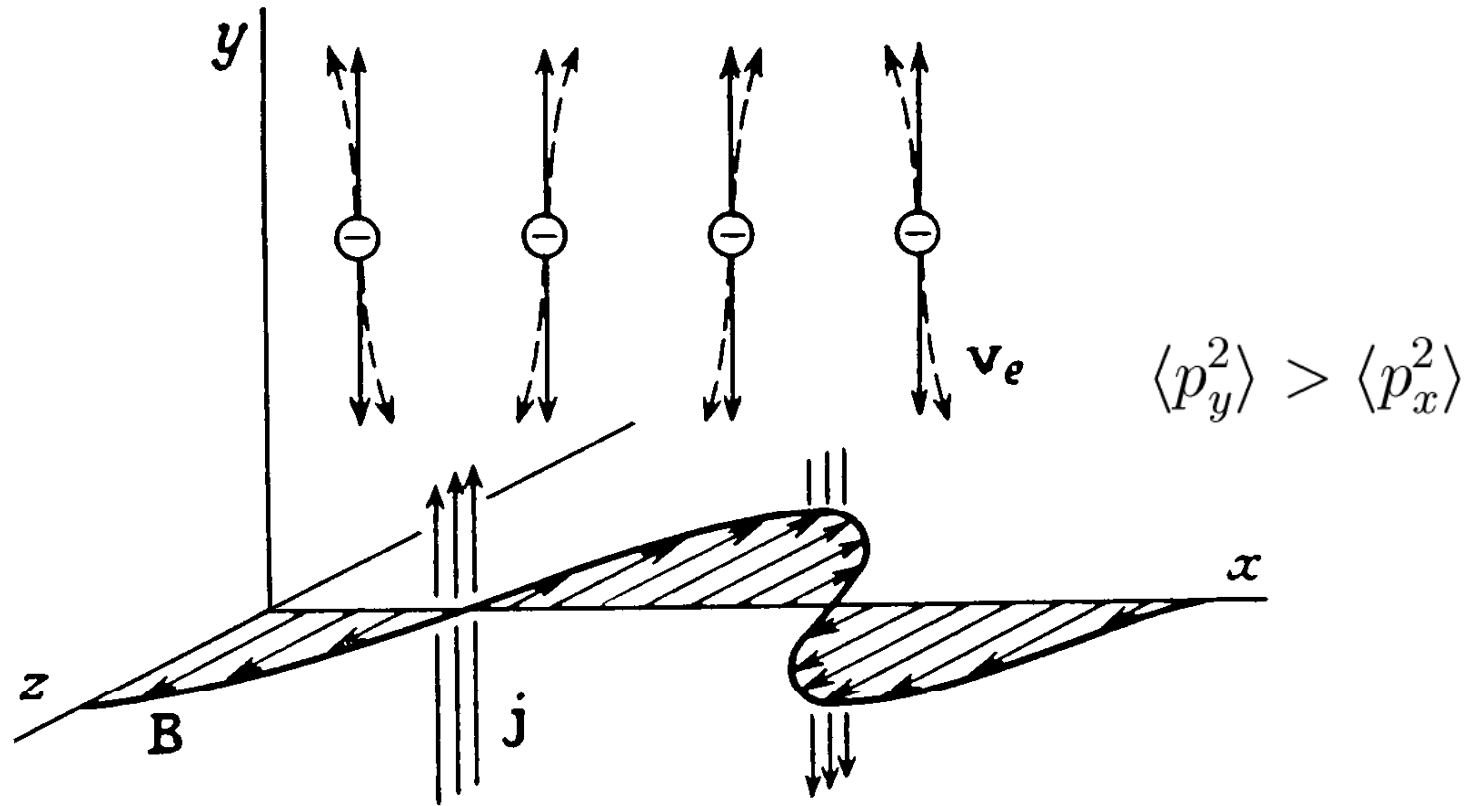
Fonseca, Silva et al (2003).

Numerical simulations of magnetic structure formation

Particle-in-cell experiments in 2D and 3D

- A. Pukhov, Rep. Prog. Phys. **66**, 47 (2003).
- L. Silva *et al*, ApJ **596**, L121 (2003).
- F. Califano, D.D. Sarto, F. Pegoraro, PRL **96**, 105008 (2006).
- K.-I. Nishikawa, C.B. Hededal *et al.*, ApJ **642**, n. 2, 1267 (2006).
- T.N. Kato, Phys. Plasmas **12**, 080705 (2005).
- A. Spitkovsky, ApJ **673**, 1, L39 (2008); U. Keshet *et al.*, ApJ **693**, L127 (2009); A. Spitkovsky, L. Sironi, ApJ **698.2** (2009).
- Haugbolle, ApJ Lett. **739**, L42 (2011).
- H.-S. Park, D.D. Ryutov, J.S. Ross, High Energy Density Physics **8**, 38 (2012); **9**, 192 (2013).
- E.V. Derishev, M.A. Garasev, MNRAS **461**, 641 (2016).

Weibel instability and its saturation



Highly anisotropic velocity distributions are unstable

$$\max(\text{Im } \omega) \sim \omega_p / \sqrt{\gamma}$$

Instability condition

$$\omega = 0, \quad k \neq 0 \Rightarrow$$

$$\sum_{\alpha} \frac{e_{\alpha}^2}{m_{\alpha}} \int \left[1 + \frac{p_y^2 k^2}{(\mathbf{k}\mathbf{p})^2} \right] \frac{f_{0\alpha}}{\gamma_a} d^3\mathbf{p} < 0$$

$$\langle p_y^2 \rangle > \langle p_x^2 \rangle$$

Saturated magnetic field

General case ($\Gamma \sim kv$, or $\Gamma \gg kv$)

$$B_{sat} \sim \frac{mc\gamma\Gamma}{|e|} \left(\frac{\Gamma}{kv} + \frac{kv}{\Gamma} \right)^{-1}$$

Weak anisotropy or small growth rate ($\Gamma \ll kv$)

$$\frac{B_{sat}^2}{8\pi} \sim \frac{1}{2} N\gamma m v^2 \left(\frac{k^2 c^2}{\omega_p^2 / \gamma} \right) \left(\frac{\Gamma^3}{k^3 v^3} \right)$$

Nonlinear evolution

- Quasineutrality
- Magnetic energy can approach equipartition
- Current filaments merge due to Ampère force
- Spatial scale increases
- Slow magnetic field decay
- Metastable configurations

Equal treatment of relativistic and non-relativistic plasma

$$\langle B^2 / 8\pi \rangle \lesssim \langle (\gamma - 1) N m c^2 \rangle$$

Analytical generalizations of Harris' solution, mainly based on modified Maxwellian distributions

- Harris, 1962
- Fadeev et al., 1965
- Hoh, 1966
- Alpers, 1969
- Kan, 1973
- Channell, 1976
- Attico and Pegoraro, 1999
- Manakova et al., 2000
- Brittnacher and Whipple, 2002
- Schindler and Birn, 2002
- Mottez, 2003
- Yoon and Lui, 2005
- Zelenyi et al., 2006
- Suzuki and Shigeyama, 2008
- Janaki, Dasgupta and Yoon, 2012, 2014

and also on kappa distributions

$$f^{\kappa}(\vec{v}) = \frac{n}{2\pi(\kappa v_{\kappa}^2)^{3/2}} \frac{\Gamma(\kappa + 1)}{\Gamma(\kappa - \frac{1}{2})\Gamma(\frac{3}{2})} \left(1 + \frac{v^2}{\kappa v_{\kappa}^2}\right)^{-(\kappa+1)}$$

- Fu, Hau, 2005
- Yoon, Lui, 2006
- Vasko, 2013

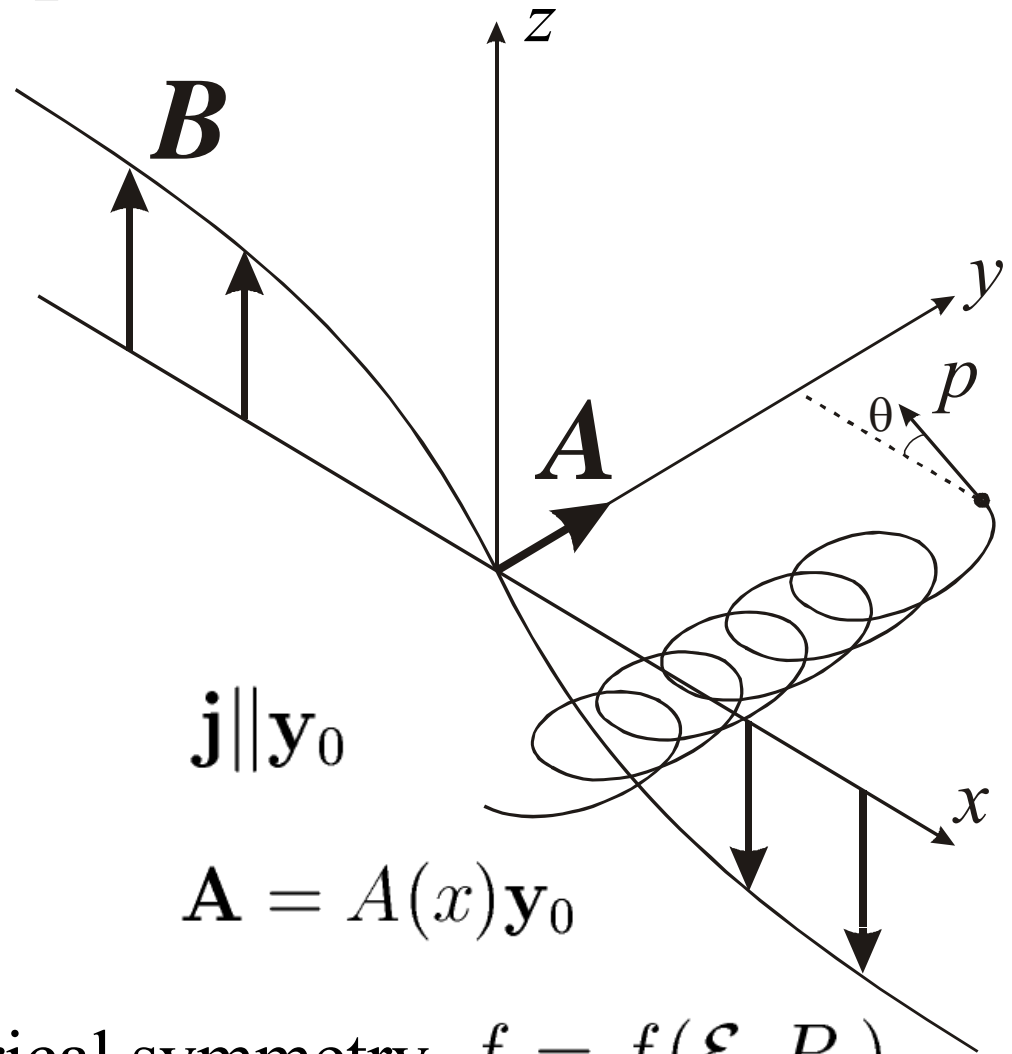
Integrals of particle motion

$$\mathcal{E} = c\sqrt{m^2c^2 + p^2}$$

$$P_y = p_y + \frac{e}{c}A_y$$

$$p_z$$

$$f = f(\mathcal{E}, P_y, p_z)$$



Special case of PDF: cylindrical symmetry, $f = f(\mathcal{E}, P_y)$

1D charged current structures with sheared magnetic field

$$\frac{d^2 \varphi}{dx^2} = -4\pi \sum_{\alpha} e_{\alpha} \iiint f_{\alpha} \left(\gamma_{\alpha} m_{\alpha} c^2 + e_{\alpha} \varphi, p_y + \frac{e_{\alpha} A_y}{c}, p_z + \frac{e_{\alpha} A_z}{c} \right) d^3 \mathbf{p}$$

$$\frac{d^2 A_{y,z}}{dx^2} = -\frac{4\pi}{c} \sum_{\alpha} \iiint \frac{e_{\alpha} p_{y,z}}{m_{\alpha} \gamma_{\alpha}} f_{\alpha} \left(\gamma_{\alpha} m_{\alpha} c^2 + e_{\alpha} \varphi, p_y + \frac{e_{\alpha} A_y}{c}, p_z + \frac{e_{\alpha} A_z}{c} \right) d^3 \mathbf{p}$$

$$\text{i.e., } \frac{d^2 A_{y,z}}{dx^2} = -\frac{4\pi}{c} \frac{dP_{xx}}{dA_{y,z}}$$

$$\frac{d^2 \varphi}{dx^2} = 4\pi \frac{dP_{xx}}{d\varphi}$$

component of the pressure tensor

$$P_{xx} = \sum_{\alpha} N_{\alpha} \iiint f_{\alpha} p_x v_x d^3 \mathbf{p}$$

Charge

- Morozov, Soloviev, 1961
- Yoon, Lui, 2004, 2006
- Cremaschini et al, 2010, 2012
- Tautz, Lerche, 2011

Shear

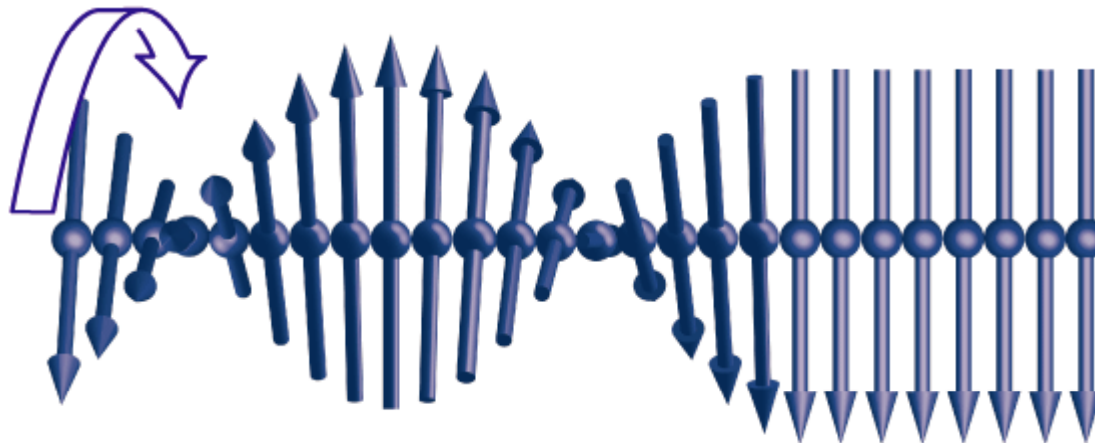
- Channell, 1976
- Mahajan, 2000
- Neukirch, 2009
- Ghosh, Janaki, Dasgupta, 2014

1D current sheets with sheared magnetic field

$$\varphi \equiv 0 \quad \frac{B_y^2 + B_z^2}{8\pi} + P_{xx} = \text{const}$$

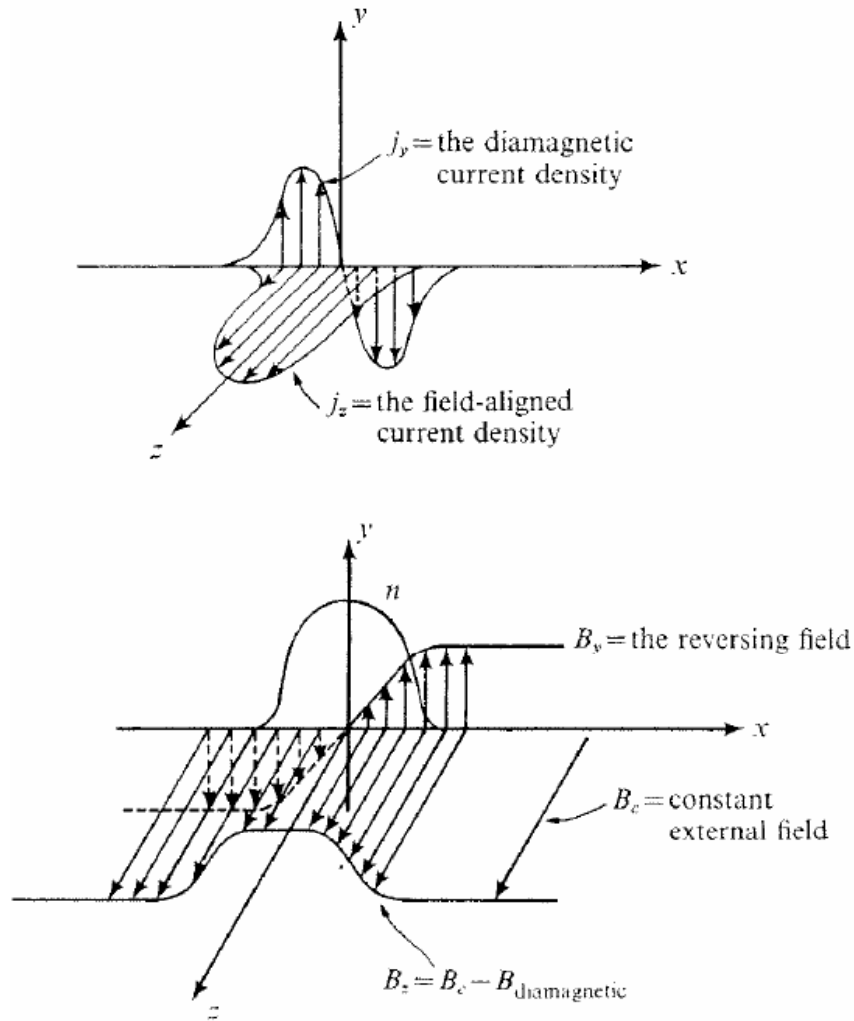
$$f_\alpha = f_\alpha^{(y)} \left(\gamma_\alpha m_\alpha c^2, p_y + \frac{e_\alpha A_y}{c} \right) + f_\alpha^{(z)} \left(\gamma_\alpha m_\alpha c^2, p_z + \frac{e_\alpha A_z}{c} \right)$$

$$U^{(y,z)}(A_{y,z}) = 4\pi P_{xx}^{(y,z)} + \text{const}$$

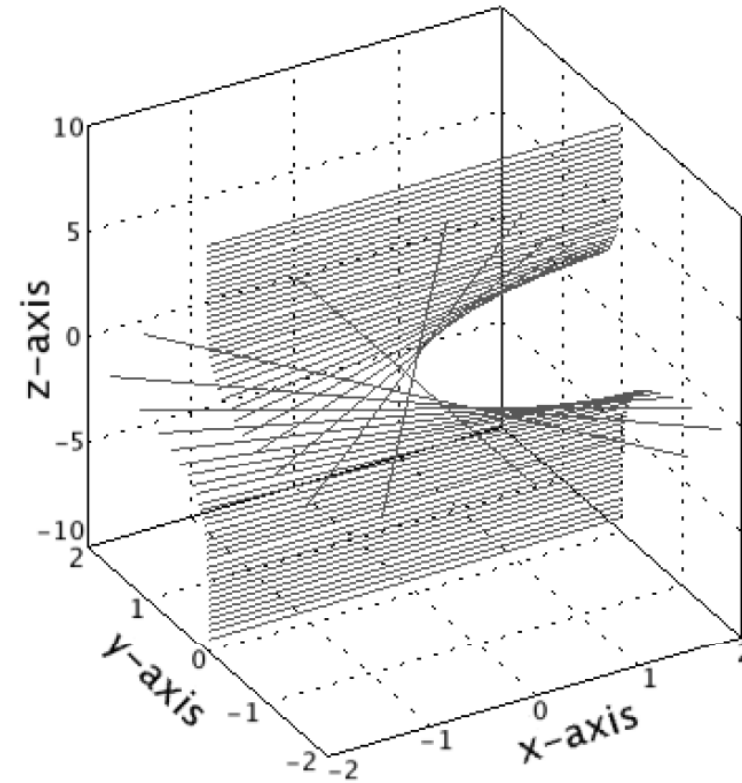


1D superposition of two current sheets with orthogonal currents and cylindrically symmetrical particle distributions $f^{(x)}, f^{(y)}$

Harris + Nicholson sheets as obtained by Kan, 1972



Force-free Harris sheet as described by Neukirch, 2011



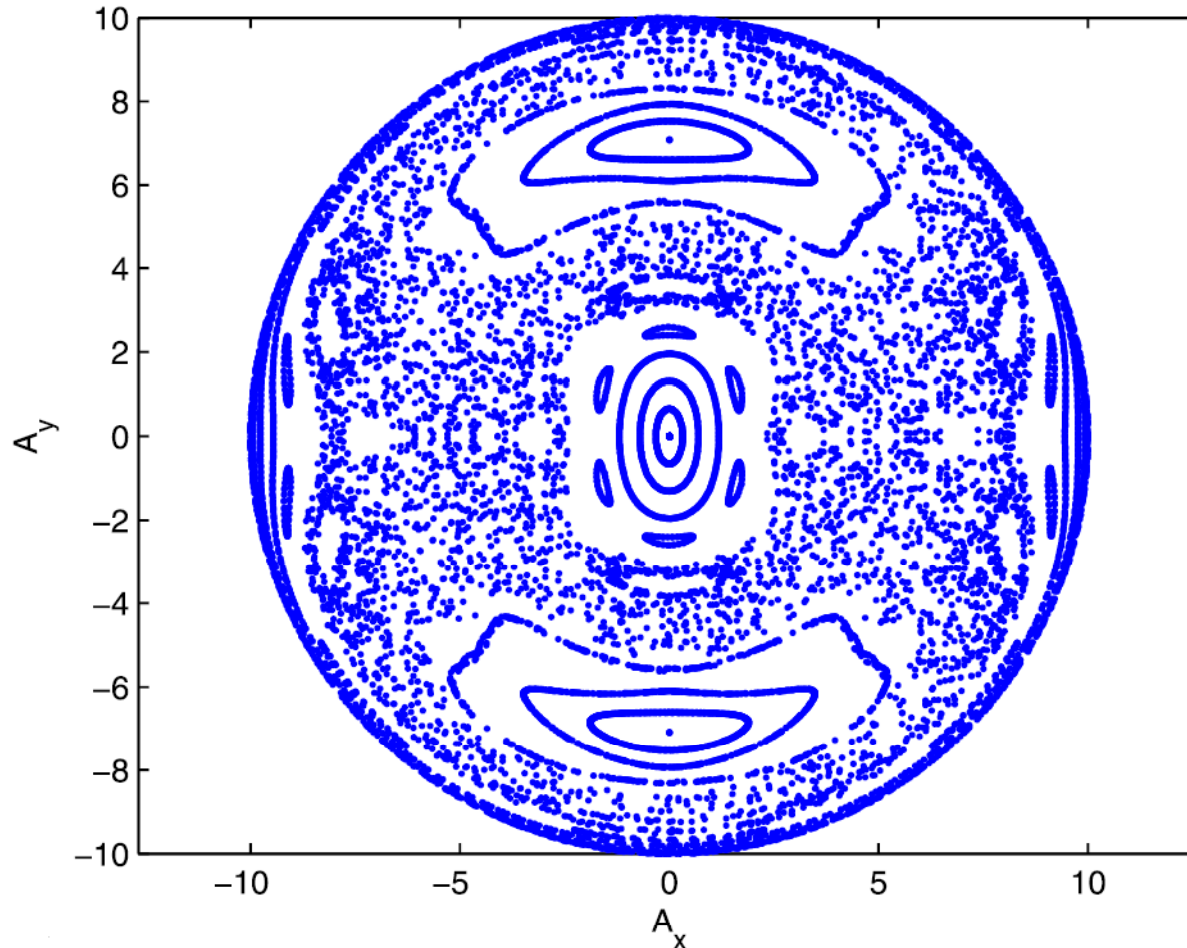
$$A_{x,ffhs} = 2B_0L \tan^{-1}(e^{z/L}),$$

$$A_{y,ffhs} = -B_0L \ln [\cosh(z/L)]$$

$$f_{s,ffhs} = \frac{n_{0s}}{(\sqrt{2\pi}v_{th,s})^3} \exp(-\beta_s H_s) [a_s \cos(\beta_s u_{xs} p_{xs}) + \exp(\beta_s u_{ys} p_{ys}) + b_s]$$

1D current sheets with sheared chaotic magnetic fields

$$\frac{d^2 A_{y,z}}{dx^2} + \beta_1 A_{y,z} + \beta_3 A_{y,z} A_{z,y}^2 = 0$$



Surface of section plots in the A_x - A_y plane at $B_y=0$ with parameter $(r_H / L)^2 = 20$, and energy $E = 50$. [Ghosh et al. (2014)]

Towards finding an analytical solution for arbitrary PDF Grad-Shafranov equation and PDF decomposition 1

$$f_{\alpha}(P_y, \mathcal{E}) = \sum_j f_{\alpha j}(\mathcal{E}) \left(\frac{P_y}{m_{\alpha} c} \right)^j$$

$$\frac{\partial^2 A}{\partial x^2} + \frac{\partial^2 A}{\partial z^2} = -\frac{\partial U}{\partial A}$$

$$U = -8\pi^2 m_{\alpha}^2 c^3 \sum_{j=0}^{\infty} \int f_{\alpha j}(\mathcal{E}) Q_j \left(\frac{e_{\alpha} A}{m_{\alpha} c^2}, \frac{p}{m_{\alpha} c} \right) \frac{p}{\gamma} dp$$

$$Q_j(A, p) = \frac{(A + p)^{j+2} [p(j + 2) - A] + (A - p)^{j+2} [p(j + 2) + A]}{(j + 1)(j + 2)(j + 3)}$$

In practice, a finite number, d , of terms in the sum \sum is considered.

Grad-Shafranov equation and PDF decomposition 2

$$f_\alpha(\mathcal{E}, P_y) = \exp\left(\zeta_\alpha \frac{P_y}{m_\alpha c}\right) \sum_{i=0}^d f_{\alpha i}(\mathcal{E}) \left(\frac{P_y}{m_\alpha c}\right)^i$$

$$\frac{\partial^2 A}{\partial x^2} + \frac{\partial^2 A}{\partial z^2} = -\frac{dU}{dA}$$

$$U = \sum_{\alpha} \exp\left(\frac{\zeta_\alpha e_\alpha A}{m_\alpha c^2}\right) \sum_{j=0}^d A^j \left\{ \sum_{i=j}^d \int f_{\alpha i}(\mathcal{E}) [Y_{\alpha ij}(p) - Y_{\alpha ij}(-p)] dp \right\}$$

$$Y_{\alpha ij}(p) = \exp\left(\frac{\zeta_\alpha p}{m_\alpha c}\right) \frac{4\pi^2 e_\alpha^j p (-\zeta_\alpha)^{j-i-3} i!}{\gamma_\alpha m_\alpha^{j-2} c^{2j-3} j! (i-j)!}$$

$$\cdot (\exp(q)\Gamma(i-j+1, q) [(i-j+2)(i-j+1) - q^2] + q^{i-j+2} + (i-j+2)q^{i-j+1})$$

$$q = -\zeta_\alpha p / m_\alpha c \quad \exp(q)\Gamma(i-j+1, q) - \text{polynomial of order } i-j$$

Harmonic solution of nonlinear problem (d=2)

$$\Delta_{\perp} A + k^2 A = 0$$

$$k^2 = \frac{32\pi^2}{3} \int f_2(\mathcal{E}) \frac{e^2 p^4}{m^3 c^4 \gamma} dp$$

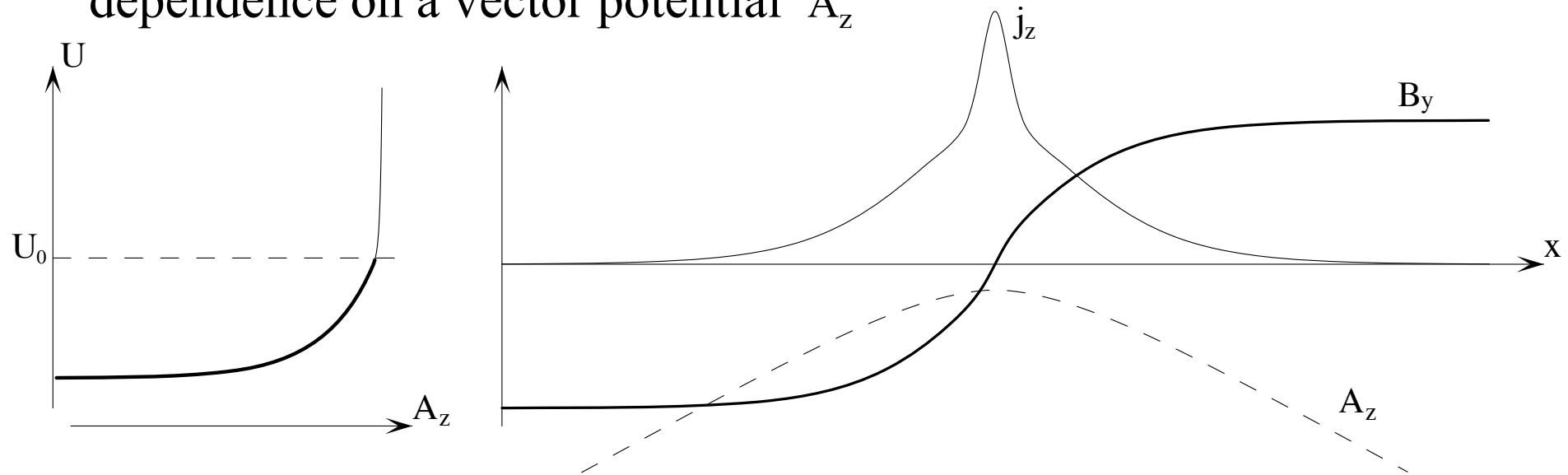
$$A = A_{\max} \cos(kx)$$

$$\frac{\langle W_B \rangle}{\langle W_e \rangle} = \frac{1}{3} \frac{\int f_2(\mathcal{E}) (v^2/c^2) \gamma p^2 dp}{\int f_2(\mathcal{E}) \gamma p^2 dp + \frac{2}{3} \int f_2(\mathcal{E}) p^2 c^2 \gamma p^2 dp / e^2 A_{\max}^2}$$

$$\frac{\langle W_B \rangle}{\langle W_e \rangle} = \frac{1}{3} \cdot \frac{1}{1 + \frac{2}{3} \frac{p^2 c^2}{e^2 A_{\max}^2}} \cdot \frac{v^2}{c^2} < \frac{1}{3}$$

Double-scale current sheet

PDF is enriched with an exponential fraction which has a fast dependence on a vector potential A_z

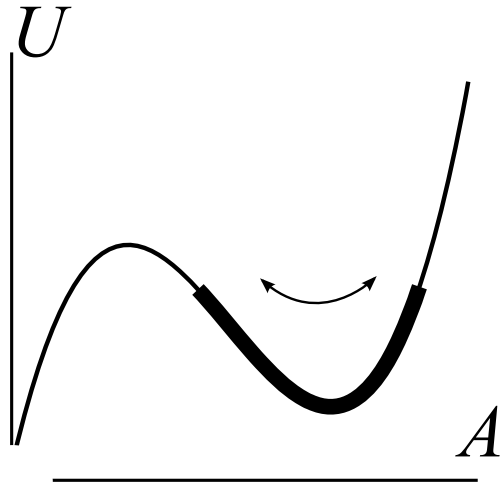


- Ratio of currents in the inner and outer layers are arbitrary.
- Particle species in two layers may be different.
- A thin layer is similar to the Harris sheet (PDF profile is unique everywhere), a thick layer is an arbitrary symmetric one.

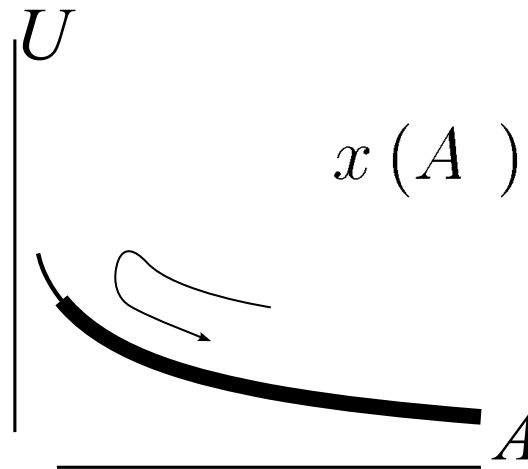
Grad-Shafranov potential and variety of solutions $A = A(x)$

$$\frac{\partial^2 A}{\partial x^2} = -\frac{dU}{dA}$$

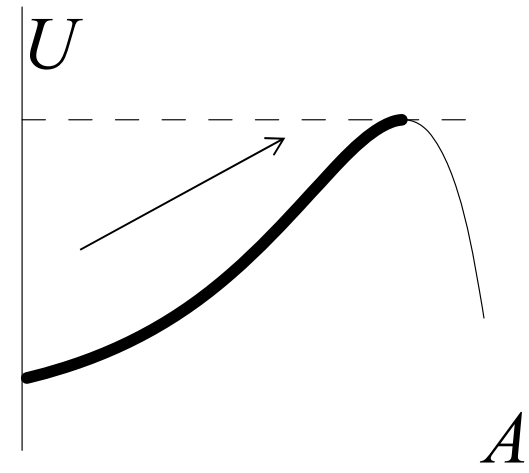
Periodic sheets



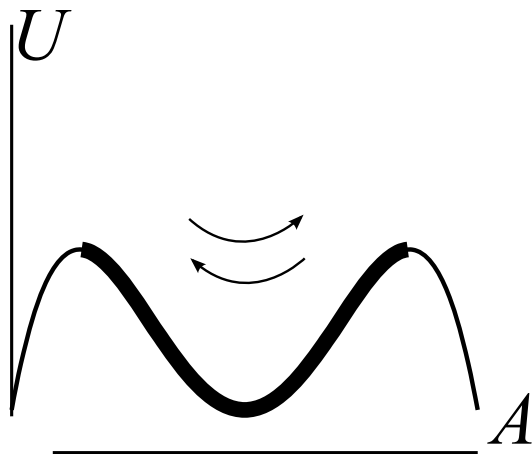
Isolated sheets ($I \neq 0$)



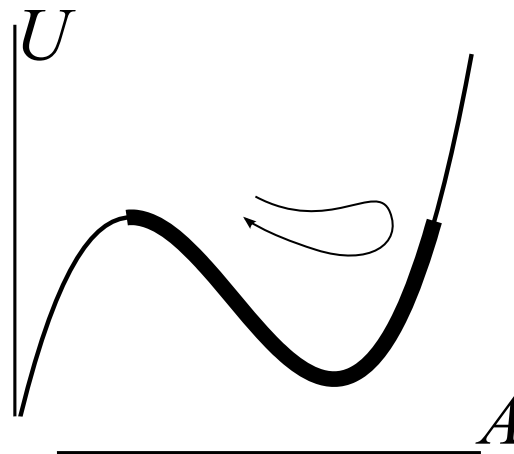
$$x(A) = \int_{A_y}^A \frac{dA'}{\sqrt{2U_0 - 2U(A')}}$$



Boundary sheets



Double sheets



Symmetrical shielded sheets

Classification of the current sheets

There are three general situations (in the absence of an external magnetic field): The magnetic field B_y with x varying from $-\infty$ to $+\infty$ (i) alters sign any number of times, or (ii) changes it but once, or (iii) retains the same sign. The corresponding classification is studied in detail. It is summarized below.

(i) If the magnetic field alters sign more than once, the self-consistent current structure is a periodic one. The function $U(A_z)$ serves as a “potential well”, the $A_z(x)$ represents oscillations (generally nonlinear) between two certain points in this well. At those “turning points”, the magnetic field vanishes.

The profiles of the magnetic field with different signs of B_y between them are mirror images of each other. The current density, which is proportional to the derivative of B_y with respect to x , is symmetric relative to any plane of a zero magnetic field.

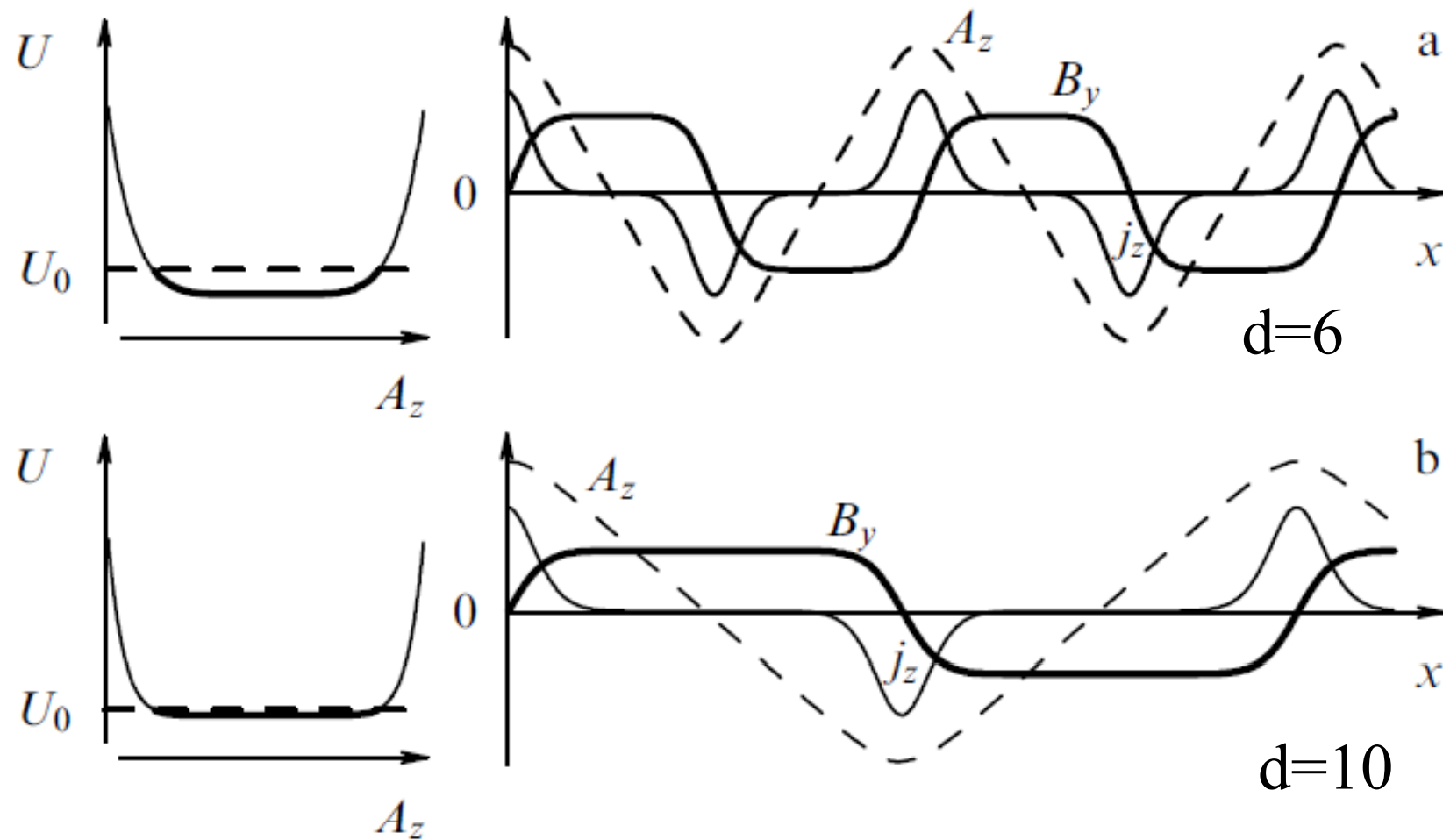


Figure 9. Profiles of the anharmonic Grad–Shafranov potential U and coordinate dependences of A_z , B_y , and j_z : (a) $U \propto A_z^6$, and (b) $U \propto A_z^{10}$.

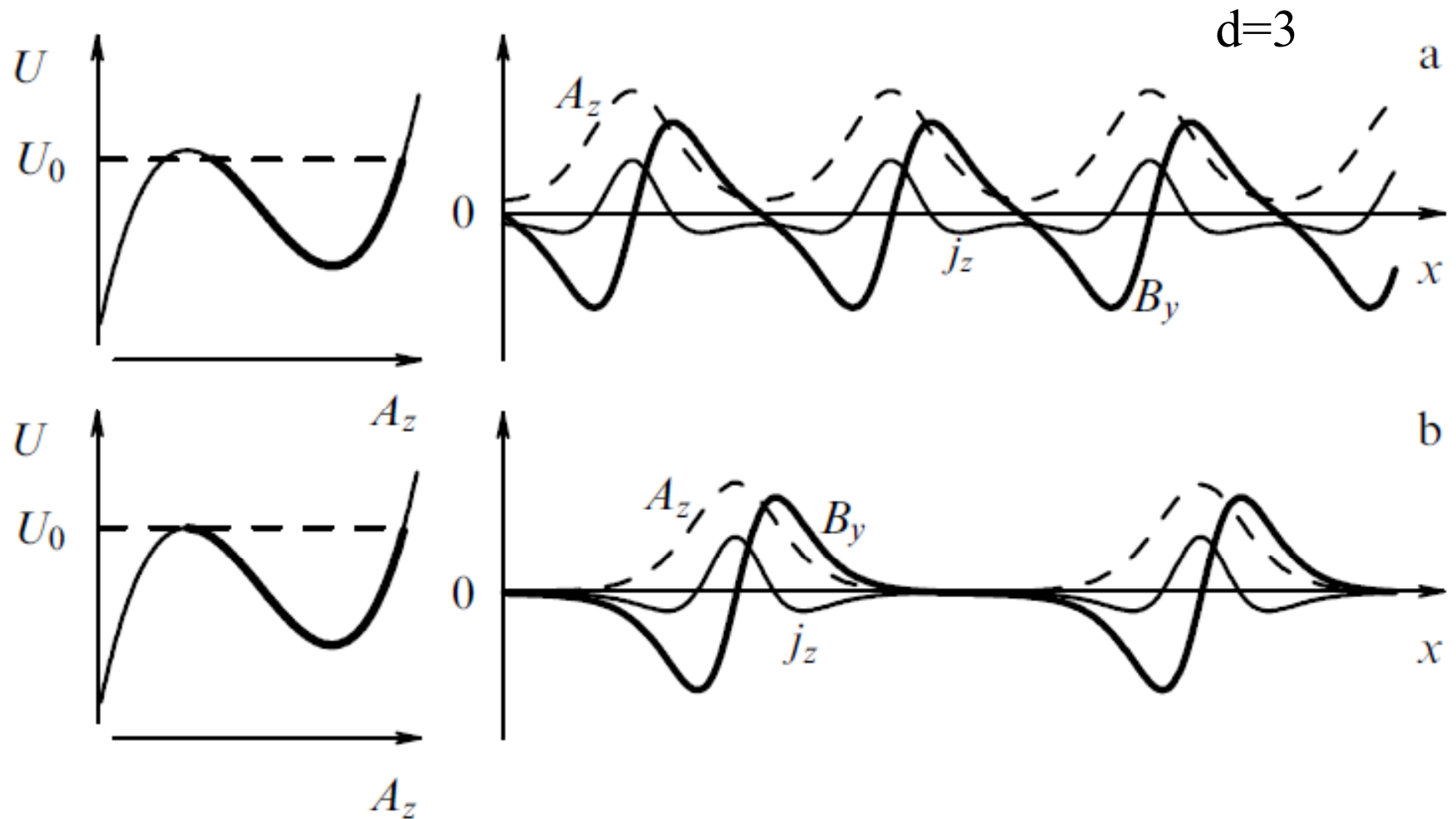


Figure 10. Typical profile of the anharmonic Grad–Shafranov potential (89) in the form of a cubic parabola and coordinate dependences of A_z , B_y , and j_z for the periodic solution at two different values of the first integral U_0 .

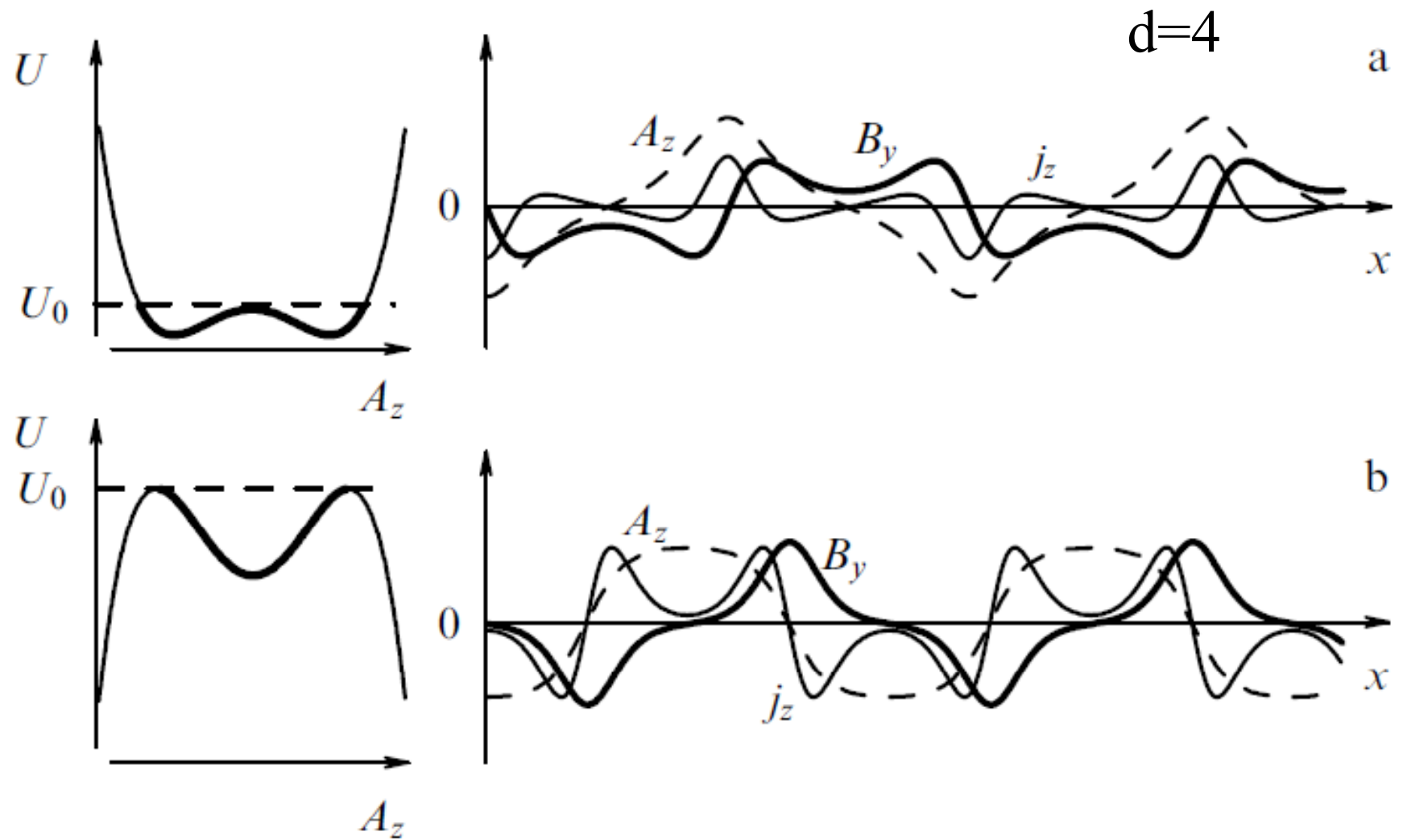


Figure 11. Variants of the profile of the Grad–Shafranov potential (89) in the form of a bi-quadratic parabola and coordinate dependences of A_z , B_y , and j_z for periodic solutions.

Example of PDF as a sum of two exponential terms

The respective Grad–Shafranov potential takes the form

$$U(A) = W_0 \cosh\left(\frac{A_z}{A_0}\right) - 2W_2 \cosh\left(\frac{A_z}{2A_0}\right) \quad (169)$$

and tends toward $+\infty$ as $A_z \rightarrow \pm\infty$, suggesting the existence of nonlinear periodic solutions. One of them can be written down in elementary functions:

$$A_z(x) = 4A_0 \operatorname{artanh}\left(\frac{\cos\left(\sqrt{(W_2 + 2W_0)}/A_0 x\right)}{\sqrt{1 + 2W_0/W_2}}\right), \quad (170)$$

$$B_y(x) = \frac{4\sqrt{A_0 W_2} \sin\left(\sqrt{(W_2 + 2W_0)}/A_0 x\right)}{1 - (W_2/(W_2 + 2W_0)) \cos^2\left(\sqrt{(W_2 + 2W_0)}/A_0 x\right)}. \quad (171)$$

When $W_2 \ll W_0$, solutions (170), (171) are close to a harmonic one; for $W_2 \gg W_0$, the solution is strongly anharmonic, because the argument of hyperbolic arctangent can be close to +1 or -1.

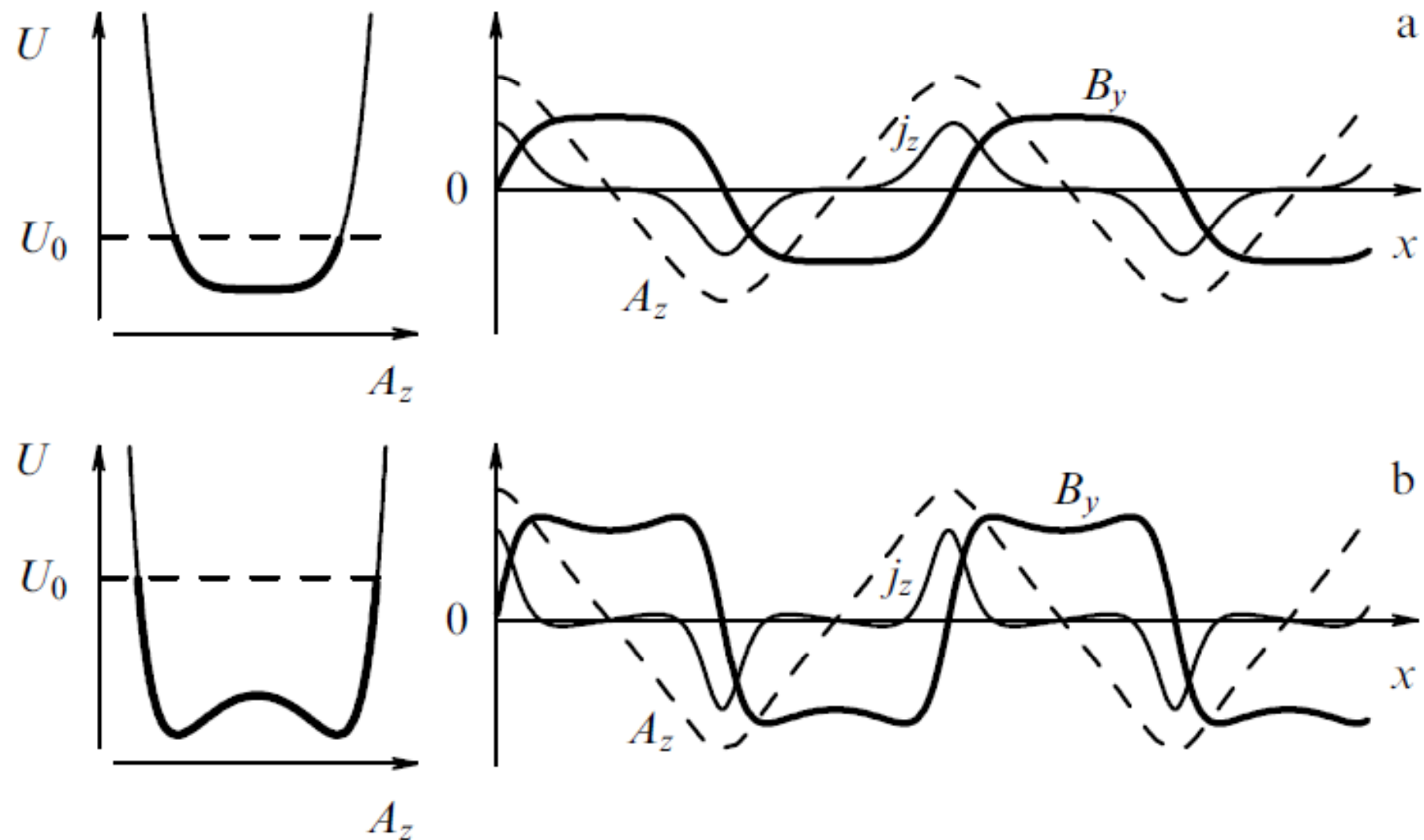
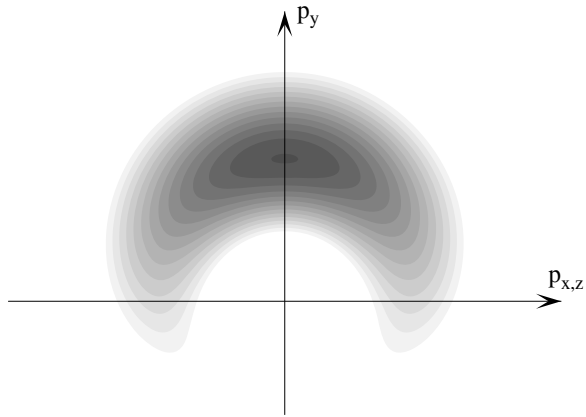


Figure 18. The profile of the Grad–Shafranov potential (169) and coordinate dependences of A_z , B_y , and j_z for the anharmonic periodic solutions (170), (171) at $W_2 = 2W_0$ (a), and $W_2 = 6W_0$ (b).

(ii) If the magnetic field changes its sign only once, the point where it vanishes can be chosen as the origin of x ; $B_y(x = 0) = 0$. In the neighborhood of $x = 0$, the magnetic field is antisymmetric, $B_y(x) = -B_y(-x)$, while the current density is symmetric. In a whole, contrary to the magnetic field, the current density either keeps a constant sign or alternates a sign any even number of times if the profile of $U(A_z)$ is non-monotonic and contains irregularities which, however, do not rise higher than $U_0 = U(A_z(x = 0))$ anywhere in the domain of A_z

The behavior of the magnetic field and the current density on the sheet's periphery at large values of x depends on the type of the Grad-Shafranov's potential profile, i.e., on the nature of the anisotropy of the particle distribution. The current is localized and its total value may be arbitrary (finite or close to zero).

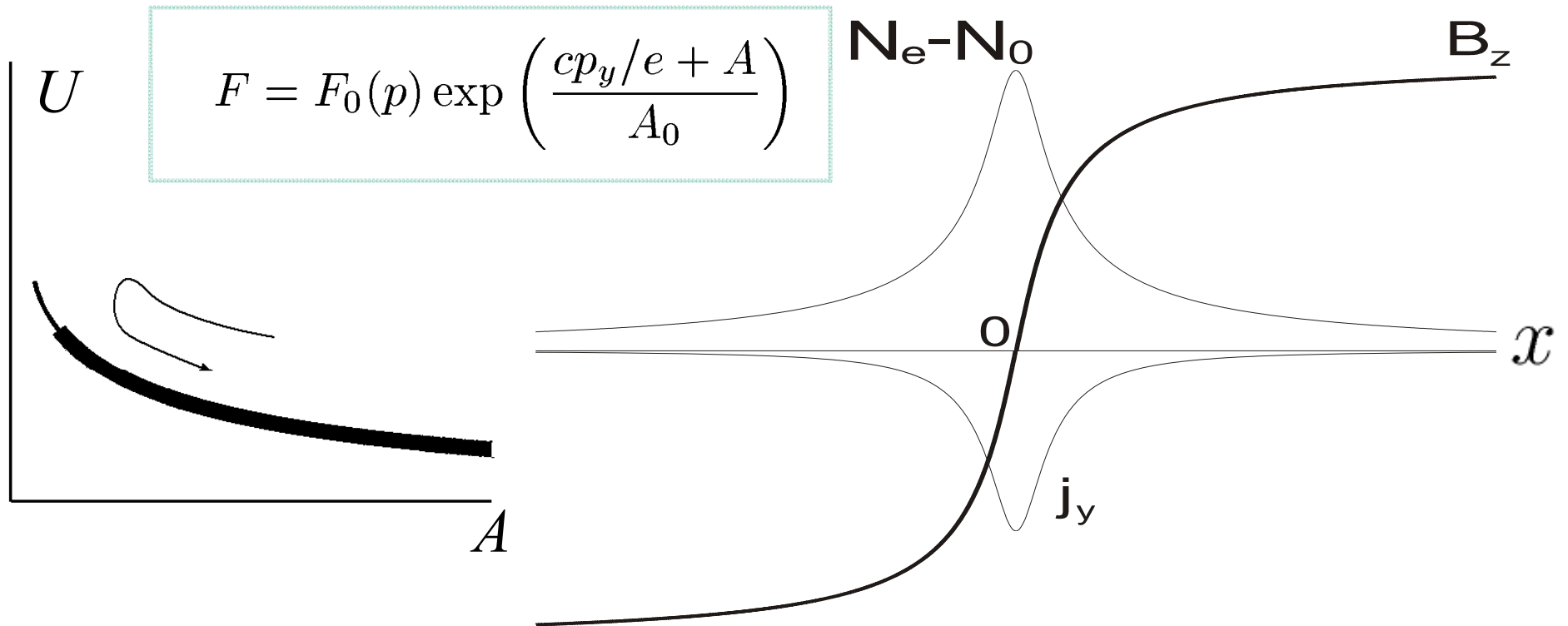
Generalized relativistic Harris current sheet ($d=0, \zeta \neq 0$)



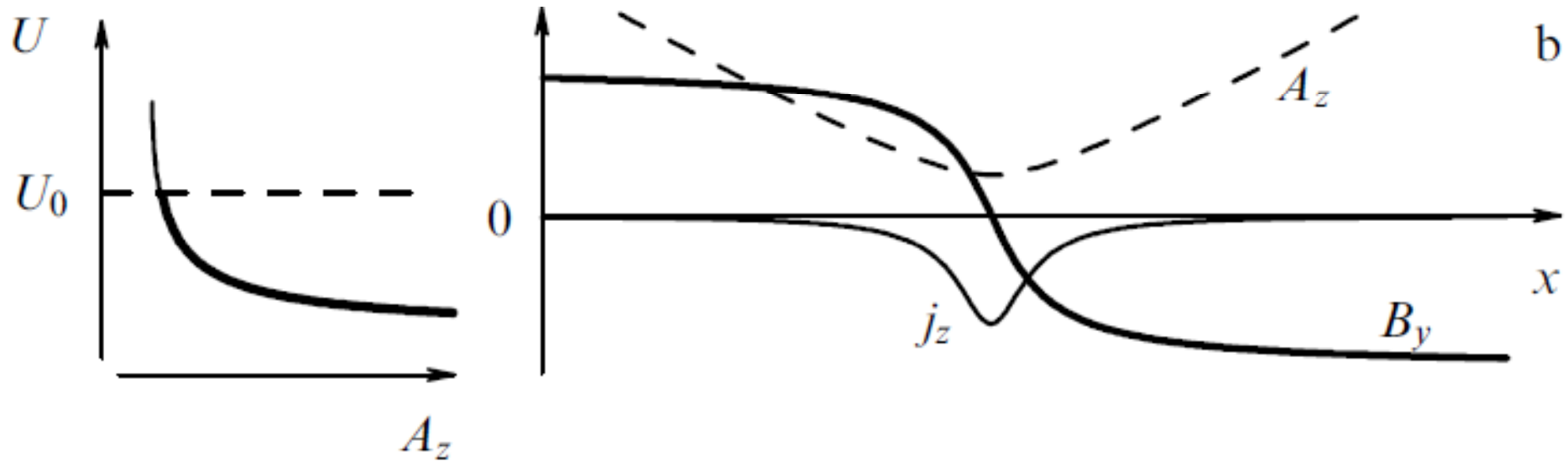
$$A = -2A_0 \ln \cosh \left(\sqrt{\alpha/2A_0} x \right) + \text{const}$$

$$B = -A_0 \sqrt{2\alpha/A_0} \tanh \left(\sqrt{\alpha/2A_0} x \right)$$

$$N_e - N_0 \propto \cosh^{-2} \left(\sqrt{\alpha/2A_0} x \right)$$



Localized current sheet with PDF of hyperbolic type ($d=-1$)

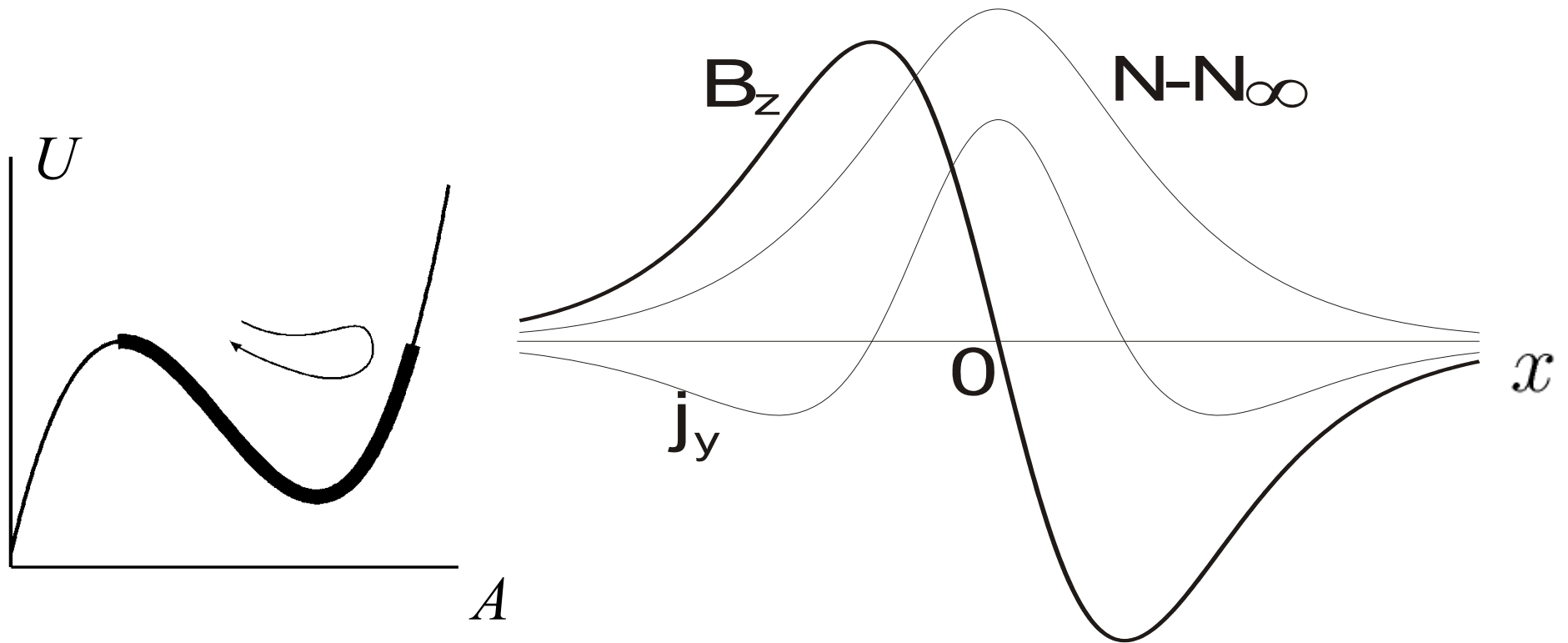


The solution is similar to the Harris one and is described by an equation

$$\frac{d^2 A_z}{dx^2} = -\frac{\partial}{\partial A_z} \left[8\pi^2 \sum_{\alpha} N_{\alpha} C_{\alpha, -1} e_{\alpha} A_z \left(1 - \sqrt{1 - \frac{c^2 p_0^2}{e_{\alpha}^2 A_z^2}} \right) \right]$$

Shielded current sheet (Taylor order $d=3$)

$$A = \frac{-mc^2 N_2}{eN_3} \text{ch}^{-2} \left(\sqrt{-\frac{\pi e^2 N_2 p_0^2}{c\gamma_0 (mc)^3}} x \right)$$



Shielded current sheet (Taylor order d=3)

$$A = \frac{-mc^2 N_2}{eN_3} \operatorname{ch}^{-2} \left(\sqrt{-\frac{\pi e^2 N_2 p_0^2}{c\gamma_0 (mc)^3}} x \right)$$

$$B_z = \frac{2m_e c^2 N_2}{e_e N_3} \sqrt{-\frac{\pi e_e^2 N_2 p_0^2}{\gamma_0 m_e^3 c^4}} \operatorname{ch}^{-2} \left(\sqrt{-\frac{\pi e_e^2 N_2 p_0^2}{\gamma_0 m_e^3 c^4}} x \right) \tanh \left(\sqrt{-\frac{\pi e_e^2 N_2 p_0^2}{\gamma_0 m_e^3 c^4}} x \right),$$

$$N_e = N_0 + \frac{N_2 p_0^2}{2m_e^2 c^2} + \frac{N_2 e_e^2 A_y^2}{m_e^2 c^4} + \frac{3N_3 p_0^2 e_e A_y}{4m_e^3 c^4} + \frac{N_3 e_e^3 A_y^3}{m_e^3 c^6},$$

$$j_y = \frac{-N_2^2 e_e c p_0^2}{N_3 \gamma_0 m_e^2 c^2} \operatorname{ch}^{-2} \left(\sqrt{-\frac{\pi e_e^2 N_2 p_0^2}{c\gamma_0 (m_e c)^3}} x \right) \left[1 - \frac{3}{2} \operatorname{ch}^{-2} \left(\sqrt{-\frac{\pi e_e^2 N_2 p_0^2}{c\gamma_0 (m_e c)^3}} x \right) \right],$$

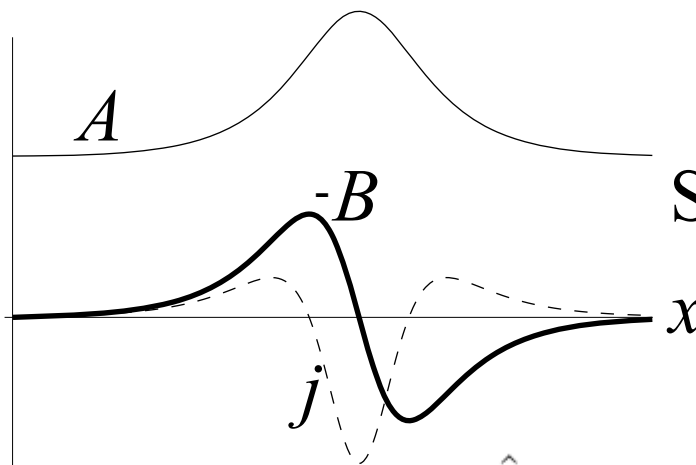
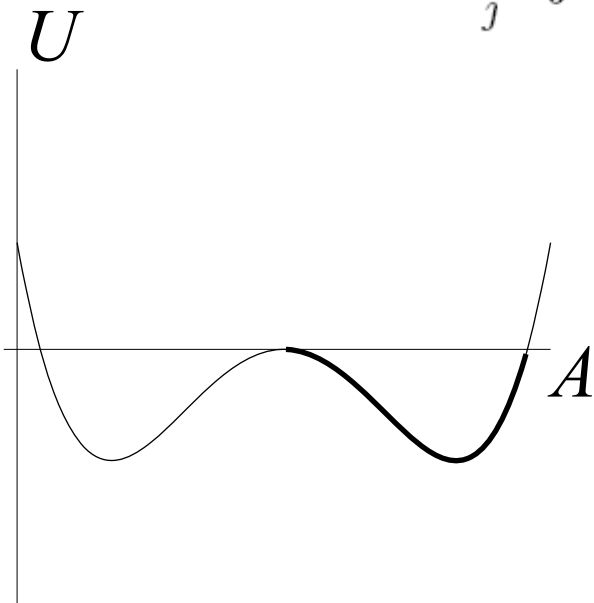
$$B_{z\max} = -\frac{4\sqrt{3} m_e c^2 N_2}{9 e_e N_3} \sqrt{-\frac{\pi e_e^2 N_2 p_0^2}{c\gamma_0 (m_e c)^3}}, \quad j_{y\max} = \frac{N_2^2 e_e c p_0^2}{2N_3 \gamma_0 (m_e c)^2}.$$

Shielded current sheet (Taylor order d=4)

$$A = (A_0/\sqrt{2})\sqrt{1 - \tanh^2 \left[\left(\sqrt{-U_0/A_0} \right) x \right]}$$

$$A_0^2 = S \left(-5 \sum_j \int \frac{\hat{F}_{j4}(p)}{m_j^5 c^8} e_j^4 p^4 \frac{dp}{\gamma_j} \right)^{-1}, \quad U_0 = \frac{16\pi^2}{15c} A_0^2 S$$

$$S = \sum_j \int \frac{[5\hat{F}_{j2}(p)m_j^2 c^2 + 6\hat{F}_{j4}(p)p^2]}{m_j^5 c^5} e_j^2 p^4 \frac{dp}{\gamma_j}$$



Stability conditions:

$$A_0^2 > 0$$

$$\mathbf{k} \perp \mathbf{z}, \mathbf{E} \parallel \mathbf{z}$$

$$\sum_j \int \frac{[5\hat{F}_{j2}(p) + 2\hat{F}_{j4}(p)p^2]}{m_j c} e_j^2 p^4 \frac{dp}{\gamma_i} > 0$$

$$\mathbf{k} \parallel \mathbf{z}, \mathbf{E} \perp \mathbf{z}$$

Kinetic features of self-consistent current structures

- $L \ll r_H$ - most of the particles are not magnetically trapped ($I \ll I_A$)
- $L \gg r_H$ - the current is formed mainly by trapped particles ($I \gg I_A$)

Degree of anisotropy is bounded by Taylor order d : $\frac{\langle p_y^2 \rangle}{\langle p_{\perp}^2 \rangle} < d$

Stability in the region where magnetic field vanishes:

Perturbations with $\mathbf{E} \perp \mathbf{y}$, $\mathbf{k} \parallel \mathbf{y}$ can be unstable for high enough $\frac{\langle p_{\perp}^2 \rangle}{\langle p_y^2 \rangle}$

For $d=4$ perturbations with $\mathbf{E} \perp \mathbf{y}$, $\mathbf{k} \parallel \mathbf{y}$ and with $\mathbf{k} \perp \mathbf{y}$, $\mathbf{E} \parallel \mathbf{y}$ are stable, if

$$\sum_{\alpha} \frac{e_{\alpha}^2}{m_{\alpha}} \left[5 \int \frac{f_{\alpha}^2(\mathcal{E})}{\gamma_a} \left(\frac{p}{mc} \right)^2 p^2 dp + 2 \int \frac{f_{\alpha}^4(\mathcal{E})}{\gamma_a} \left(\frac{p}{mc} \right)^4 p^2 dp \right] > 0$$

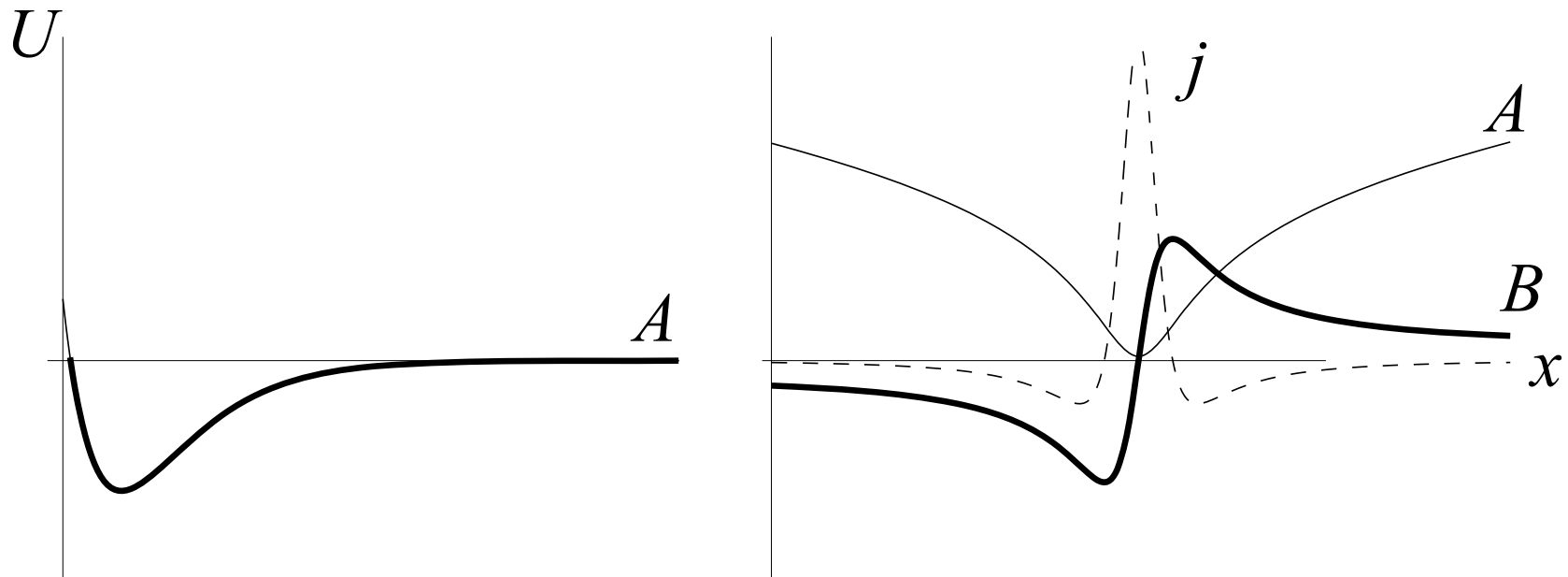
$$\sum_{\alpha} \frac{e_{\alpha}^2}{m_{\alpha}} \left[5 \int \frac{f_{\alpha}^2(\mathcal{E})}{\gamma_a} \left(\frac{p}{mc} \right)^2 p^2 dp + 6 \int \frac{f_{\alpha}^4(\mathcal{E})}{\gamma_a} \left(\frac{p}{mc} \right)^4 p^2 dp \right] < 0$$

Shielded current sheet (two exponent PDF)

$$U = -\frac{2U_0}{\alpha} \exp\left(-\frac{A}{A_0}\right) + \frac{2U_0}{\alpha^2} \exp\left(-\frac{2A}{A_0}\right)$$

$$A = -A_0 \ln \frac{\alpha}{1 + (U_0/A_0^2)x^2}$$

It resembles Harris sheet, but with decaying magnetic field $B \sim 1/x$



Partially or completely shielded current sheets

$$U(A_z) = W_0 \exp\left(\frac{A_z}{A_0}\right) + 2W_2 \exp\left(\frac{A_z}{2A_0}\right). \quad (137)$$

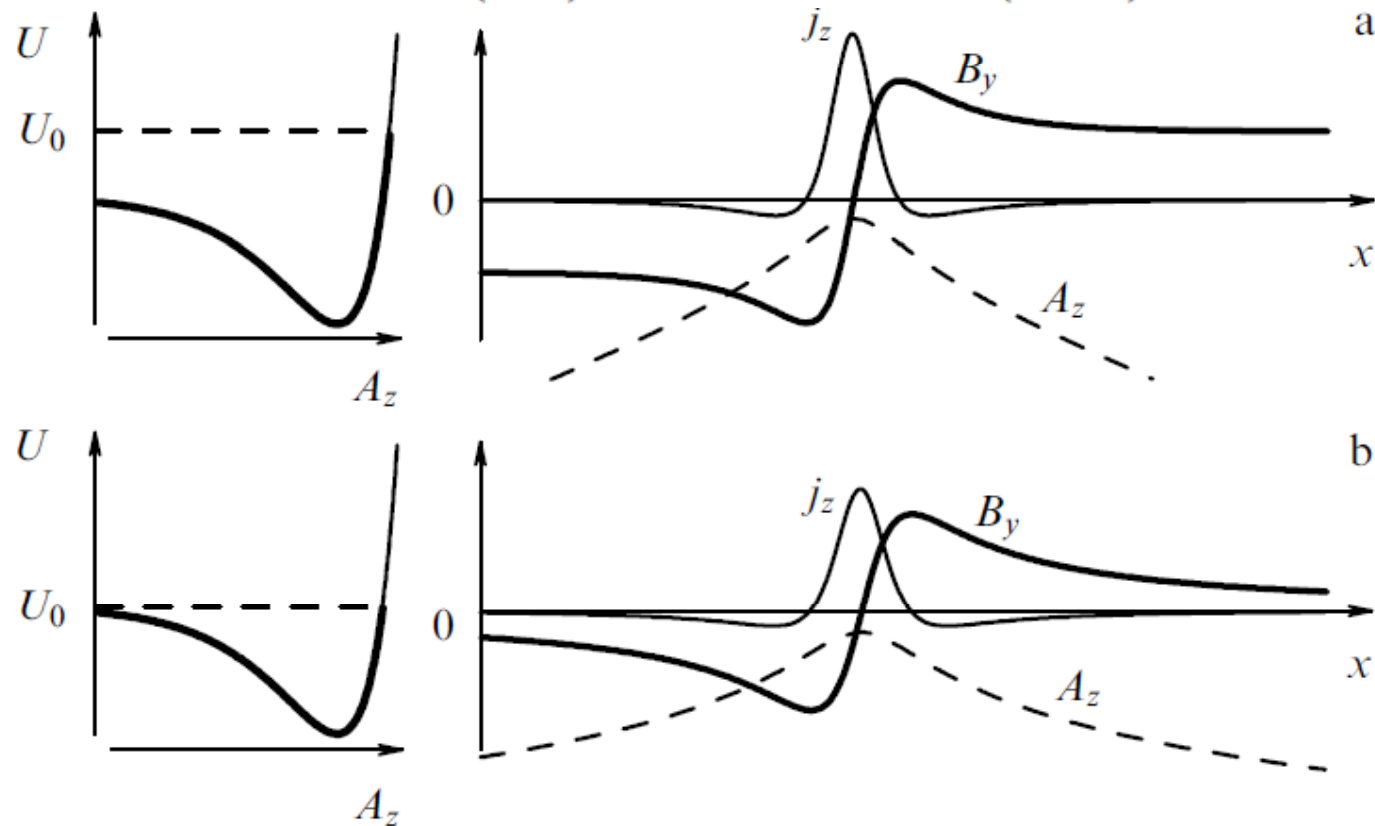


Figure 14. Profile of the Grad–Shafranov potential (137) for $W_0 > 0$, $W_2 < 0$ and coordinate dependences of A_z , B_y , and j_z characteristic of: (a) a partly screened current sheet, $U_0 > 0$, and (b) a completely screened current sheet, $U_0 = 0$.

All profiles are described analytically

Examples of PDF as a sum of two exponential terms

$$U(A_z) = W_1 \exp\left(\frac{A_z}{A_0}\right) + W_2 \exp\left(\frac{A_z}{wA_0}\right)$$

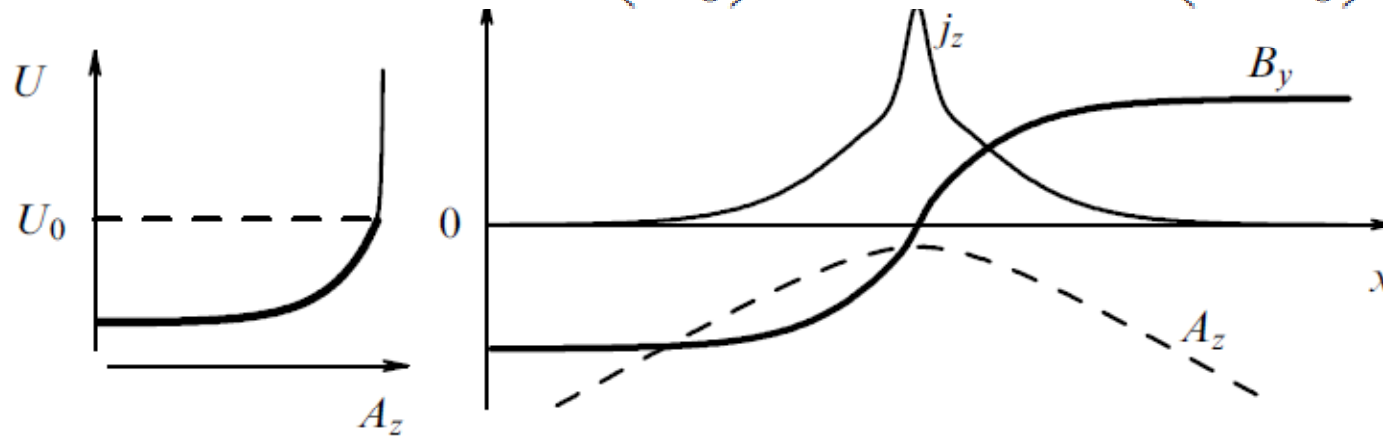
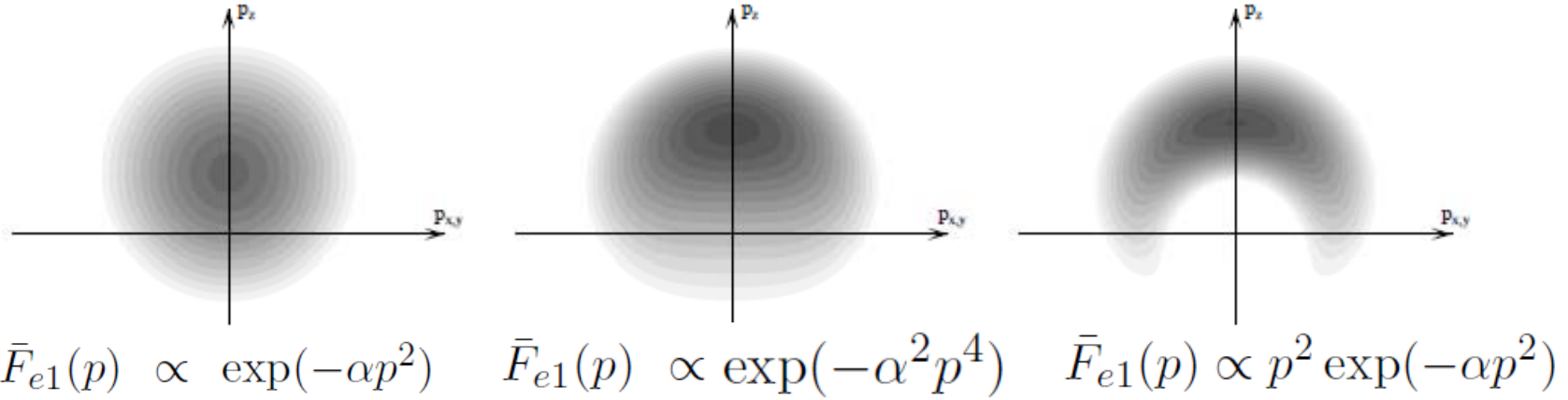


Figure 17. The profile of the Grad–Shafranov potential (137) for $W_0 > 0$, $W_2 > 0$, $w = 30$ and coordinate dependences of A_z , B_y , and j_z characteristic of a nested current sheet.

Noice, without going into the details of the resultant solutions, that if $w \gg 1$ or $w \ll 1$ and both quantities W_1 and W_2 are positive, the current density profile can be a double-scale one, i.e., have the shape of current sheets of markedly different thicknesses embedded within each other, so that various kinds of ions make up current sheets of different scales. The example of such embedding is presented in Fig. 17.



$$f_{i1} \left(p, p_z + \frac{e_{i1}}{c} A_z \right) = \bar{F}_{i1}(p) \exp \left(\zeta_{i1} \frac{p_z + e_{i1} A_z / c}{m_{i1} c} \right)$$

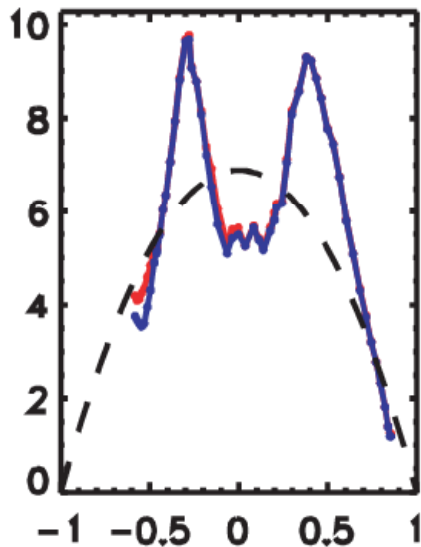
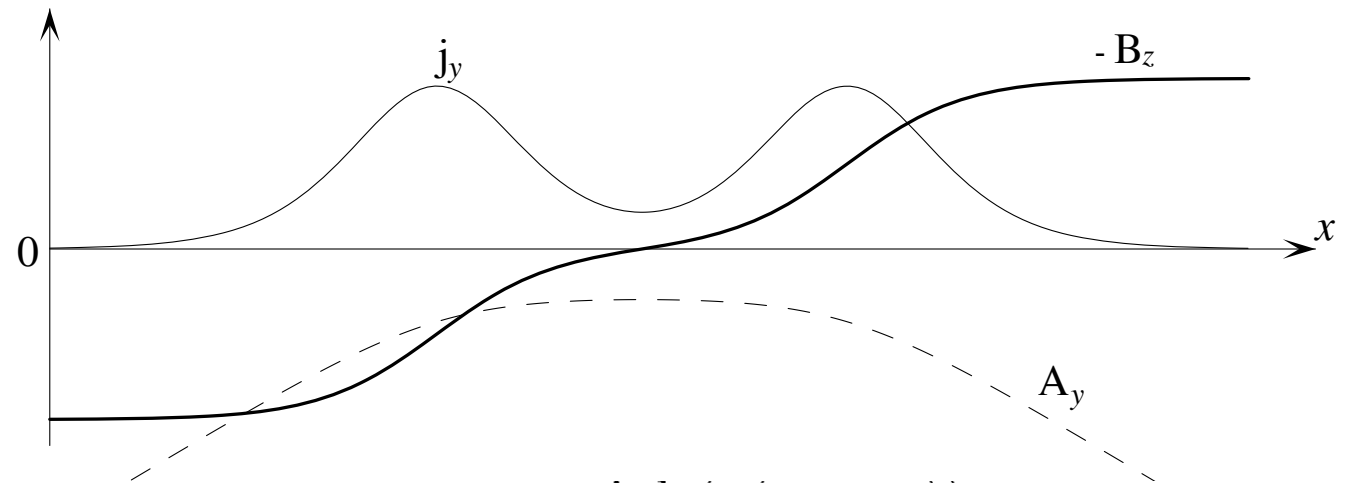
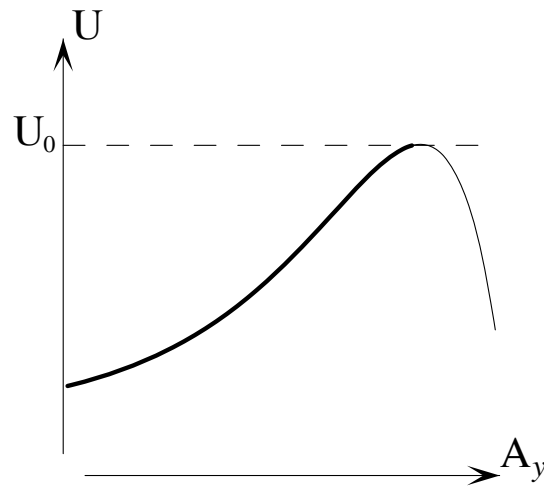
$$f_{i2} \left(p, p_z + \frac{e_{i2}}{c} A_z \right) = \bar{F}_{i2}(p) \exp \left(\zeta_{i2} \frac{p_z + e_{i2} A_z / c}{m_{i2} c} \right)$$

$$U(A_z) = W_1 \exp \left(\frac{A_z}{A_0} \right) + W_2 \exp \left(\frac{A_z}{w A_0} \right)$$

$$A_0 = \frac{c^2 m_{i1}}{\zeta_{i1} e_{i1}}, \quad w = \frac{m_{i2} \zeta_{i1} e_{i1}}{m_{i1} \zeta_{i2} e_{i2}}$$

Bifurcated current sheet with two peaks

$$\frac{d^2 A_y}{dx^2} = -\frac{W_1}{A_0} \exp\left(\frac{A_y}{A_0}\right) - \frac{W_2}{wA_0} \exp\left(\frac{A_y}{wA_0}\right)$$



$$B_y = 2\kappa A_0 \frac{\sinh(\kappa(x - x_0))}{\cosh(\kappa(x - x_0)) + W_2/\sqrt{W_2^2 + 2\kappa^2 A_0^2 W_0}},$$

$$j_z = \frac{c\kappa^2 A_0}{2\pi} \frac{1 + \left(W_2/\sqrt{W_2^2 + 2\kappa^2 A_0^2 W_0}\right) \cosh(\kappa(x - x_0))}{\left(\cosh(\kappa(x - x_0)) + W_2/\sqrt{W_2^2 + 2\kappa^2 A_0^2 W_0}\right)^2}$$

CLUSTER data

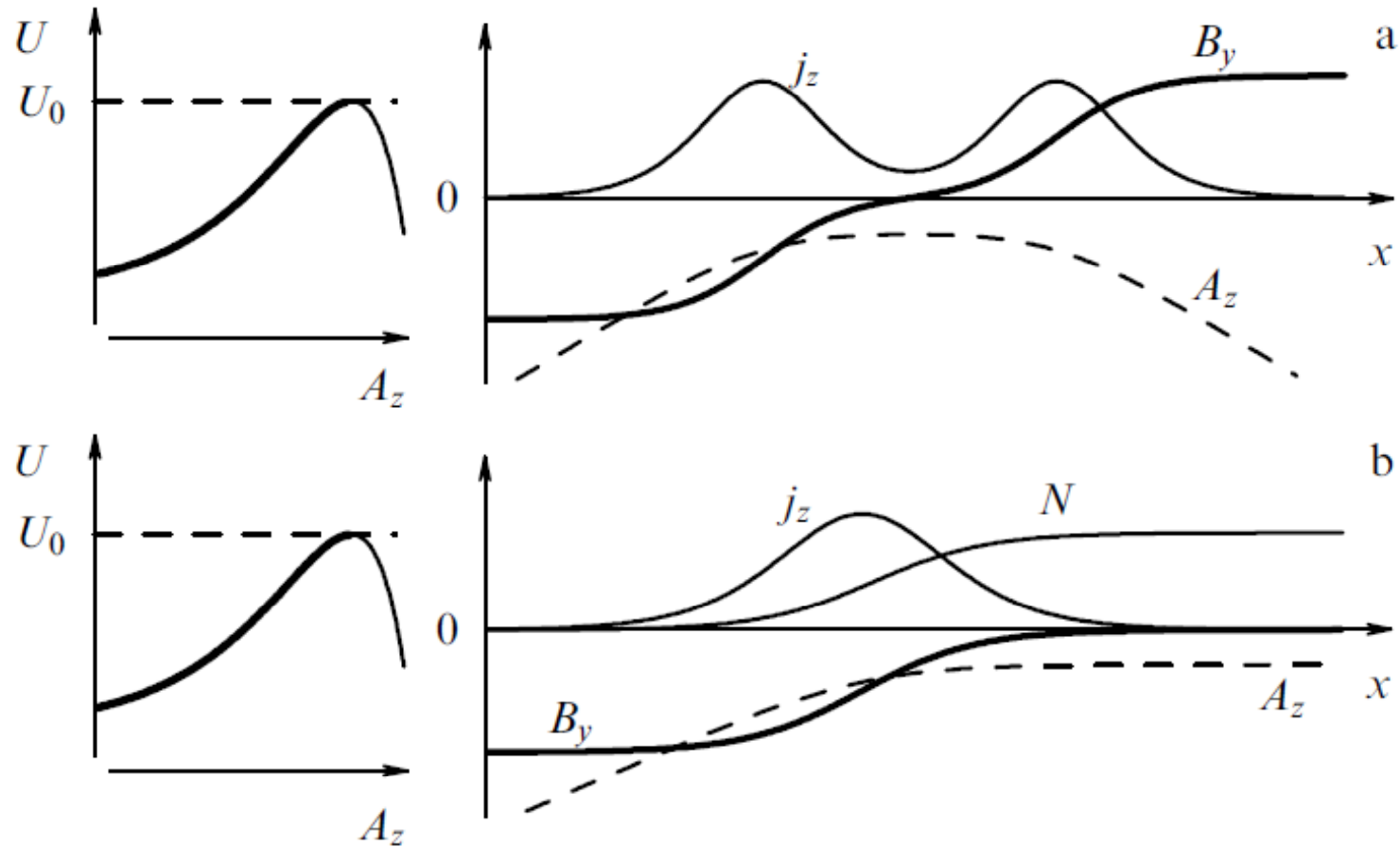
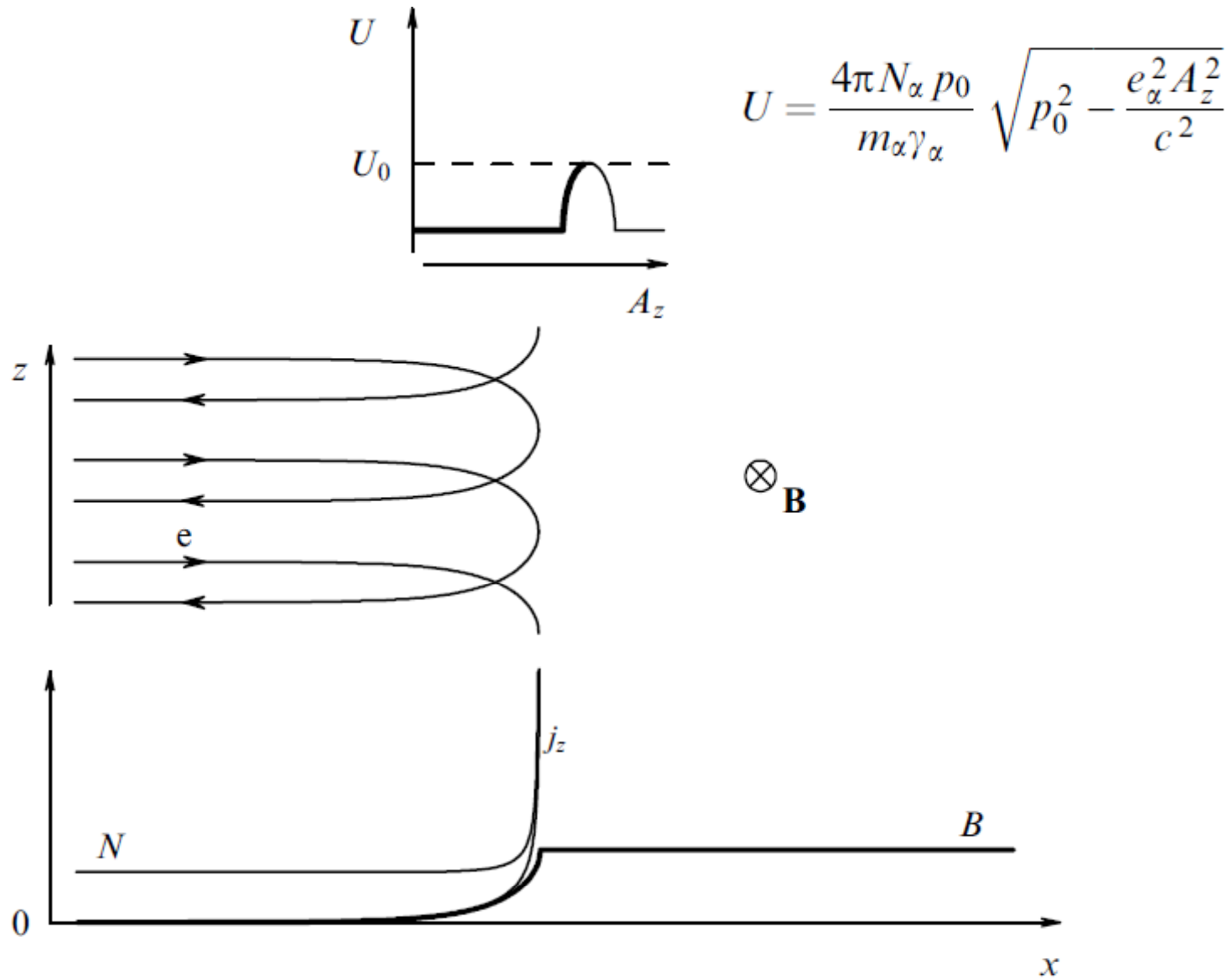


Figure 15. Profile of the Grad–Shafranov potential (137) for $W_0 < 0$, $W_2 > 0$ and the coordinate dependences of A_z , B_y , and j_z characteristic of (a) the split current sheet with U_0 close to $-W_2^2/W_0$, and (b) the symmetric transition sheet (from a homogeneous plasma to a vacuum with a uniform magnetic field; N is the particle concentration) realized at $U_0 = -W_2^2/W_0$.

(iii) In the case when the magnetic field is of constant sign, the function $U(A_z)$ varies monotonically and the current density alters the sign at least once, while the total current of the structure is zero. If the range of A_z is limited, the oscillator (i.e., A_z) moves down from a summit (hilltop) of a height U_0 and then moves up another hill of the same height U_0 . In the generic case, the potential near both summits is approximately parabolic, the magnetic field and the current density decline exponentially to zero as the distance from the sheet grows.

If the range of A_z is unlimited, the potential $U(A_z)$ tends to U_0 when the A_z goes to positive or negative infinity that cause a decrease of the magnetic field, while the current structure is asymmetrical — with an exponential decline of the current density on the one side and a power-law decline on the other (not faster than x^{-2}).



$$U = \frac{4\pi N_\alpha p_0}{m_\alpha \gamma_\alpha} \sqrt{p_0^2 - \frac{e_\alpha^2 A_z^2}{c^2}}$$

Figure 19. Grad–Shafranov potential (208), electron trajectories, and profiles of the magnetic field, current density, and particle concentration at the boundary of a uniform magnetic field and a two-beam plasma (at $U_0 = U_{\max}$).

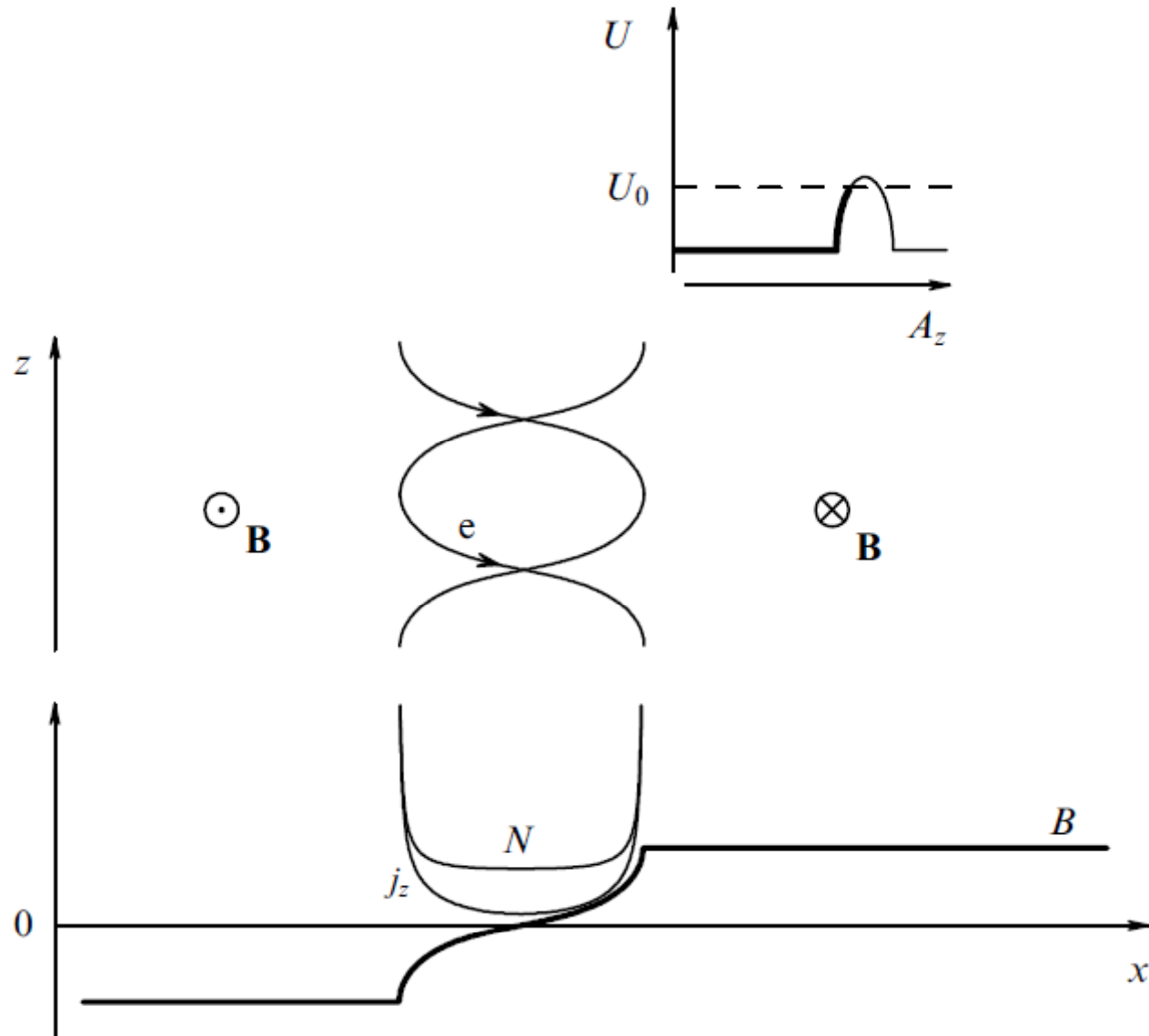


Figure 20. Grad-Shafranov potential (208), electron trajectories, and profiles of the magnetic field, current density, and particle concentration for a sheet with an antisymmetric magnetic field (for $U_0 < U_{\max}$).

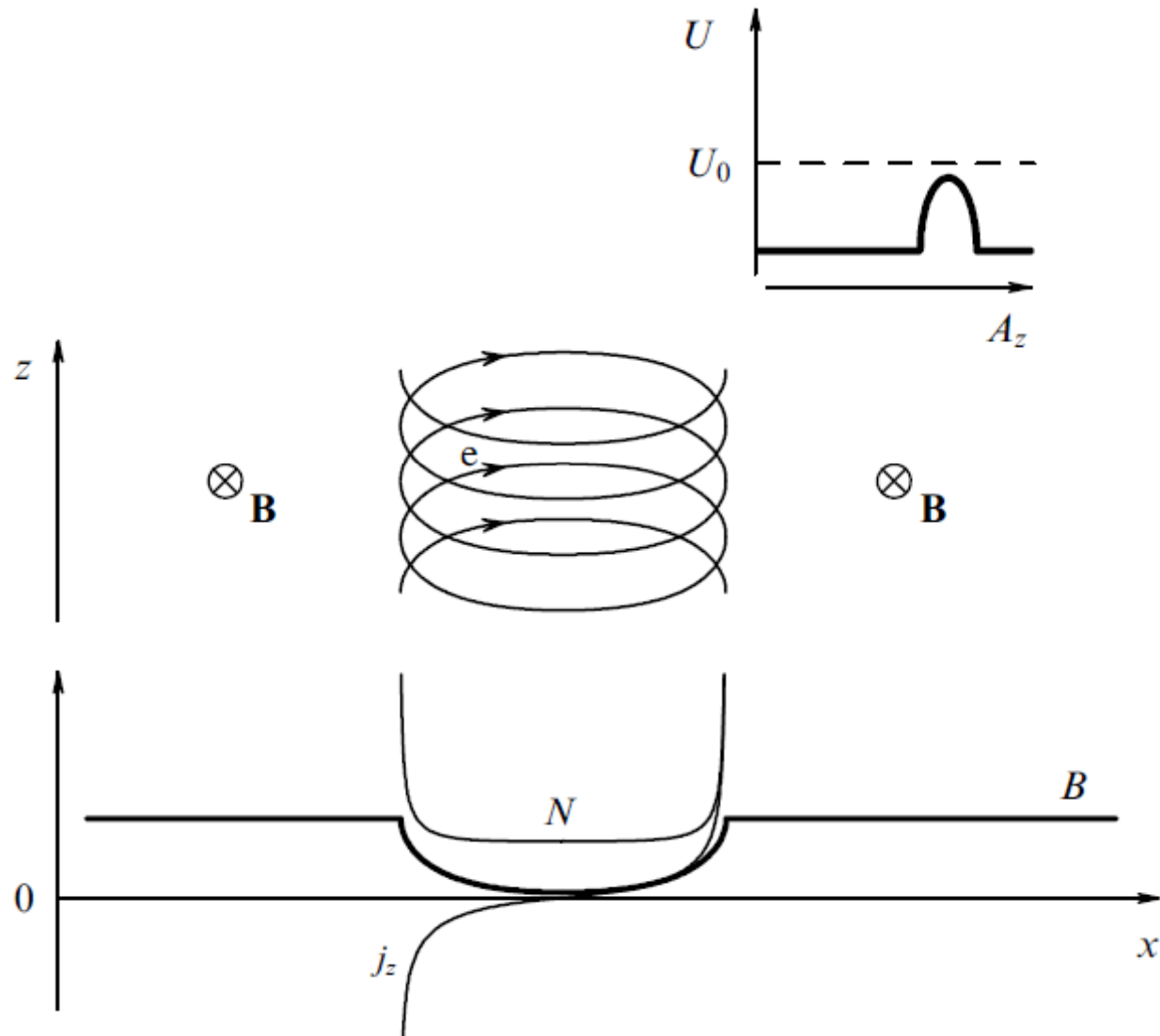


Figure 21. Grad–Shafranov potential (208), electron trajectories, and profiles of the magnetic field, current density, and particle concentration for a sheet with a symmetric magnetic field (for $U_0 > U_{\max}$).

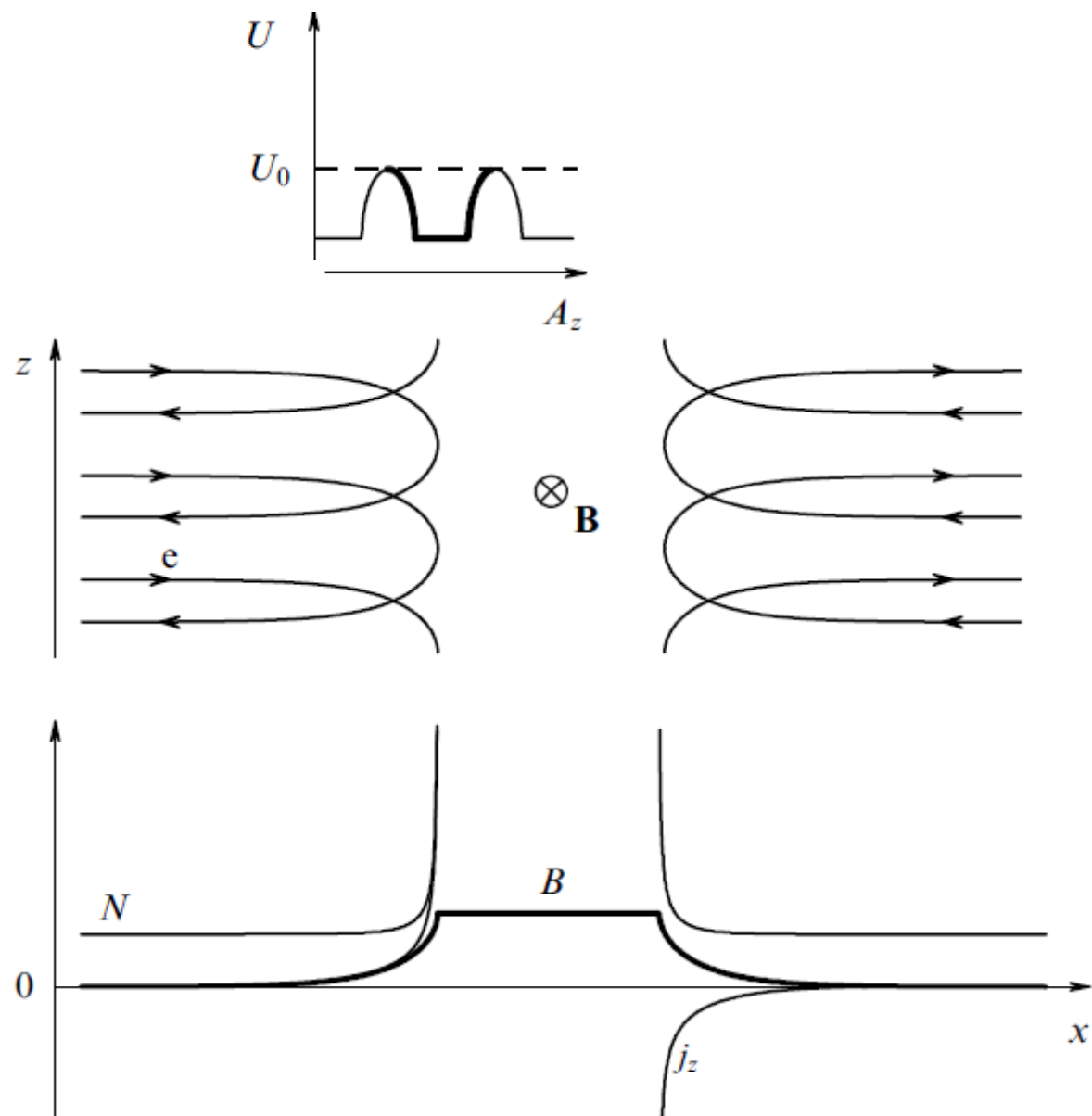


Figure 22. Grad-Shafranov potential, electron trajectories, and profiles of the magnetic field, current density, and particle concentration for two spatially separated fractions of particles (at $U_0 = U_{\max}$).

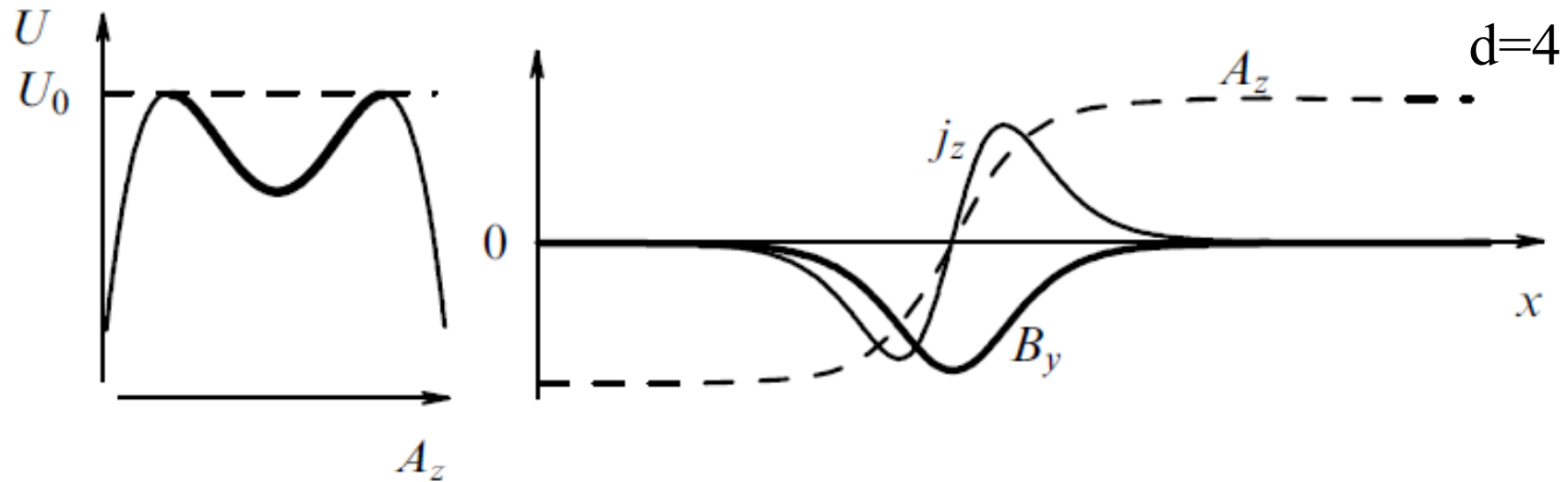


Figure 12. Profile of the Grad–Shafranov potential $U(A_z)$ and coordinate dependences of A_z , B_y , and j_z characteristic of the double current sheet.

$$U(A_z) = A_z^4 \sum_{\alpha} \int_0^{\infty} \hat{F}_{\alpha 4}(p) \frac{16\pi^2 N_{\alpha} p^4 e_{\alpha}^4}{3m_{\alpha}^5 \gamma_{\alpha} c^8} dp$$

$$A_z = A_{\max} \tanh\left(\frac{x}{D}\right),$$

$$+ A_z^2 \sum_{\alpha} \int_0^{\infty} \left(\hat{F}_{\alpha 2}(p) \frac{16\pi^2 N_{\alpha} p^4 e_{\alpha}^2}{3m_{\alpha}^3 \gamma_{\alpha} c^4} + \hat{F}_{\alpha 4}(p) \frac{32\pi^2 N_{\alpha} p^6 e_{\alpha}^2}{5m_{\alpha}^5 \gamma_{\alpha} c^6} \right) dp$$

$$B_y = \frac{A_{\max}}{D} \cosh^{-2}\left(\frac{x}{D}\right),$$

$$j_z = \frac{c A_{\max}}{2\pi D^2} \cosh^{-2}\left(\frac{x}{D}\right) \tanh\left(\frac{x}{D}\right)$$

Pair of current sheets ($d=4, \zeta=0$): $A_z = A_{\max} \tanh\left(\frac{x}{D}\right)$

$$D = \left[\sum_{\alpha} \int_0^{\infty} \left(\hat{F}_{\alpha 2}(p) \frac{16\pi^2 N_{\alpha} p^4 e_{\alpha}^2}{3m_{\alpha}^3 \gamma_{\alpha} c^4} + \hat{F}_{\alpha 4}(p) \frac{32\pi^2 N_{\alpha} p^6 e_{\alpha}^2}{5m_{\alpha}^5 \gamma_{\alpha} c^6} \right) dp \right]^{-1/2}$$

$$A_{\max} = \left[-2D^2 \sum_{\alpha} \int_0^{\infty} \hat{F}_{\alpha 4}(p) \frac{16\pi^2 N_{\alpha} p^4 e_{\alpha}^4}{3m_{\alpha}^5 \gamma_{\alpha} c^8} dp \right]^{-1/2}$$

$$B_z = \frac{\sqrt{\pi} p_0 (2N_2 m_e^2 c^4 + 3N_4 p_0^2 c^2)}{\sqrt{-4N_4 \gamma_0 m_e^5 c^8}} \operatorname{ch}^{-2} \left(\sqrt{\frac{2\pi e_e^2}{c\gamma_0} \frac{N_2 p_0^2}{(m_e c)^3} + \frac{3\pi e_e^2}{c\gamma_0} \frac{N_4 p_0^4}{(m_e c)^5}} x \right),$$

$$N_e = N_0 + \frac{N_2 p_0^2}{2m_e^2 c^2} + \frac{3N_4 p_0^4}{8m_e^4 c^4} + \left(\frac{N_2 e_e^2}{m_e^2 c^4} + \frac{3N_4 e_e^2 p_0^2}{m_e^4 c^6} \right) A_y^2 + \frac{N_4 e_e^4}{m_e^4 c^8} A_y^4,$$

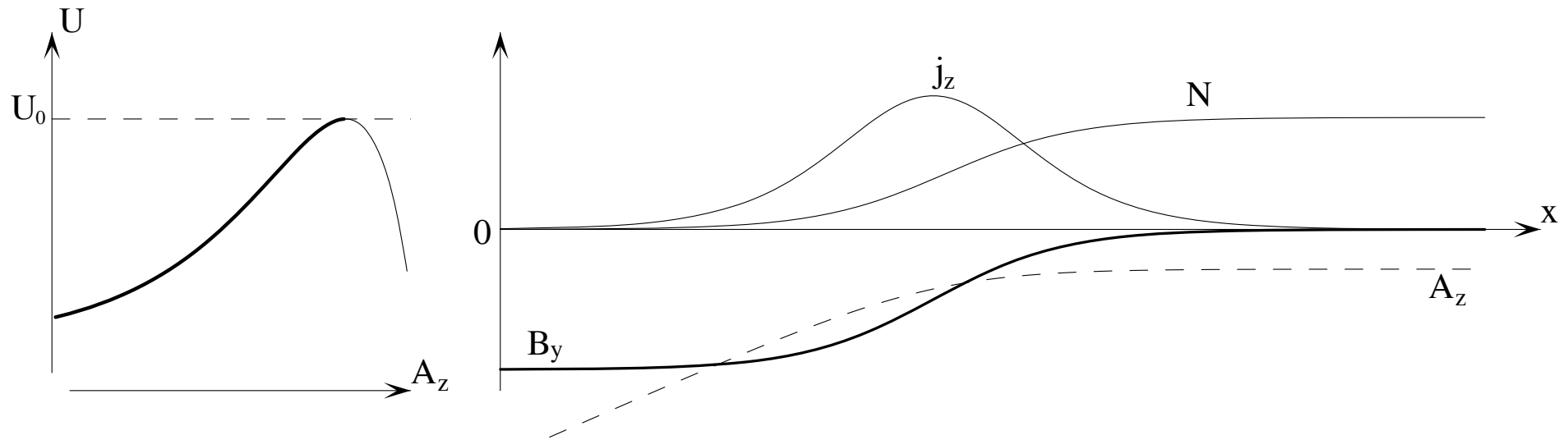
$$j_y = \left(\frac{e_e^2}{\gamma_0} \frac{N_2 p_0^2}{(m_e c)^3} + \frac{3e_e^2}{2\gamma_0} \frac{N_4 p_0^4}{(m_e c)^5} \right) A_y + \frac{2e_e^4}{c^2 \gamma_0} \frac{N_4 p_0^2}{(m_e c)^5} A_y^3.$$

(iv) The case of an external magnetic field

When the magnetic field does not change sign, the Grad–Shafranov equation can be used to describe nonself-consistent current structures located in the *external magnetic field*. In this case, as $x \rightarrow \pm\infty$, the magnetic field tends toward two, generally speaking, different constants, with at least one of them being nonzero, and at least one of the limits, $U(A_z \rightarrow -\infty)$ or $U(A_z \rightarrow +\infty)$, finite and smaller than U_0 . If $U(A_z)$ is everywhere smaller than U_0 , while limits $U(A_z \rightarrow -\infty)$ and $U(A_z \rightarrow +\infty)$ are equal, it suggests an existence of a current structure localized in the external uniform magnetic field, having zero total current. If $U(A_z)$ is everywhere smaller than U_0 and the above limits are not equal, then the current structure has nonzero total current,

At one side of a current sheet, the screening of the external magnetic field may be partial or complete.

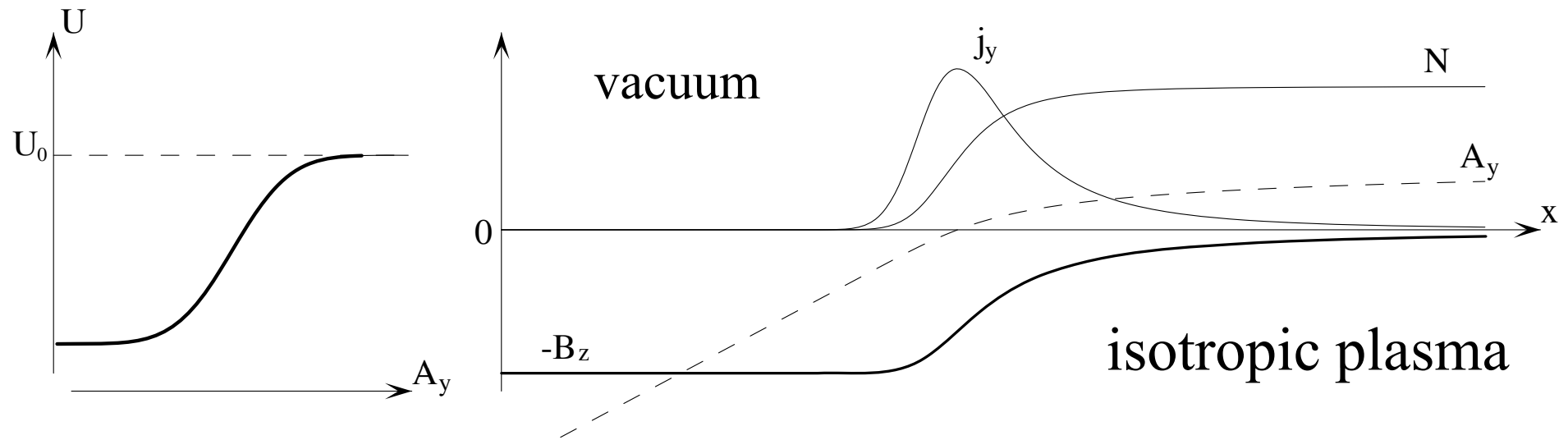
Boundary current sheet



Current profile is similar to the Harris one, but PDF is different.

$$\frac{d^2 A_y}{dx^2} = -\frac{W_1}{A_0} \exp\left(\frac{A_y}{A_0}\right) - \frac{W_2}{wA_0} \exp\left(\frac{A_y}{wA_0}\right)$$

Asymmetric current sheets in external magnetic field as a boundary layer separating plasmas with different parameters



$$F = F_0(p) H \left(\frac{cp_y/e + A}{A_0} \right)$$

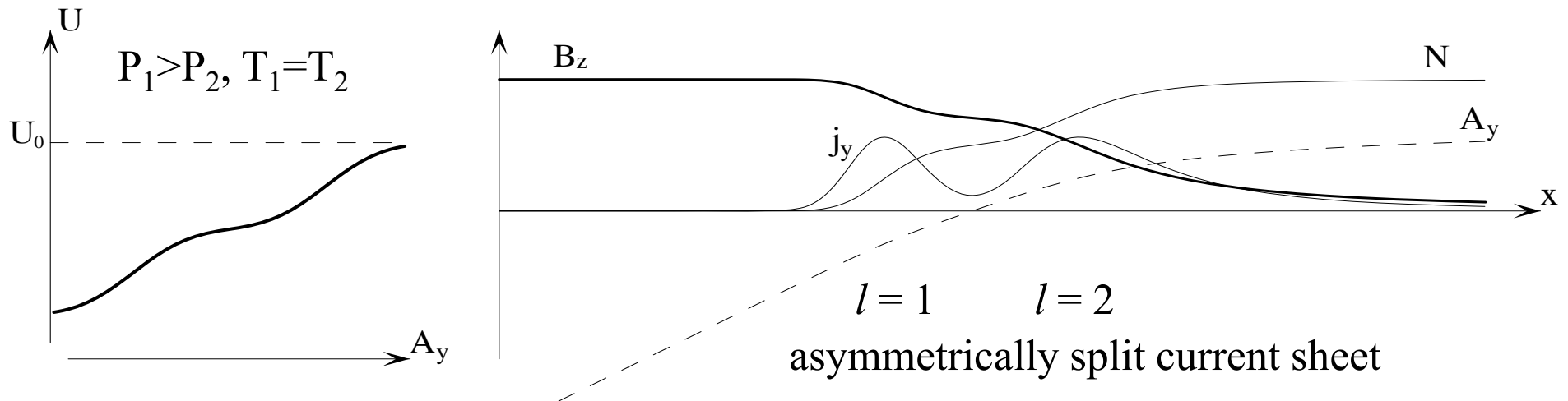
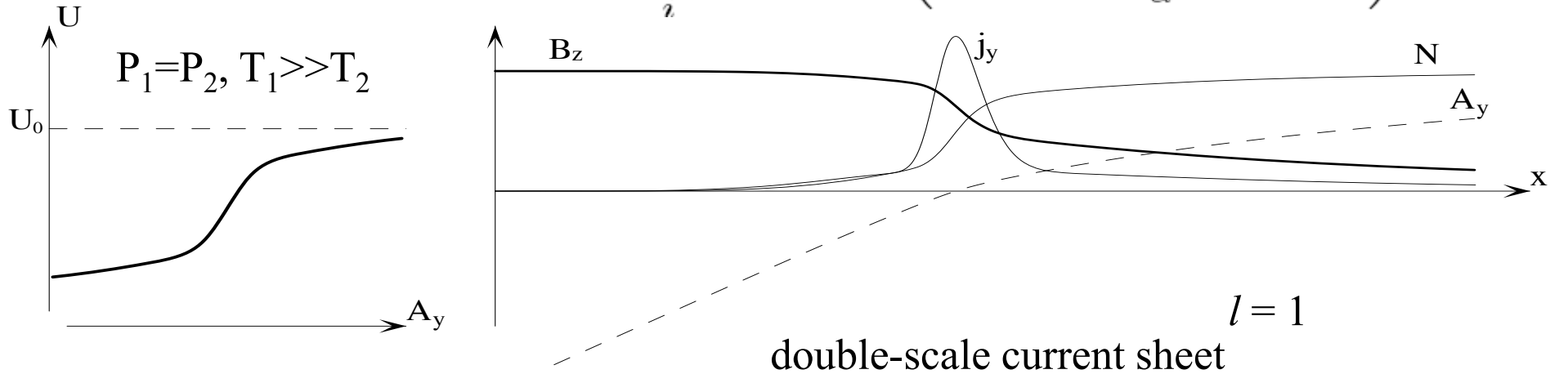
For maxwellian PDF, the Grad-Shafranov potential is the following

$$U(A) = \sum_{\alpha} 2\pi N_{\alpha} k_B T \operatorname{erf} \left(\frac{e_{\alpha} A / c}{\sqrt{2m_{\alpha} k_B T}} \right)$$

Boundary current sheets with step-functions in PDF

$i=1,2$

$$f_{\alpha} \left(p, p_z + \frac{e_{\alpha}}{c} A_z \right) = \sum_i \bar{F}_{\alpha i}(p) H \left(\frac{p_z + e_{\alpha} A_z / c - P_i(p)}{m_{\alpha} c} \right)$$

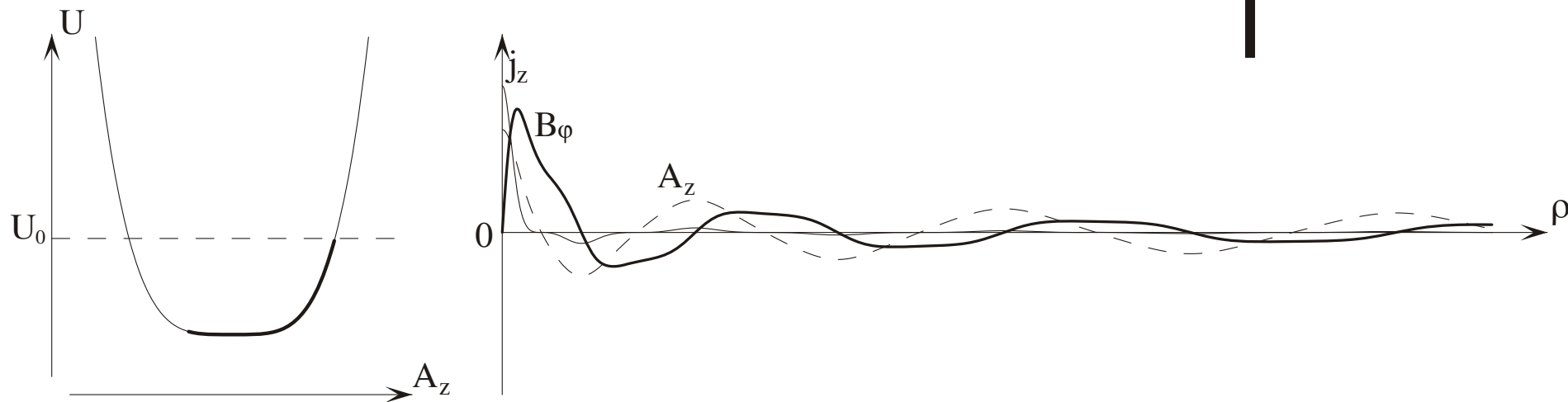
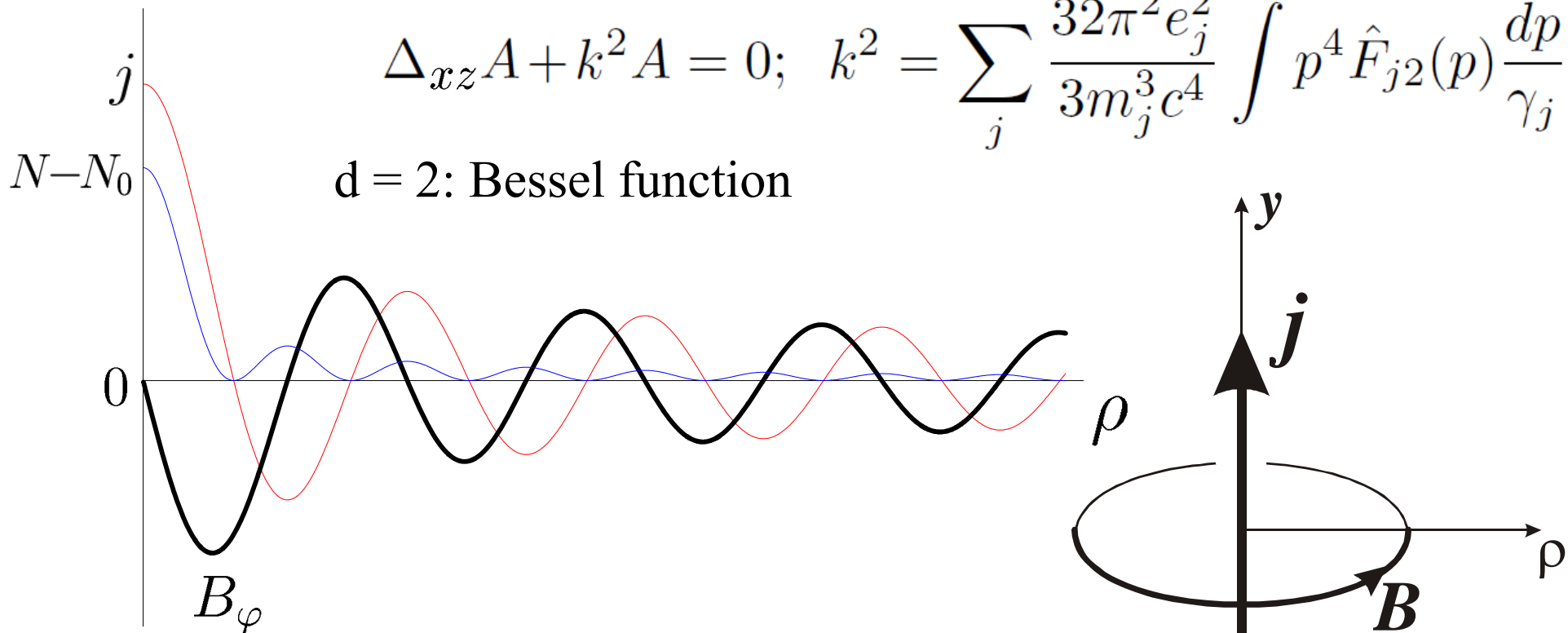


Plasma is isotropic in the regions with homogeneous magnetic field

Cylindrical configurations (current filaments)

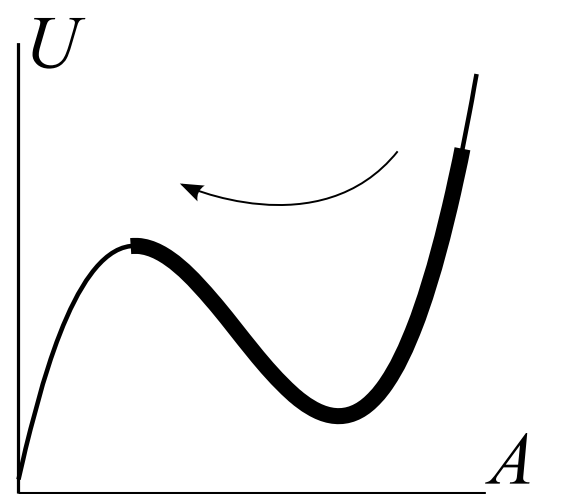
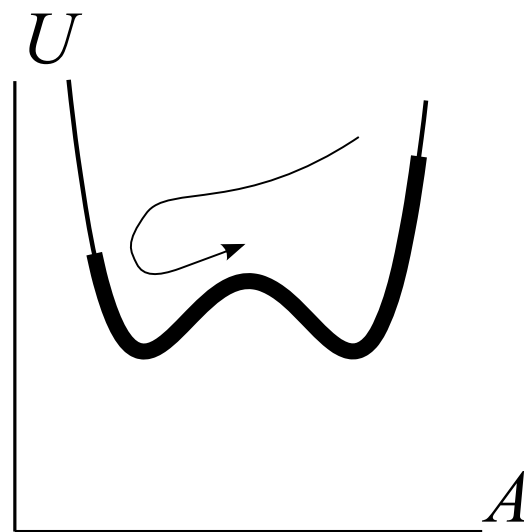
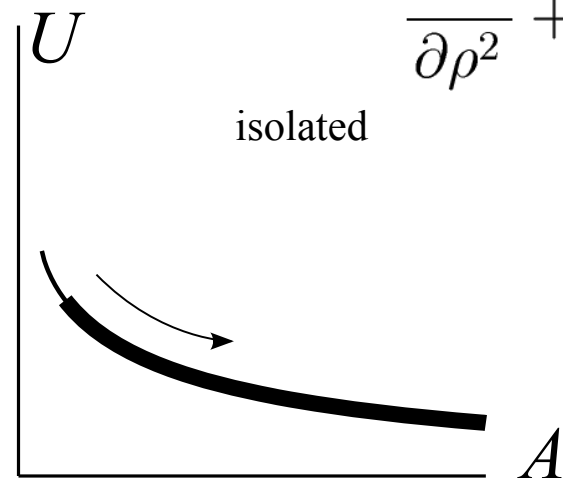
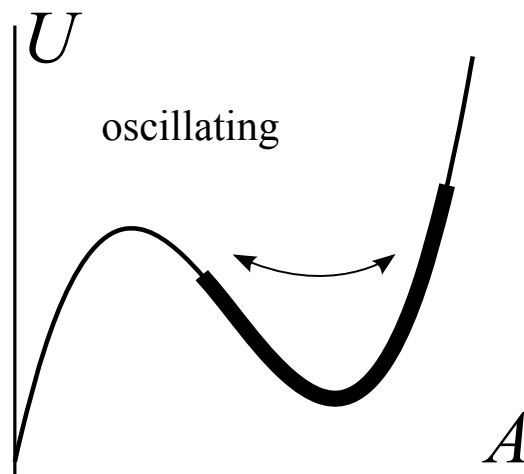
$$\Delta_{xz} A + k^2 A = 0; \quad k^2 = \sum_j \frac{32\pi^2 e_j^2}{3m_j^3 c^4} \int p^4 \hat{F}_{j2}(p) \frac{dp}{\gamma_j}$$

$d = 2$: Bessel function



Cylindrically symmetric solutions (effective viscous damping)

$$\frac{\partial^2 A}{\partial \rho^2} + \frac{1}{\rho} \frac{\partial A}{\partial \rho} = -\frac{\partial U}{\partial A}$$



shielded

Classification of the current filaments

For the cylindrically symmetrical filaments with a purely azimuthal magnetic field, the method of particle motion invariants admits only the following three qualitatively different types of the self-consistent structures.

I. The first type assumes an unlimited value of the vector potential A_z . This implies that the A_z is a monotonic function and the azimuthal component of the magnetic field is of the same sign for all values of the radial variable ρ . The current density may be sign-changing, although the current through any circular area perpendicular to z with a center on z has the same sign. A total current can be either finite or zero. The plasma can be localized near axis z , with its density exponentially vanishing with an increasing distance from the axis.

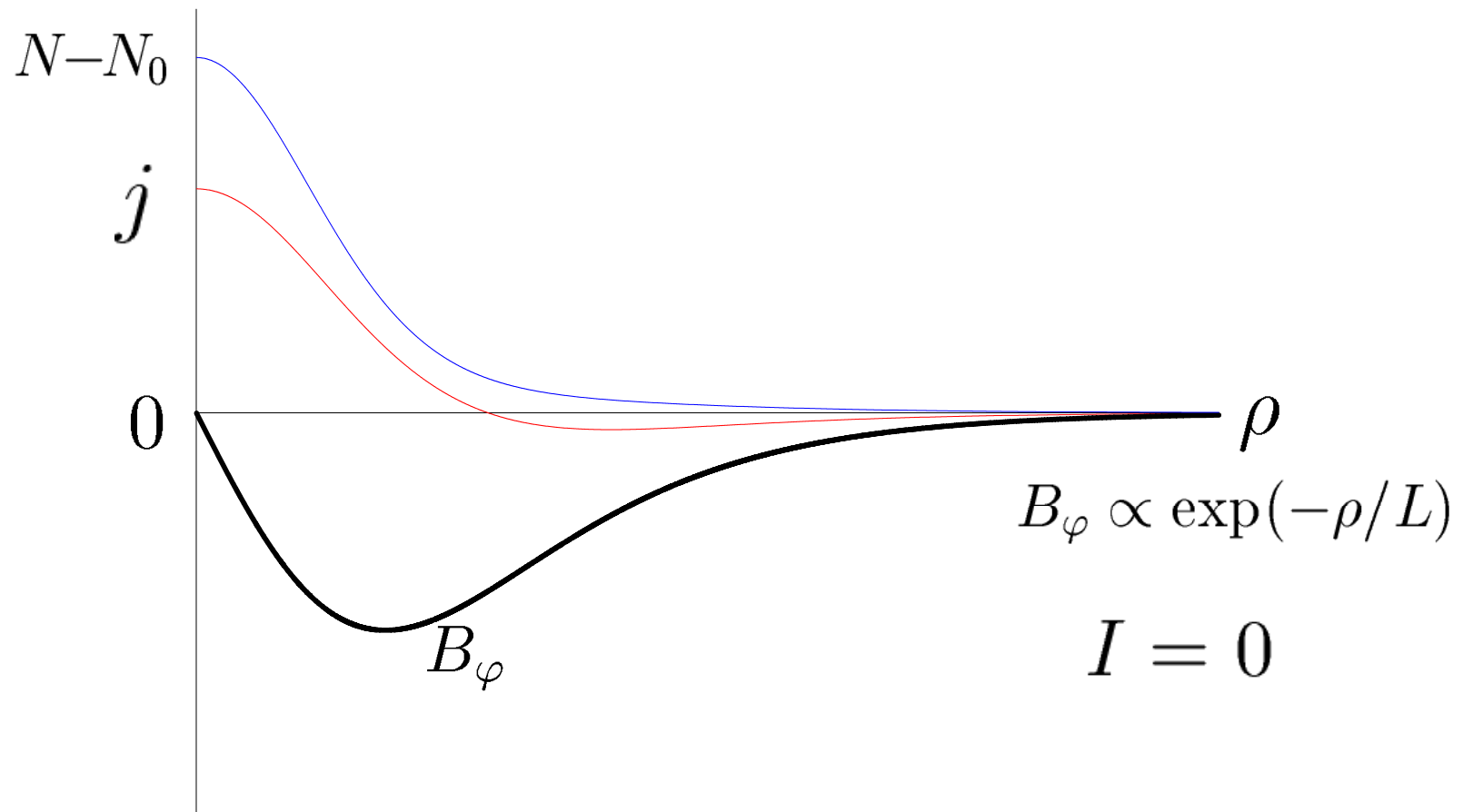
II. In the second type, the range of values of A_z is limited and its derivative with respect to ρ (the azimuthal component of magnetic field) changes sign a finite number of times. So, the “motion” of the oscillator (i.e., A_z) in the Grad-Shafranov potential starts at $\rho = 0$ with sliding down the slope of the well and ends on a local summit or, in a degenerate case, at the point where the first two derivatives of $U(A_z)$ with respect to A_z vanish.

A bottom of the potential well cannot be reached in an infinitely slow monotonic manner since a general solution to the oscillator equation with a viscous friction and a zero right-hand side is $A_z = c_1 + c_2 \cdot \ln \rho$. So, even for a completely flat bottom the motion is unlimited and the “friction” cannot stop the motion at a finite distance. Between the beginning and the end of the motion, there could be a few reflections from the potential walls that are higher than the final summit. The total current is absent, the magnetic field declines faster than $1/\rho$ with the increase of ρ . In the general case, the summit (hilltop) on the vector potential's profile has a quadratic form. Hence, the magnetic field and the current density decline exponentially.

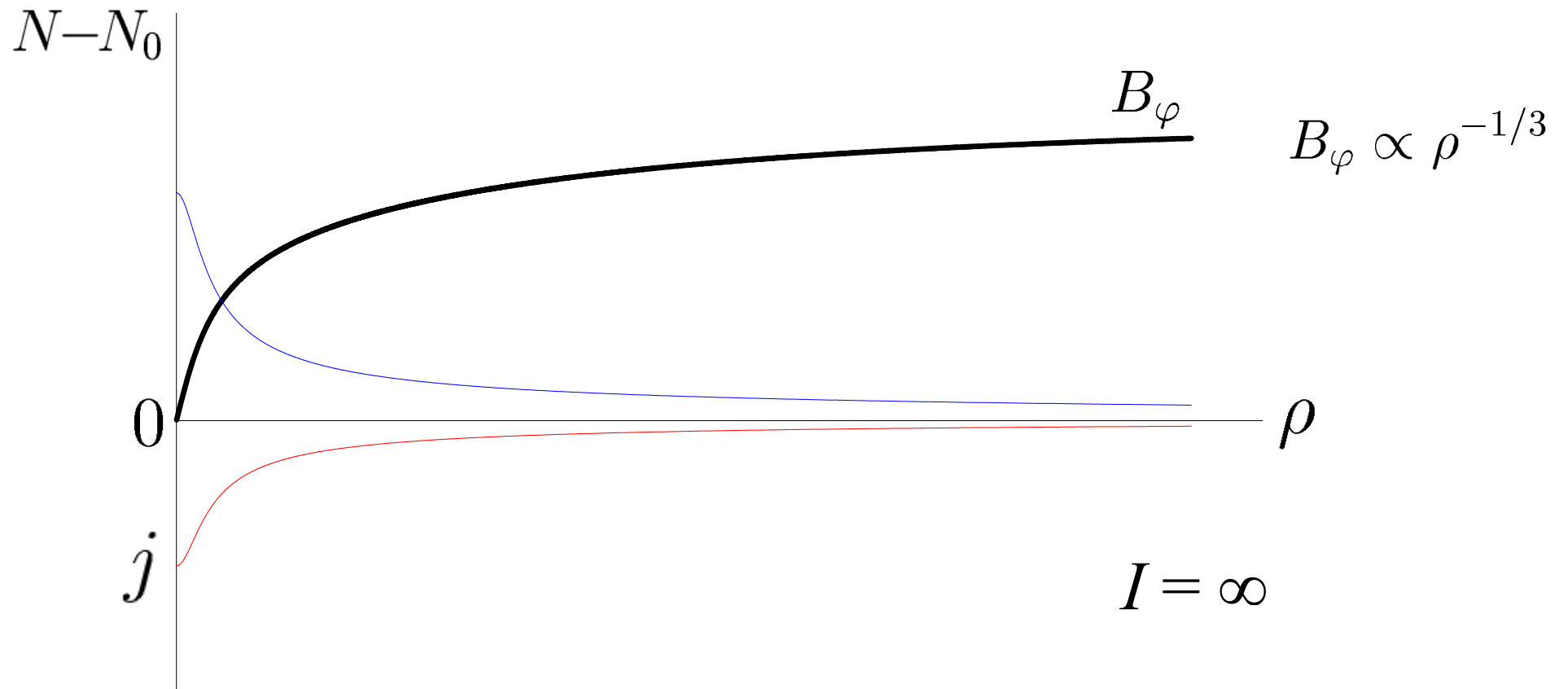
III. In the third type, the range of values of A_z is limited, the A_z oscillates infinitely many times near the well's bottom with the increase of ρ . In a general case, as the amplitude of these oscillations decreases, the profile of the well's bottom can be approximated by a parabola, which yields a Bessel-type solution. The amplitudes of oscillations of A_z , the magnetic field and the current density decrease as $1/\rho$ when ρ increases.

In the case when the series expansion of the Grad-Shafranov potential near the bottom starts with a term higher than quadratic, the infinitely many oscillations also exist, although their period grows with ρ . The resulting current configuration constitutes a finite or infinite collection of concentric current cylinders, among which the ones on the outside have, as a rule, a larger value of the total current and a lower current density than the inside ones.

Shielded current filament (Taylor order $d=3$)

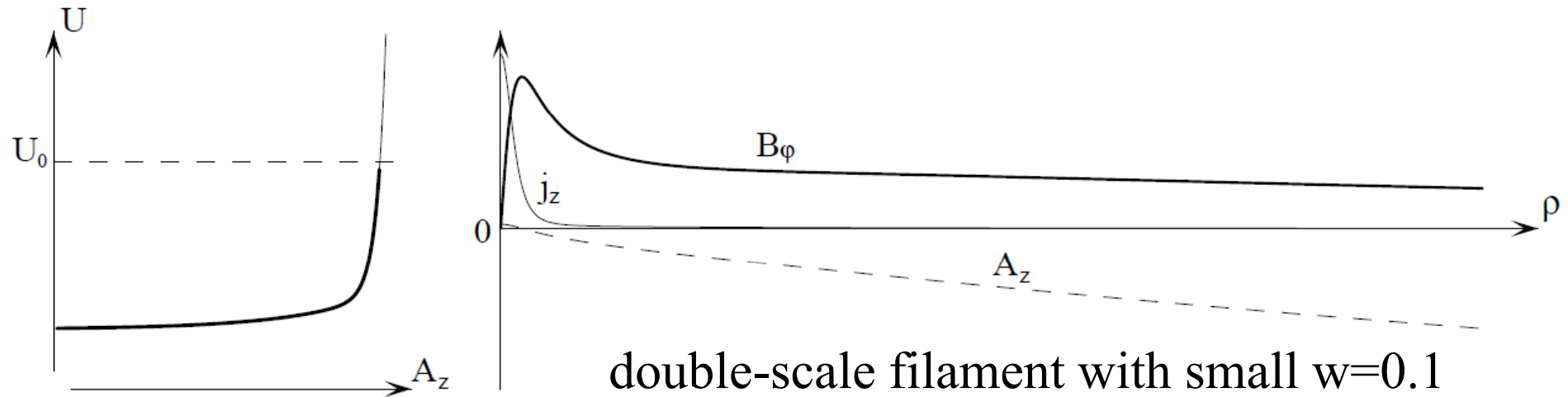


Single current filament (Taylor order $d = -1$)



Generalized relativistic Bennett pinch

$$\frac{d^2 A_y}{d\rho^2} + \frac{1}{\rho} \frac{dA_y}{d\rho} = -\frac{W_1}{A_0} \exp\left(\frac{A_y}{A_0}\right) - \frac{W_2}{wA_0} \exp\left(\frac{A_y}{wA_0}\right)$$



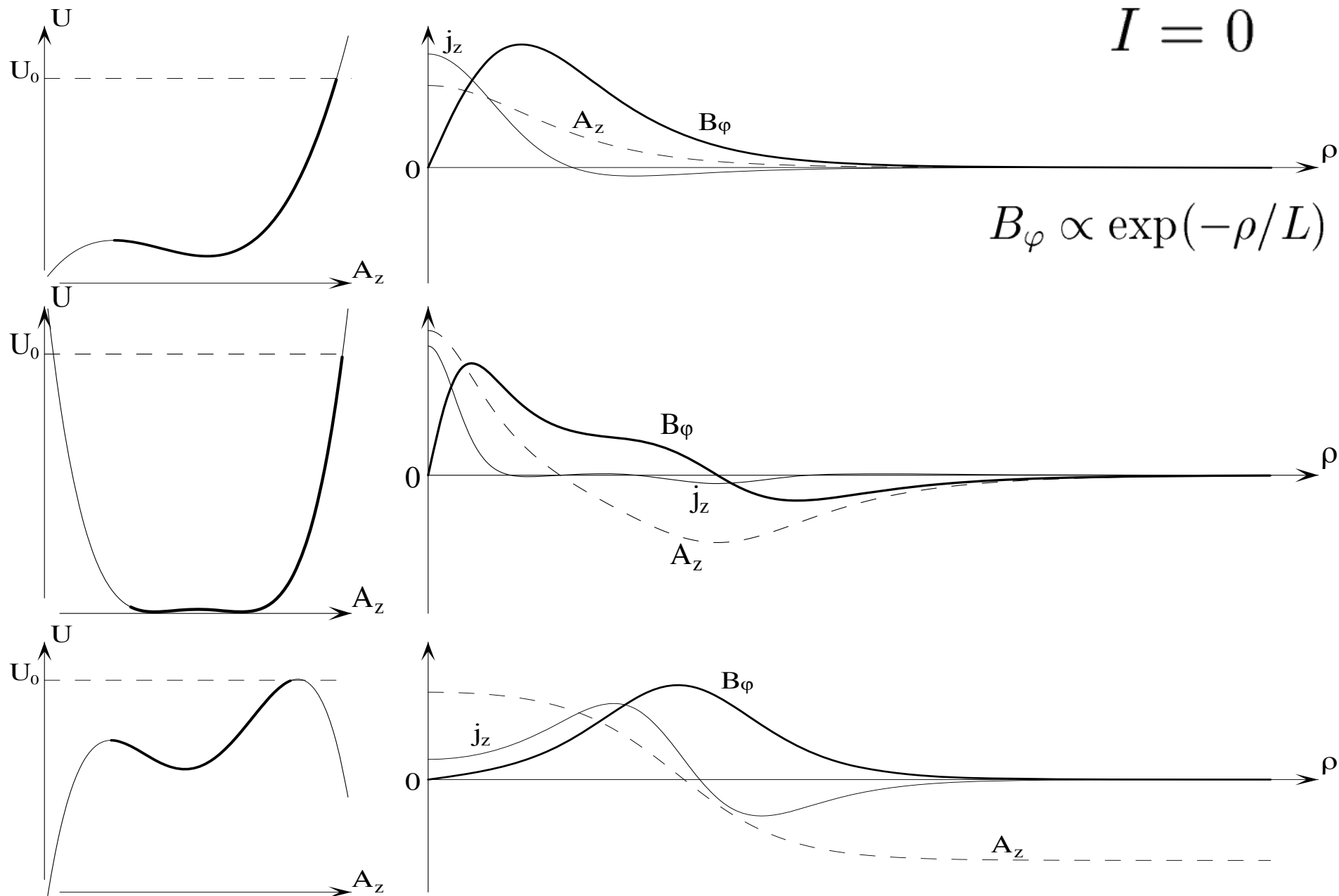
Limiting case of Bennett pinch with current along a wire on the axis $I = (1-q)cA_0$. If $q > 1$, the latter is opposite to the pinch current, which is expelled from the axis area and localized in a hollow tube.

$$B_\varphi = \frac{2A_0 (1 - q + (1 + q)(\kappa\rho)^{2q})}{\rho(1 + (\kappa\rho)^{2q})}$$

$$j_z = \frac{2cA_0 q^2 \kappa^2}{\pi((\kappa\rho)^{1-q} + (\kappa\rho)^{1+q})^2}$$

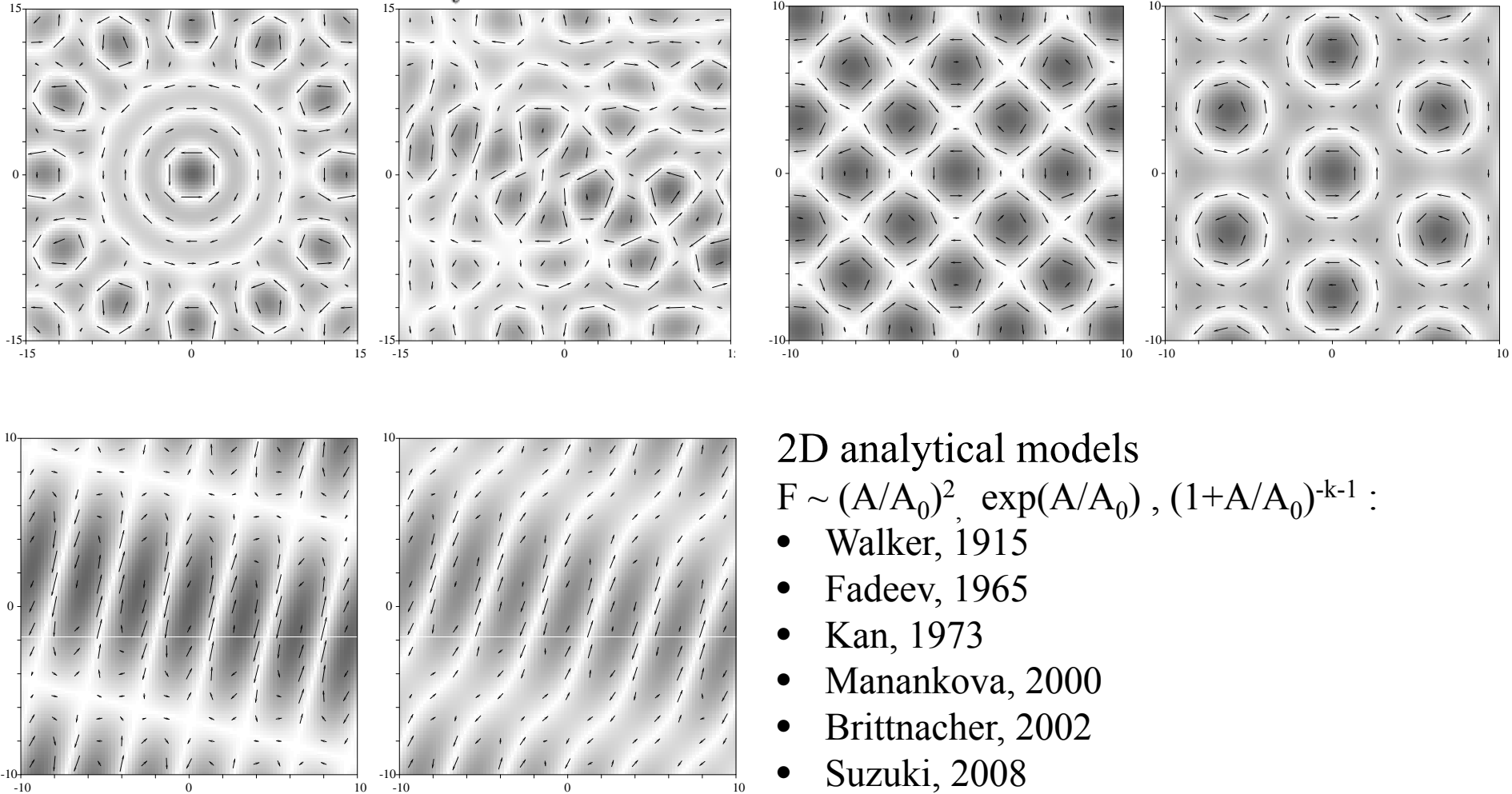
Shielded current filaments (Taylor order $d=3$, $d=4$)

$$I = 0$$



Two-dimensional current structures $j(x,z)$ ($d=2$)

$$A = \sum_l A_l \cos(k z \cos \theta_l + k y \sin \theta_l + \varphi_l)$$



2D analytical models

$F \sim (A/A_0)^2, \exp(A/A_0), (1+A/A_0)^{-k-1} :$

- Walker, 1915
- Fadeev, 1965
- Kan, 1973
- Manankova, 2000
- Brittnacher, 2002
- Suzuki, 2008
- Vasko, 2013

Arbitrary PDF in a generalization of Harris current sheet

$$\hat{F}_j(p, p_z + e_j A/c) = \hat{F}_j(p) \exp\left(\frac{cp_z/e_j + A}{A_0}\right) + \hat{f}_j(p)$$

$$\Delta_{xy} A = -\alpha \exp\left(\frac{A}{A_0}\right)$$

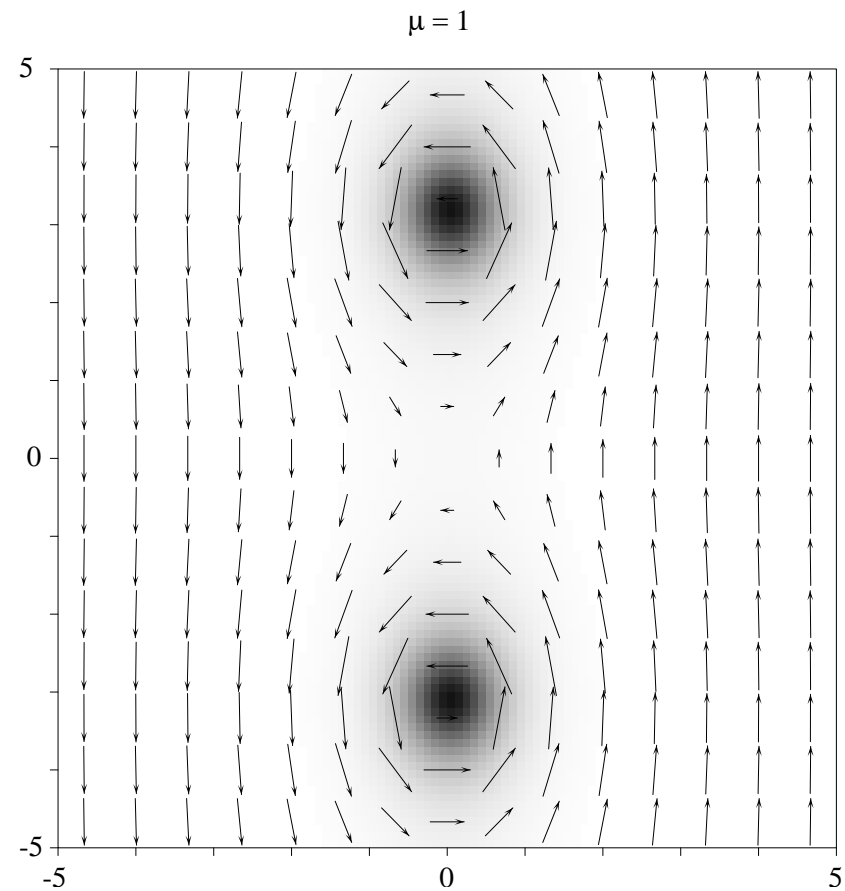
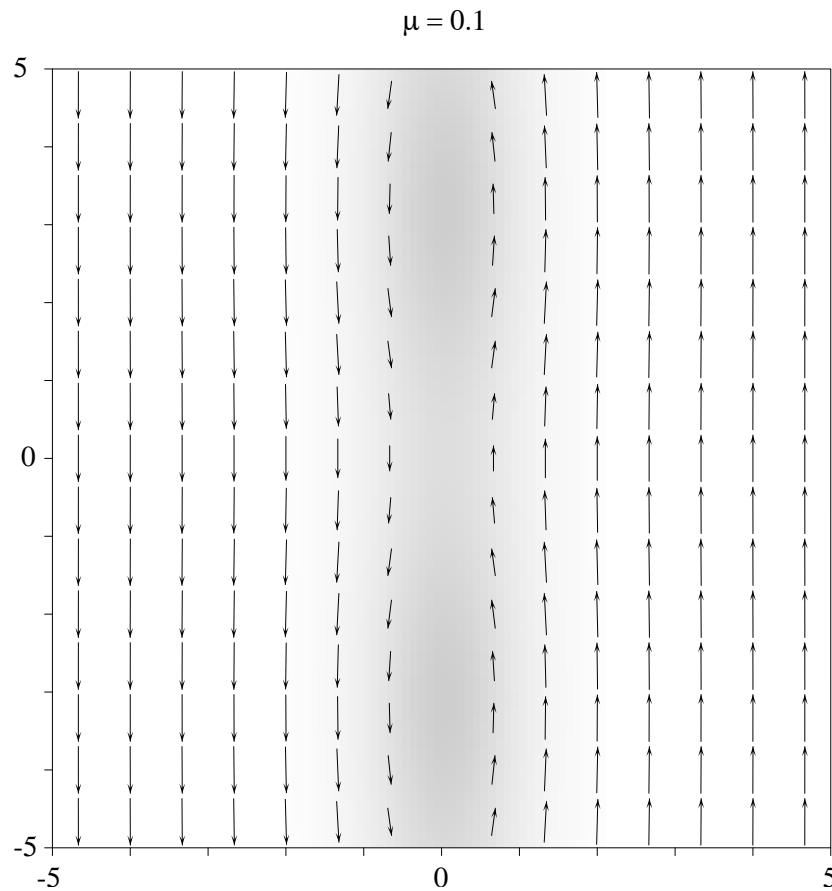
$$\alpha = \sum_j \frac{8\pi^2 e_j^3 A_0^2}{m_j c^3} \int \left[\left(\frac{cp}{e_j A_0} - 1\right) \exp\left(\frac{cp}{e_j A_0}\right) + \left(\frac{cp}{e_j A_0} + 1\right) \exp\left(-\frac{cp}{e_j A_0}\right) \right] \frac{p}{\gamma_j} \hat{F}_j(p) dp$$

$$A = -2A_0 \ln \cosh \sqrt{\frac{\alpha}{2A_0}} x, \quad B_y = -\sqrt{2A_0 \alpha} \tanh \sqrt{\frac{\alpha}{2A_0}} x$$

$$N_j = N_{j\max} \cosh^{-2} \sqrt{\frac{\alpha}{2A_0}} x$$

Two-dimensional Fadeev-like solution (exponential PDF)

$$A = -2A_0 \ln \left[\mu \cos \sqrt{\frac{\alpha}{2A_0}} z + \sqrt{1 + \mu^2} \cosh \sqrt{\frac{\alpha}{2A_0}} x \right]$$



Conclusions

- Closed analytical forms of the nonlinear Grad-Shafranov equation obtained on the basis of several simple decompositions of particle distribution functions (PDFs) in collisionless relativistic multicomponent plasma.
- Exact solutions of magnetostatic Vlasov-Maxwell equations describing a broad variety of current sheets and filaments with arbitrary energy PDFs.
- Various properties of self-consistent current sheets and filaments, including magnetic energy content, gyroradius to thickness ratio, PDF anisotropy.
- a way to new analytical models of current structures observed in cosmic and laboratory plasmas as well as obtained in numerical simulations.

Some open problems

- (1) How representative are distribution functions depending only on particle motion invariants compared with a variety of distribution functions describing all stationary self-consistent current structures? How adequately do the first distributions represent qualitatively (physically) similar current structures described by more general particle distributions?
- (2) What self-consistent current structures are most (or least) stable and what is the hierarchy of their instabilities? For which particle distribution is the structure with a given current density profile most stable?
- (3) To what degree do the classes of stationary current structures extend (or contract) under the effect of a magnetic field imposed, for example, across the current sheet and/or boundary conditions, e.g., in prescribing the input and output particle flows at the borders of the current structure?
- (4) Is there a possibility of quasi-adiabatic (slow) deformation of current structures without their appreciable destruction and, if yes, under which conditions does it occur? Is it possible to macroscopically describe any current structure deformation or their interaction with each other without a detailed analysis of PDF evolution?
- (5) How do interparticle collisions, quasi-stationary electric fields, and higher-frequency electromagnetic fields influence self-consistent current structures? When does this influence result in their destruction or evolution of their macroscopic parameters without destruction, even if with a loss of energy content?